論文 / 著書情報
Article / Book Information

題目(和文)	
Title(English)	Study of electrical double layer structure at solid-liquid interfaces by atomic force microscopy
著者(和文)	新井(富取)豊子
Author(English)	Arai Tomitori Toyoko
出典(和文)	学位:博士(理学), 学位授与機関:東京工業大学, 報告番号:甲第3247号, 授与年月日:1996年3月26日, 学位の種別:課程博士, 審査員:
Citation(English)	Degree:Doctor (Science), Conferring organization: Tokyo Institute of Technology, Report number:甲第3247号, Conferred date:1996/3/26, Degree Type:Course doctor, Examiner:
学位種別(和文)	博士論文
Type(English)	Doctoral Thesis

Study of Electrical Double Layer Structure at Solid-Liquid Interfaces by Atomic Force Microscopy

1996

Tokyo Institute of Technology

Toyoko Arai Tomitori

Table of Contents

Chapter 1

General Introduction

1-1. Historical Introduction of Electrical Double Layers

Electrical double layers, which are formed at the interfaces between metal electrodes and aqueous electrolyte solutions, have been investigated for more than a century. About one hundred and fifty years ago, Helmholtz [1] discovered that the interface exhibits the properties of an electric capacitor in the solution. To account for this phenomenon, Helmholtz proposed a model of the interface: all the excess charges on the metal are located at the surface, and a rigidly held layer consisting of oppositely charged ions is formed to be a plane parallel and close to the surface of the electrode in the solution. This is the so-called Helmholtz model of a parallel-plate-capacitor for the electrical double layer. Figure 1-1(a) and (b) schematically show the Helmholtz model and the potential across the interface, respectively. This model takes no account of the dependence of the measured capacitance on the potential or the solution concentration, although the change in the values of capacitance in different electrolytes could be attributed to the variation of the layer thickness d including the adsorbed ion radius.

A different model, which predicts a dependence of the measured capacitance on both the potential and the electrolyte concentration, was proposed by Gouy [2] and Chapman [3] independently. An electric field at the interface is induced by an excess charge on a metal surface. A positive charge, for example, on the electrode attracts the negative ions and repels the positive

ions in the solution. Figure1-2(a) and (b) schematically show the Gouy-Chapman model and the corresponding potential across the interface, respectively. The fundamental equations, which describe the diffuse double layer, are the Boltzmann distribution equation and the Poisson's equation. The Gouy-Chapman model improved the Helmholtz model essentially, since a dependence of the differential capacitance on both the potential and the concentration can be predicted by it. However, wide discrepancies were found between the theoretical predictions and the experimental results.

The next model describing the physical situation of the double layer at the interface was suggested by Stern [4]: it was a combination of the two previous models with a more realistic way. The schematic diagram and the corresponding potential across the interface of the Stern model are shown in Fig.1-3(a) and (b), respectively. In the Stern model, two capacitors, C_H from the Helmholtz layer and C_D from the diffuse layer determine the total differential capacitance of the interface. Since the two regions are linked in space, the two capacitors act in series. Thus the total capacitance C is given by

$$\frac{1}{C} = \frac{1}{C_H} + \frac{1}{C_D} \qquad (1.1.1)$$

Stern also recognized the effect of specific interactions and suggested a distinction between the ions adsorbed on the electrode and the ions which merely approached to it at the closest distance. This picture was adopted by Grahame [5] to develop a model of the interface, which consists of three regions, although it was still commonly referred to as the double layer. The first region extends from the electrode surface to a plane passing through the centers of the specifically adsorbed ions: this is the inner Helmholtz plane

(IHP) and its potential is denoted by Ψ_1. The boundary to the next region is the outer Helmholtz plane (OHP), which passes through the centers of the hydrated ions at the closest distance on the approach to the electrode. The potential is denoted by Ψ_2. Beyond the OHP lies the diffuse double layer. The Grahame model is schematically shown in Fig.1-4.

The model of the double layer proposed by Devanathan, Bockris, and Müller [6], which explicitly takes into account the predominant existence of the solvent at the interface, is shown in Fig.1-5 for water as the solvent. The electrode surface is mostly covered with a layer of oriented water molecules. On some sites, the water molecules are replaced by specific adsorbed ions, usually anions.

To understand the structures of electrical double layer, the detailed analysis was carried out for the surface excess and the surface charge density by measuring the electric capacitance, the surface tension and so on. The surface tension and the electric capacitance can be measured directly by the methods proposed by Grahame [7], Parsons [8,9], Delahay [10] and others. They investigated the structures of the electrical double layer on Hg surfaces in aqueous solutions.

1-2. Interaction between Surfaces in Aqueous Solution

About fifty years ago, Derjaguin, Landau, Verwey and Overbeek developed a quantitative theory, which is called the DLVO theory [11,12], to describe the stability between identically charged colloidal particles in an aqueous solution. According to the theory, the interaction between identically charged colloidal particles can be separated into two contributions: an attractive van der Waals interaction and a repulsive electrostatic force. The

total interaction is taken as a sum of these two terms. The physical dimensions of the surfaces allow the use of the Derjaguin approximation to relate the force (F) between the sphere with a radius (R) and the flat plate in terms of the interaction free energy per unit area between two parallel plates made of the same material. In the Derjaguin approximation [13] the force F between the sphere and the plate has the form

$$F/R = 2\pi (V_A + V_R) \qquad (1.2.1)$$

where V_A is the attractive van der Waals interaction free energy per unit area and V_R is the electrical double layer interaction free energy per unit area between two flat plates made of the same material.

At present, the theory has been proved to hold for the interaction between dissimilar surfaces [14-16]. In general, the van der Waals contribution is attractive for dissimilar metal oxide surfaces interacting across water. However, if the interacting surfaces have dissimilar charges, the electrical double layer contribution can be either attractive or repulsive.

On the other hand, experimental direct measurement techniques of surface forces have been investigated since the measurement performed by Derjaguin in 1954 [17]. The Surface Force Apparatus (SFA), with which the surface forces can be measured at angstrom resolution, was developed by Israelachvili and coworkers [18,19]. The SFA, schematically shown in Fig. 1-6, has identified and quantified the fundamental interactions occurring between mica surfaces in controlled vapors or immersed in liquids. The molecular-smooth mica sheets are glued onto curved silica discs, which is locally equivalent to a sphere near a flat surface. The interaction forces are measured using a force-measuring spring, on which one of the silica disks is, and the

force sensitivity is about 10^{-8} N. The separation between the two surfaces from microns down to molecular contact is measured by use of an optical technique using multiple beam interference fringes called the Fringes of Equal Chromatic Order (FECO). The separation resolution is about 0.1 nm. The SFA is a powerful tool to investigate the fundamental interactions occurring between surfaces in aqueous solutions. These include the attractive van der Waals force [20], the repulsive electrostatic double layer forces [21], oscillatory (solvation or structural) forces [22], repulsive hydration forces [23], and attractive hydrophobic forces [24].

The interaction forces measured by the SFA are the average between macro surfaces, even though the surfaces are not uniform. The SFA has an angstrom-order sensitivity of separation, but can not resolve the interaction laterally. In general, the real surfaces are usually not uniform and have lateral distributions, chemically and electrically. The analysis of the interaction between inhomogeneous surfaces requires the other techniques.

1-3. Application of Scanning Probe Microscopy for the Force Measurements

Since the invention of scanning tunneling microscopy (STM) by G. Binnig and H. Rohrer in 1981, STM has revealed surface topography and electronic structures on atomic scale [25]. The STM is a representative of a family of scanning probe microscopy (SPM), which can depict the topography by scanning an atomically sharpened needle (tip) over the sample surface. During the scanning the separation between the tip and the sample surface is kept constant by monitoring and referring some interaction between the tip apex and the sample surface. For STM, the interaction means "tunneling

current" of the electrons passing through the vacuum barrier between the tip and the sample by the quantum effect. Thus the scanning of the tip can be performed without touching to the sample surface. The tip on scanning is 3-dimensionally positioned mechanically by piezo ceramics driven by changing applied voltages. At present, one can see "the atoms" on the surfaces of semiconductors, metals and other conductive materials by the STM. However, the surfaces of electrically insulating materials can not be depicted by the STM, where the tunneling electrons are trapped so that the current flow is interrupted.

When five years had passed after the STM was invented, G.Binnig invented another new SPM, atomic force microscopy (AFM) [26]. It utilizes "force" exerting between the tip apex and the sample surface, measured by a micro cantilever with a sharpened tip. The cantilever bends proportionally to the force. Then, if the cantilever deflection can be measured precisely, the force can be estimated from the bending, and the surface topography is depicted by maintaining a constant force while scanning the tip over the sample surface. The first AFM used an STM to measure the deflection of the cantilever on nanoscale, schematically shown in Fig.1-7(a). The other fine mechanism was also similar to that in the STM. After the invention of AFM, the stability and the resolution have been rapidly improved: the detection system of the cantilever deflection was devised; (1) utilizing an interferometer consisting of an exit of an optical fiber leading a laser beam and a mirrored backface of the cantilever, in Fig.1-7(b) [27]; (2) utilizing a position detector of a sectored photodetector, which detects the incident position of the laser beam reflected from the cantilever backface, in Fig.1-7(c) [28]; (3) measuring a capacitance of the gap between a small metal plate and the cantilever

backface, in Fig.1-7(d) [29].

The AFM has two operation modes of the tip-sample contact and non-contact: (1) in the contact mode, the tip slightly touches the sample surface on scanning; (2) in the non-contact mode, the tip position is slightly retracted and modulated vertically to the sample without touching the sample, and the change in the resonance frequency is detected, which is sensitive to the force change. In the early days of the AFM invention, the contact mode was popular exhibiting higher resolution easily, although the non-contact mode gave less damage to the samples, the feature of which suits to soft materials such as biomaterials. At present, since the Q value of the cantilever was improved, the non-contact mode also exhibits an atomic resolution as high as that in STM [30].

The spatial resolution of the AFM is determined by the tip radius. The cantilever with a tip is microfabricated from silicon or silicon nitride and has a spring constant of 0.02-0.7 N/m for the contact mode. To improve the spatial resolution, a pyramidal tip and a sharpened tip apex are usually formed at the end of the cantilever with a radius of 50 nm and 10-30 nm, respectively. By contriving new integrated tips, many groups uncovered various phenomena including surface topography and the lateral distribution of forces due to chemical [31-33], electrical [34-36], and magnetic interactions [37]. The friction force on scanning between the tip and the sample surface was also detected simultaneously with the AFM operation with a 4-sectored photodetector, in Fig.1-7(c) and in Fig.1-8, which detects the torsion of the cantilever caused by the friction. This method is called friction force microscopy (FFM) [38,39]. Furthermore, the AFM can be operated in air, liquid and vacuum [40-42]. Thus, the AFM is a promising method to

investigate interactions between a tip and a sample in liquid on nanoscale and reveal the electrical double layers.

On the other hand, one of the force measurement tools, the SFA, can measure the force and analyze the structure of the double layer with a high vertical resolution to the surface [43-45], although the measure is smeared laterally over the wide area. Since the theoretical analyses usually assume that the surfaces are homogeneous and charged uniformly, the theory can predict the experimental results macroscopically over the whole surfaces on the average. However, the charge distribution on the real surfaces is not uniform. For example, since both anionic and cationic groups exist on the amphoteric surface of a protein, even at an isoelectric point (IEP), at which potential the total charge is zero, the charge density is not zero locally on the surface. Thus local probing methods with a high lateral resolution as AFM are required to map the inhomogeneous charges and to analyze the double layer laterally.

1-4. Contents in this Thesis

In Chapter 2 of this thesis, the author shows a mathematical treatment of the force-distance analysis, which is assumed that the force consists of the van der Waals force and the electrical double layer force according to the DLVO theory without the low potential approximation. The effect of the AFM tip shape, the surface potential, and the ion concentration on the theoretical interaction force is described.

In Chapter 3, the force-distance curves measured with AFM in an electrolyte solution are compared to the theoretical curves calculated in chapter 2. The good agreement between measured and calculated force is shown. The force-distance curves between a Si_3N_4 tip and several oxides, such

as SiO_2, SnO_2, and Al_2O_3 are measured in aqueous electrolytes by using AFM. The IEP of these materials are evaluated.

In Chapter 4, the surface force analysis is applied to the modified quartz surfaces with hydrocarbon monolayer. The effects of the surface modification are described. The electrical double layer forces due to the concentration profile of the counterions at the oxide/water interface are discussed in terms of acid-base reactions of -OH groups on the oxide surface.

In Chapter 5, the electrical double layers on potential controlled gold electrodes are analyzed by force measurement with AFM. A Au-covered or a bare Si_3N_4 tip is used as a probe. The electrode and the tip potentials are controlled electrochemically by a potentiostat. The author discusses the specific adsorption of anions and the potential of the outer Helmholtz plane on gold electrode with the result of the force measurements.

In Chapter 6, the author suggests a novel method to measure a change in surface tension on a solid electrode with applied bias voltage, using AFM, which utilizes the laser beam deflection to measure the displacement of a microfabricated cantilever.

In Chapter 7, the author summarizes this thesis.

References

1. H.L.F.von Helmholtz, Pogg. Ann., **89** (1853) 211.
2. G.Gouy, Ann. de Phys., **7** (1917) 129.
3. D.L.Chapman, Phil. Mag., **25** (1913) 475.
4. O.Stern, Z. Elektrochem., **30** (1924) 508.
5. D.C.Grahame, Chem. Revs., **41** (1947) 441.
6. M.A.V.Devanathan, J.O'M.Bockris, and K.Müller, Proc. Roy. Soc. London, A **274** (1963) 55.
7. D.C.Grahame, Ann. Rev. Phys. Chem., **6** (1955) 337.
8. R.Parsons, Modern Aspects of Electrochemistry, vol. 1, O'M. Bockris, editor, Butterwoths, LOndon, (1954) pp.103-179.
9. R.Parsons, Chem. Rev., **90** (1990) 813.
10. P.Delahay, *Double Layer and Electrode Kinetics*, Interscience, New York, (1965).
11. B. V. Derjaguin and L. Landau, Physicochim., URSS **14**, 633 (1941).
12. E. J. W. Verwey and J. T. G. Overbeek, *Theory of the Stability of Lyophobic Colloids*, Elsevier, Amsterdam, (1948).
13. B. V. Derjaguin, Kolloid Zeits., **69** (1934) 155.
14. R. Hogg, T. W. Healy, and L. R. White, Trans. Faraday Soc., **62** (1966) 1638.
15. D. Y. C. Chan, T. W. Healy, and L. R. White, J. Chem. Soc., Faraday Trans 1, **72** (1976) 2845.
16. D. McCormack, S. L. Carnie, D. Y. C. Chan, J. Colloid Interface Sci., **169** (1995) 177.
17. B. V. Derjaguin and I. I. Abrikossova, Discuss. Faraday Soc., **18** (1954)

24.

18. J. N. Israelachvili and G. E. Adams, J. Chem. Soc. Faraday Trans. 1, **74** (1978) 975.
19. J. N. Israelachvili, Accounts Chem. Res., **20** (1987) 415.
20. J. N. Israelachvili and D. Tabor, Proc. R. Soc. Lond. A, **331** (1972) 19.
21. R. M. Pashley, J. Colloid Interface Sci., **80** (1981) 153.
22. J. N. Israelachvili and R. M. Pashley, Nature, **306** (1983) 249.
23. R. M. Pashley and J. N. Israelachvili, Colloids Surf., **2** (1981) 169.
24. J. N. Israelachvili and R. M. Pashley, Nature, **300** (1982) 341.
25. G.Binnig and H.Rohrer, Review of Modern Phys., **59** (1987) 615.
26. G. Binnig, C. F. Quate, and Ch. Gerber, Phys. Rev. Lett. **56** (1986) 930.
27. Y.Martin, C. C. Williams and H. K. Wickramsinghe, J. Appl. Phys., **61** (1987) 4723.
28. G.Meyer and N. M. Amer, Appl. Phys. Lett., **53** (1988) 1045.
29. G. Neubauer, S. R. Cohen, G. M. McClelland, D. Horne, and C. M. Mate, Rev. Sci. Instrum., **61** (1990) 2296.
30. F.Ohnesorge and G. Binnig, Science, **260** (1993) 1451.
31. G. U. Lee, D. A. Kidwell, and R. J. Colton, Langmuir **10** (1994) 354.
32. E.-L. Florin, V. T. Moy, and H. E. Gaub, Science **264** (1994) 415.
33. U. Dammer, D. Anselmetti, M. Dreier, M. Hegner, W. Huber, J. Hurst, G. Misevic, and H.-J. Güntherodt, *Force in Scanning Probe Methods*, H.-J. Güntherodt, D. Anselmetti, and E. Meyer Eds., Kluwer Academic Publishers (1995) p.625.
34. M. Nonnenmacher, M. O'Boyle, and H. K. Wickramsinghe, Appl. Phys. Lett. **58** (1991) 2921.
35. M. Fujihira and H. Kawate, Thin solid films, **242** (1994) 163.

36. H. Yokoyama and T. Inoue, Thin solid films, **242** (1994) 33.
37. D. Rugar, H. J. Mamin, P. Guethner, S. E. Lambert, J. E. Stern, I. R. McFadyen, and T. Yogi, J. Appl. Phys. **68** (1990) 1169.
38. C. M. Mate, G. M. McClelland, R. Erlandsson, and S. Chiang, Phys. Rev. Lett., **59** (1987) 1942.
39. G. Meyer and N. M. Amer, Appl. Phys. Lett., **57** (1990) 2089.
40. A. L. Weisenhorn, J. F. Macdougall, S. A. C. Gould, S. D. Cox, W. S. Wise, J. Massie, P. Maivald, V. B. Elings, G. D. Stucky, and P. K. Hansma, Science **247** (1990) 1330.
41. F. Schabert and A. Engel, Force in Scanning Probe Methods, H.-J. Güntherodt, D. Anselmetti, and E. Meyer Eds., Kluwer Academic Publishers (1995) p.607.
42. T. J. Senden, C. J. Drummond, and P. Kekicheff, Langmuir **10** (1994) 358 .
43. J.N.Israelachvili and P.M.Macguiggan, J. Mater. Res., **5** (1989) 2223.
44. Y.H.Tsao, S.X.Yang and D.F.Evans, Langmuir, **8** (1992) 1188.
45. V.E.Shubin and P.Kekicheff, J. Colloid Interface Sci., **155** (1993) 108.

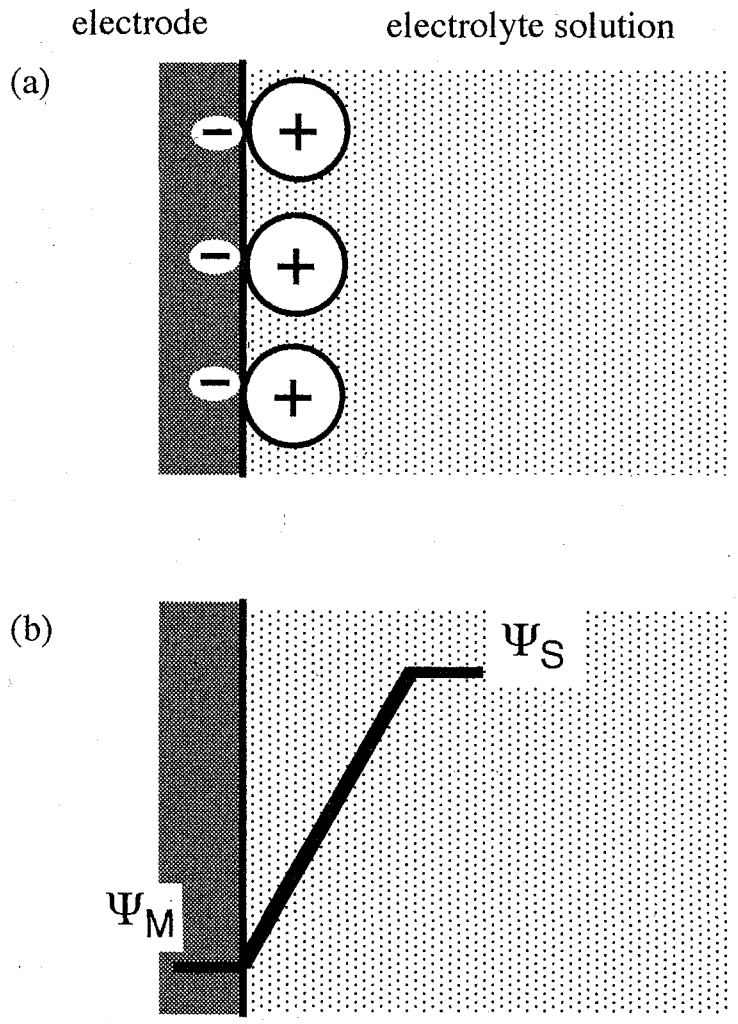

Figure 1-1. (a) Schematic of the Helmholtz model and (b) the corresponding potential across the interface.

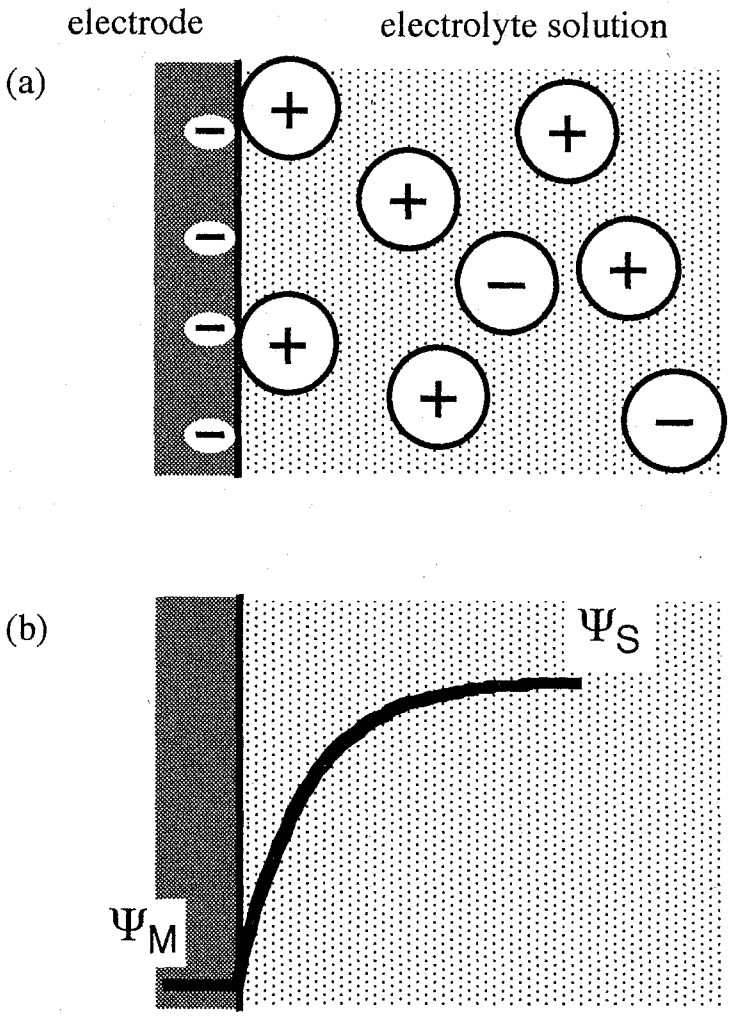

Figure 1-2. (a) Schematic of the Gouy-Chapman model and (b) the corresponding potential across the interface.

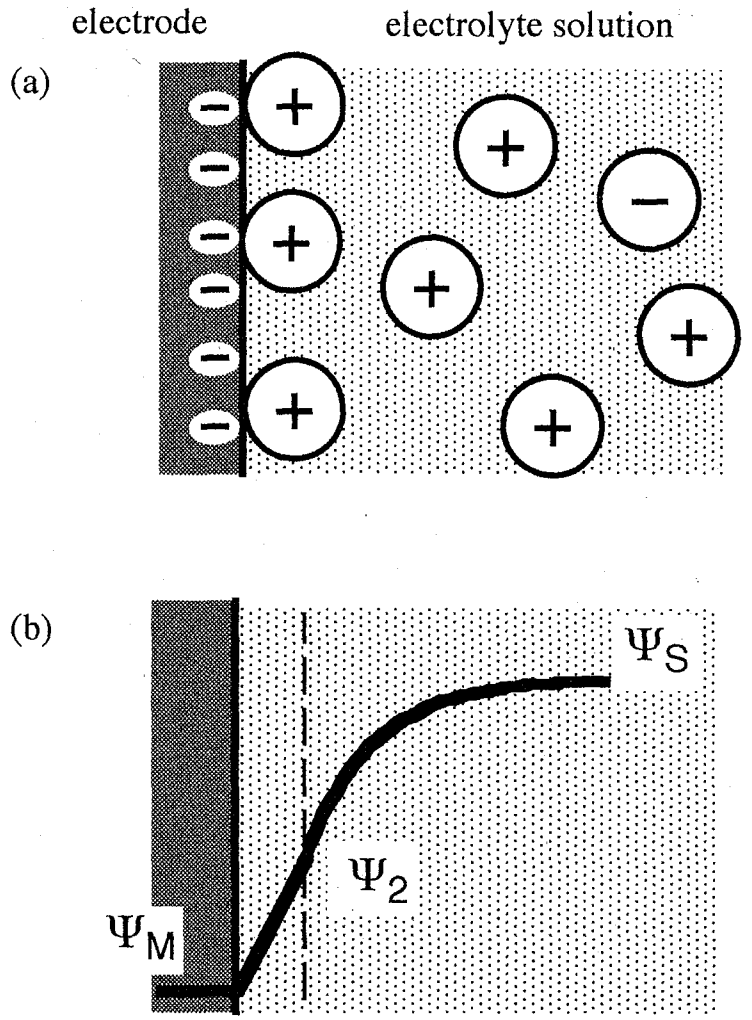

Figure 1-3. (a) Schematic of the Stern model and (b) the corresponding potential across the interface.

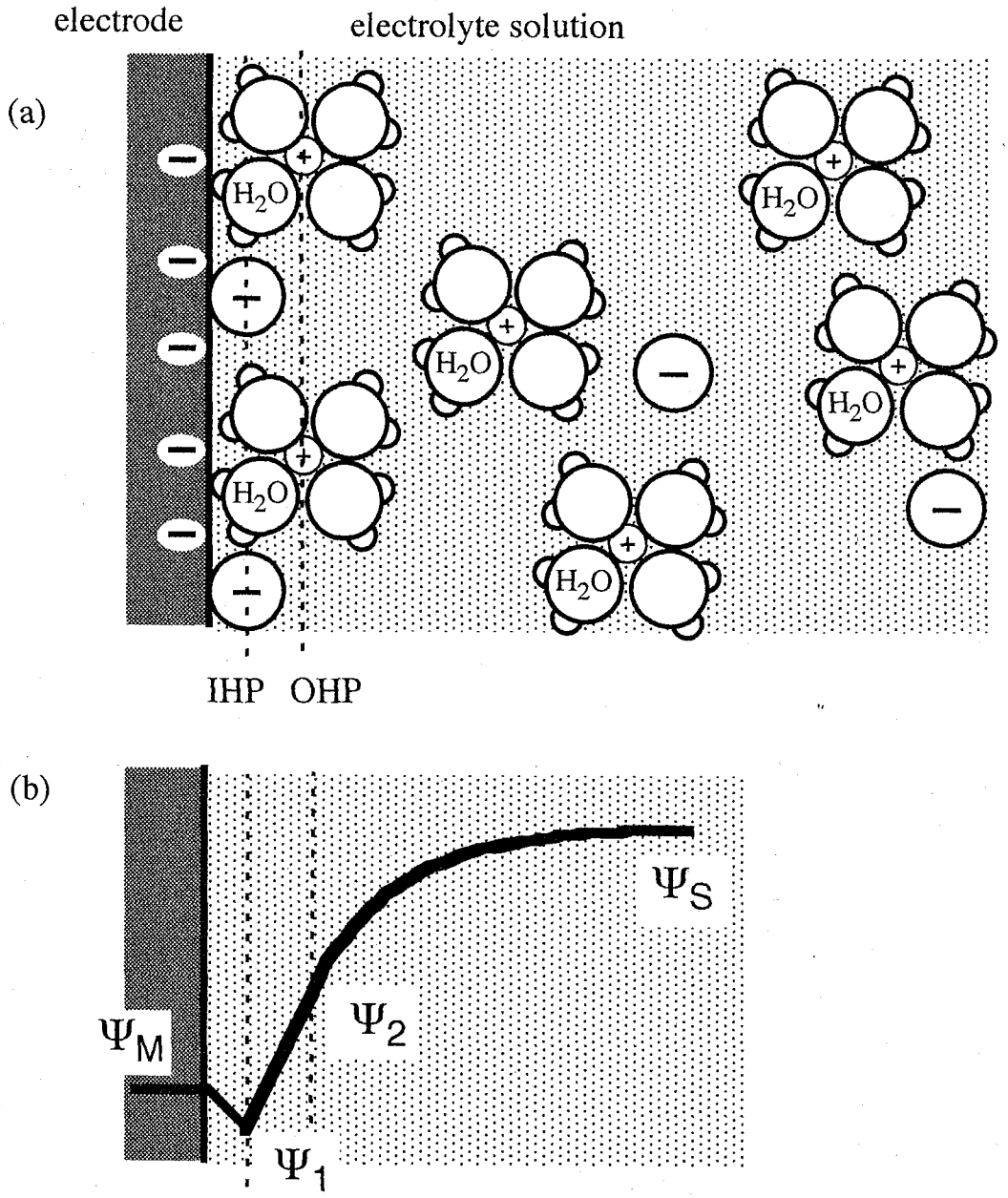

Figure 1-4. (a) Schematic of the Grahame model and (b) the corresponding potential across the interface.

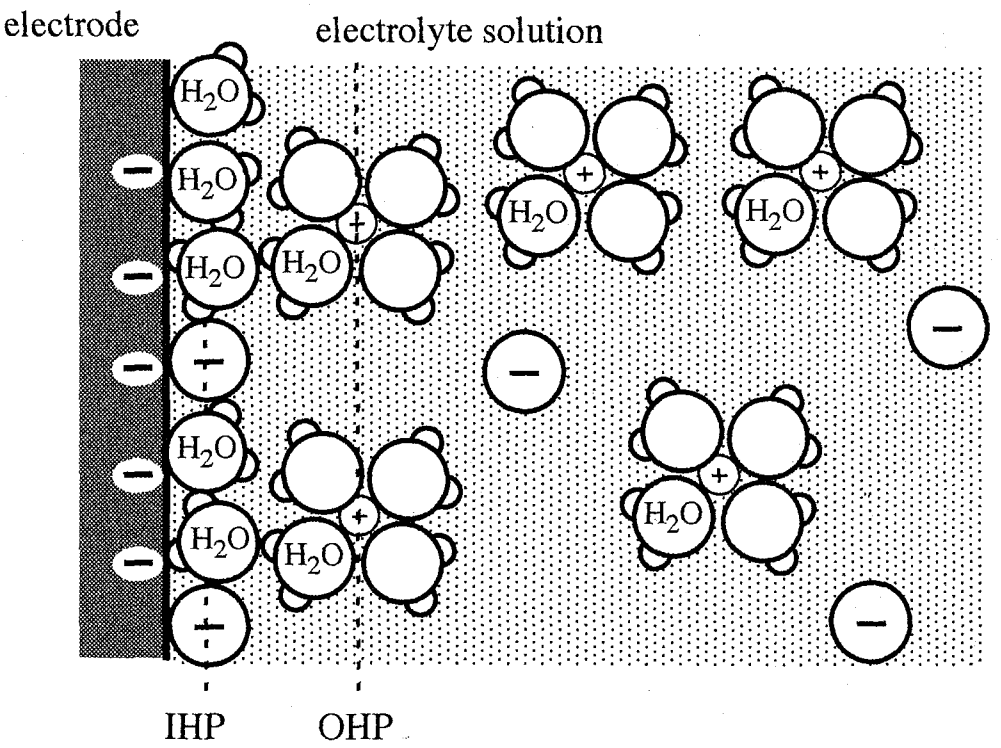

Figure 1-5. Schematic of the Devanathan, Bockris, and Müller model.

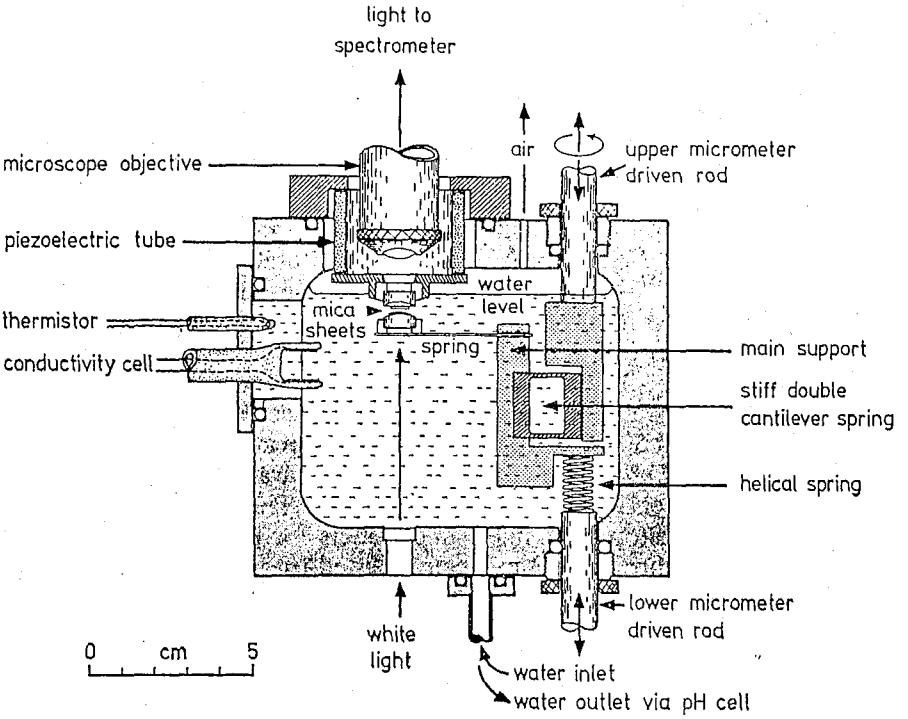

Figure 1-6. Schematic diagram of Surface Force Apparatus (SFA) [Ref. 18].

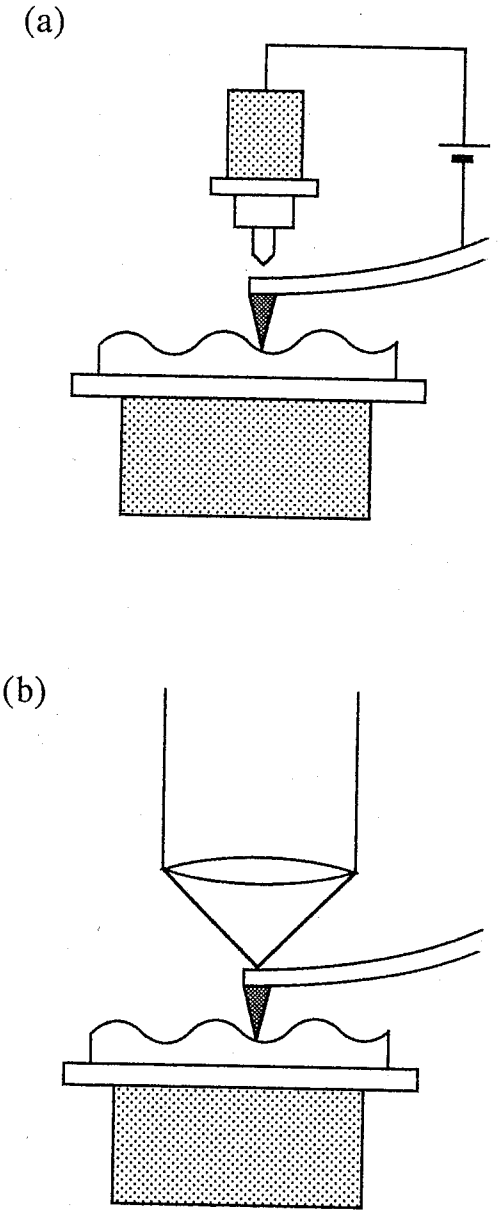

Figure 1-7. Schematic diagram of Atomic Force Microscopy (AFM) with a force detection system, which utilizes (a) tunneling current (STM), and (b) optical interferometry,

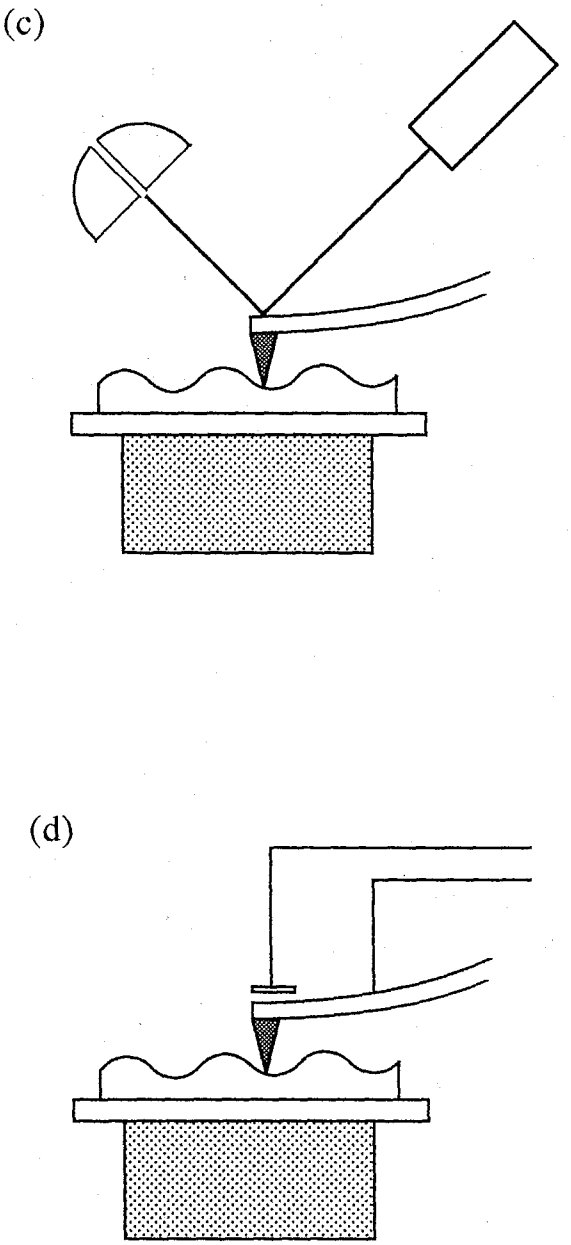

Figure 1-7. Continued.
(c) laser beam deflection, and (d) gap capacitance.

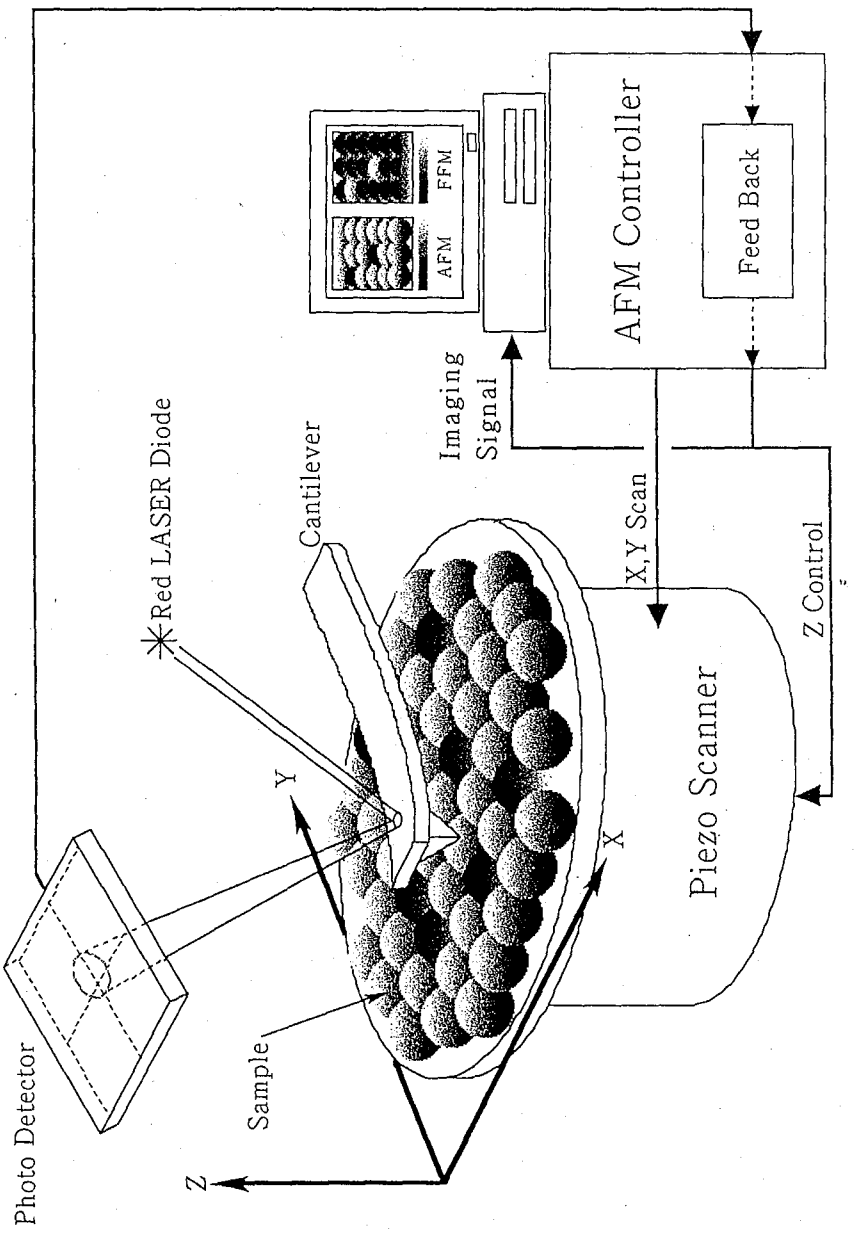

Figure 1-8. Schematic diagram of AFM and FFM.

Chapter 2

Theoretical Treatments for Force Measurements by AFM in Aqueous Solutions

2-1. Introduction

Since the invention of the AFM [1], the force exerting between a tip and a sample surface has been utilized to obtain the topography of the sample, and the AFM has successfully demonstrated to be a powerful tool to investigate sample surfaces on a nanometer scale. The AFM can afford not only topography of sample surfaces, but also the force-distance curve even in an electrolyte. The measured force-distance curves should be carefully compared with the theoretically calculated curves [2-4]. But the theory was based upon the simplified geometrical configuration of the tip and the sample surface. For example, the DLVO theory [5,6] can be applied to the force-distance curves measured only by a cantilever with a silica sphere (3.5 mm in radius) as a tip [2]. In AFM, it is advantageous to use a cantilever with a sharp tip to improve the resolution for sample surfaces with a local variation of morphology or charge distribution. Nowadays, cantilevers with a tip apex of 10-30 nm in radius are commercially available. The theoretical simplification does not apply to this sharp tip at a small separation between the tip and the sample surface. The interaction with the tip shank is not negligible.

This chapter reports a mathematical treatment of the force-distance analysis, which is assumed that the force consists of the van der Waals force and the force caused by the electrical double layers, and a tip has a spherical

apex and the circumscribing tapered shank. In the calculation of the electrical double layer force, the constant surface potentials at the tip and the sample and the Boltzmann distribution of the ion concentration are assumed. The effects of surface potential are also evaluated excluding the low potential approximation.

2-2. Application of the DLVO Theory for forces between Dissimilar Surfaces

To clarify the tip shape dependence of the measured force-distance curves, we calculated the force-distance relation based on the van der Waals force and the electrical double layer force in the AFM with a flat sample surface and a realistic tip, as shown in Fig.2-1. The tip has a spherical apex and the circumscribing tapered shank: R the radius of the apex sphere, 2θ the cone angle of the tapered shank, D the separation distance between the flat sample and the tip apex, and z the coordinate vertical to the sample surface being zero at the surface. This model is suitable for a small separation between the tip and the sample, where the interaction with the tip shank cannot be neglected.

2-2-1. Van der Waals force between a tip and a flat surface

The van der Waals potential energy, $-C/r^6$ (C is a constant and r is the interdistance), was volume-integrated over the whole sample and the realistic tip, treating the tip as an assembly of infinite thin disks and utilizing the formula of the van der Waals force between a semi-infinite plane and the infinitesimal volume [7]. Then we obtained the total energy,

$$W_{vdW,tip\text{-}flat}(D) = -\frac{A}{6\pi}\int_{D}^{D+L}\frac{S(z)}{z^3}\,dz \qquad (2.2.1)$$

Here A is the Hamaker constant [8], and S(z) is the cross sectional area of the infinite thin disk of the tip as follows,

$$S(z) = \pi\{2R - (z - D)\}(z - D) \quad \left(D \le z \le D+R(1-\sin\theta) \right), \text{ and}$$

$$S(z) = \pi \tan^2\theta \left\{z-D+R\left(1/\sin\theta - 1\right)\right\}^2 \quad \left(D+R(1-\sin\theta) \le z \le D+L \right) \qquad (2.2.2)$$

Thus, the total energy W(D) is expressed as follows:

$$W_{vdW,tip\text{-}flat}(D) = -\frac{A}{6}\left\{\int_D^{D+R(1-\sin\theta)} \frac{\{2R-(z-D)\}(z-D)}{z^3} + \tan^2\theta \int_{D+R(1-\sin\theta)}^{D+L} \frac{\left\{z-D+R\left(1/\sin\theta-1\right)\right\}^2}{z^3}\right\}$$

$$= \frac{3D+2R}{2D} - \frac{2(D+R)}{D+R\left(1-\sin\theta\right)} + \frac{D^2+2DR}{2\left\{D+R\left(1-\sin\theta\right)\right\}^2} + \ln\frac{D}{\left\{D+R\left(1-\sin\theta\right)\right\}}$$

$$+ \tan^2\theta \left[-\frac{2\left\{D-R\left(1/\sin\theta-1\right)\right\}}{D+R\left(1-\sin\theta\right)} + \frac{\left\{D-R\left(1/\sin\theta-1\right)\right\}^2}{2\left\{D+R\left(1-\sin\theta\right)\right\}^2} + \frac{2\left\{D-R\left(1/\sin\theta-1\right)\right\}}{D+L}\right.$$

$$\left. - \frac{\left\{D-R\left(1/\sin\theta-1\right)\right\}^2}{2\,(D+L)^2} + \ln\frac{D+L}{\left\{D+R\left(1-\sin\theta\right)\right\}}\right] \qquad (2.2.3)$$

Here L is the length from the apex to the root of the tip.

The force $F_{vdW,tip\text{-}flat}(D)$ between the tip and the sample is derived by differentiating the total energy $W_{vdW,tip\text{-}flat}(D)$ with the separation D on the assumption of L»,R,D,

$$F_{vdW,tip\text{-}flat}(D) = -\frac{dW}{dD}$$

$$= -\frac{A}{6}\left\{-\frac{1}{D}+\frac{R}{D^2}+\frac{1+\tan^2\theta}{D+R(1-\sin\theta)}\right\} \qquad (2.2.4)$$

2-2-2. Electrical double layer force

For calculation of the electrical double layer force, the pressure P related with the electrostatic potential Ψ is derived from the Helmholtz free energy for an electrolyte [7],

$$P = -\frac{1}{2}\varepsilon_r\varepsilon_0\left(\frac{d\Psi}{dz}\right)_z^2 + kT\left(\sum_i \rho_{zi} - \sum_i \rho_{\infty i}\right) \qquad (2.2.5)$$

where ε_r and ε_0 are the relative and the vacuum dielectric constant, respectively, and k the Boltzmann constant, T the temperature, ρ_{zi} the number density of the specific ions denoted by i at a position of z. Thus the electrostatic potential Ψ should be calculated to estimate the electrical double layer force per unit area, i.e. the pressure P.

According to the Gouy-Chapman theory, when there is one surface of an isolated matter in an electrolyte, the electrostatic potential Ψ at a position of z far from the surface is described as follows [9],

$$\sum_i \rho_{zi} = \sum_i \rho_{\infty i} + \frac{\varepsilon_r\varepsilon_0}{2kT}\left(\frac{d\Psi}{dz}\right)_z^2 \qquad (2.2.6)$$

For a 1:1 electrolyte on the assumption that the ionic density r is distributed according to the Boltzmann statistics, Eq.(2.2.6) gives

$$\frac{d\Psi}{dz} = \sqrt{\frac{8kT\rho_\infty}{\varepsilon_r\varepsilon_0}}\sinh\left(\frac{e\Psi_z}{2kT}\right) \qquad (2.2.7)$$

Integrating the above equation, we obtain

$$\Psi_z = \frac{4kT}{e} \operatorname{arctanh}\left(\gamma e^{-\kappa z}\right) \qquad (2.2.8)$$

where

$$\gamma = \tanh\left(\frac{e\Psi_0}{4kT}\right) \qquad (2.2.9)$$

and

$$\kappa = \left(\frac{e^2 \sum_i \rho_{\infty i}}{\varepsilon_r \varepsilon_0 kT}\right)^{1/2} \qquad (2.2.10)$$

Here $1/\kappa$ is the Debye length, and Ψ_0 is a surface potential.

When there are two surfaces independently charged, which is the case for electrochemical AFM, we assumed that the potential Ψ_z at point z between two surfaces is given simply by the sum of the potentials tailed from each surface as follows,

$$\Psi_z = \frac{4kT}{e} \left\{\operatorname{arctanh}\left(\gamma_1 e^{-\kappa z}\right) + \operatorname{arctanh}\left(\gamma_2 e^{-\kappa(D-z)}\right)\right\} \qquad (2.2.11)$$

where

$$\gamma_1 = \tanh\left(\frac{e\Psi_{0,1}}{4kT}\right), \quad \text{and} \quad \gamma_2 = \tanh\left(\frac{e\Psi_{0,2}}{4kT}\right) \qquad (2.2.12)$$

Here D is the distance between the two surfaces, and $\Psi_{0,1}$ and $\Psi_{0,2}$ are surface potentials, where the subscription indexes 1 and 2 correspond to one surface located at z=0 and the other surface at z=D, respectively.

A. Two flat surfaces with the same signed charges

If two faced surfaces are charged at the same polarity, the position z=m exists, at which $d\Psi/dz=0$ is satisfied, as shown in Fig.2-2.

Differentiating Eq.(2.2.11) we obtain

$$\frac{d\Psi}{dz} = \frac{4kT}{e}\left\{ \frac{-\kappa\gamma_1 e^{-\kappa z}}{1-\left(\gamma_1 e^{-\kappa z}\right)^2} + \frac{\kappa\gamma_2 e^{-\kappa(D-z)}}{1-\left(\gamma_2 e^{-\kappa(D-z)}\right)^2} \right\} \qquad (2.2.13)$$

At the point z=m, $(d\Psi/dz)_{z=m} = 0$, hence

$$e^{-\kappa m} = \sqrt{\frac{\gamma_2}{\gamma_1} e^{-\kappa D}} \qquad (2.2.14)$$

Then substituting Eq.(2.2.14) into Eq.(2.2.11),

$$\Psi_m = \frac{8kT}{e} \operatorname{arctanh}\left(\sqrt{\frac{\gamma_2}{\gamma_1} e^{-\kappa D}}\right) \qquad (2.2.15)$$

Using Eq.(2.2.5) the pressure at the point z=m is obtained as follows,

$$P = kT\left(\sum_i \rho_{mi} - \sum_i \rho_{\infty i}\right) \qquad (2.2.16)$$

For a 1:1 electrolyte this gives

$$P = kT\rho_\infty \left\{\left(e^{-e\Psi_m/kT}-1\right) + \left(e^{e\Psi_m/kT}-1\right)\right\}$$

$$= 4kT\rho_\infty \sinh^2\left(\frac{e\Psi_m}{2kT}\right) \qquad (2.2.17)$$

Incorporating Eq.(2.2.15) into this,

$$P = \frac{32\,\varepsilon_r\varepsilon_0\,(kT)^2}{e^2}\,\kappa^2\gamma_1\gamma_2 e^{-\kappa D}\,\frac{\left(1+\gamma_1\gamma_2 e^{-\kappa D}\right)^2}{\left(1-\gamma_1\gamma_2 e^{-\kappa D}\right)^4} \qquad (2.2.18)$$

The interaction free energy per unit area $W_{E1,flat\text{-}flat}(D)$, which causes the above pressure, is obtained by integrating P with respect to D,

$$W_{E1.flat\text{-}flat}(D) = \int_D^\infty P\,dD$$

$$= \frac{32\varepsilon_r\varepsilon_0\,(kT)^2}{3e^2}\,\kappa\gamma_1\gamma_2 e^{-\kappa D}\left\{\frac{1}{\left(1-\gamma_1\gamma_2 e^{-\kappa D}\right)} - \frac{2}{\left(1-\gamma_1\gamma_2 e^{-\kappa D}\right)^2} + \frac{4}{\left(1-\gamma_1\gamma_2 e^{-\kappa D}\right)^3}\right\} \qquad (2.2.19)$$

B. Two flat surfaces with the opposite signed charges

If two faced-surfaces are charged at the opposite polarity, the position z=m exists, at which $\Psi=0$ is satisfied, as shown in Fig.2-3.

At the point z=m, $\Psi_{z=m} = 0$, hence

$$\operatorname{arctanh}\left(\gamma_1 e^{-\kappa m}\right) + \operatorname{arctanh}\left(\gamma_2 e^{-\kappa(D-m)}\right) = 0$$

so that

$$e^{-\kappa m} = \sqrt{-\frac{\gamma_2}{\gamma_1}\,e^{-\kappa D}} \qquad (2.2.20)$$

Using Eq.(2.2.5) the pressure at the point z=m is obtained as follows,

$$P = -\frac{1}{2}\,\varepsilon_r\varepsilon_0\left(\frac{d\Psi}{dz}\right)^2_{z=m} \qquad (2.2.21)$$

Incorporating Eq.(2.2.13 and 20) into this,

$$P = \frac{32\,\varepsilon_r\varepsilon_0\,(kT)^2}{e^2}\,\frac{\kappa^2\gamma_1\gamma_2 e^{-\kappa D}}{\left(1+\gamma_1\gamma_2 e^{-\kappa D}\right)^2} \qquad (2.2.22)$$

The interaction free energy per unit area $W_{E2,flat\text{-}flat}(D)$, which causes the above pressure gives

$W_{E2.flat\text{-}flat}(D)$

$$= \frac{32\,\varepsilon_r\varepsilon_0\,(kT)^2}{3\,e^2}\,\kappa\,\gamma_1\gamma_2 e^{-\kappa D}\left\{\frac{1}{\left(1+\gamma_1\gamma_2 e^{-\kappa D}\right)} + \frac{1}{\left(1+\gamma_1\gamma_2 e^{-\kappa D}\right)^2} + \frac{1}{\left(1+\gamma_1\gamma_2 e^{-\kappa D}\right)^3}\right\} \qquad (2.2.23)$$

C. Electrical double layer force between a tip and a flat surface

The force $f_{flat\text{-}flat}(D)$ per unit area between the flat surfaces is derived from the differentiation of $W_{flat\text{-}flat}(D)$ with the separation D. Then the force $F_{tip\text{-}flat}(D)$ between the realistic tip and the flat surface is given by surface-integrating $f_{flat\text{-}flat}(D)$ over the tip surface regarding the tip as an assembly of thin cylindrical tubes, as follows,

$$F_{tip\text{-}flat}(D) = \int_D^{D+L} dS\, f_{flat\text{-}flat}(z)$$

$$= 2\pi \int_D^{D+R(1-\sin\theta)} (D+R-z)\, f_{flat\text{-}flat}(z)\, dz + 2\pi \tan^2\theta \int_{D+R(1-\sin\theta)}^{D+L} \left\{z-D+R\left(1/\sin\theta-1\right)\right\} f_{flat\text{-}flat}(z)\, dz$$

For L » R,D, this gives

$$F_{tip\text{-}flat}(D) = 2\pi\left\{RW_{flat\text{-}flat}(D) - \int_{D}^{D+R(1-\sin\theta)} W_{flat\text{-}flat}(z)dz + \tan^2\theta \int_{D+R(1-\sin\theta)}^{\infty} W_{flat\text{-}flat}(z)dz\right\} \quad (2.2.24)$$

Next, Eq.(2.2.19) and Eq.(2.2.23) are incorporated into Eq.(2.2.24). The former expresses the interaction free energy per unit area $W_{E1,flat\text{-}flat}(D)$ for two surfaces with the same signed charge and the latter for two surface with the opposite signed charged.

For the same signed charge:

$F_{E1,tip\text{-}flat}(D)$

$$= \frac{64\pi\varepsilon_r\varepsilon_0(kT)^2}{3e^2}\left[R\kappa\gamma_1\gamma_2 e^{-\kappa D}\frac{3+\left(\gamma_1\gamma_2 e^{-\kappa D}\right)^2}{\left(1-\gamma_1\gamma_2 e^{-\kappa D}\right)^3} - \frac{2\gamma_1\gamma_2 e^{-\kappa D}}{\left(1-\gamma_1\gamma_2 e^{-\kappa D}\right)^2} + \ln\left(1-\gamma_1\gamma_2 e^{-\kappa D}\right)\right.$$

$$\left. -\left(1-\tan^2\theta\right)\left\{\frac{-2\gamma_1\gamma_2 e^{-\kappa\left(D+R(1-\sin\theta)\right)}}{\left(1-\gamma_1\gamma_2 e^{-\kappa\left(D+R(1-\sin\theta)\right)}\right)^2} + \ln\left(1-\gamma_1\gamma_2 e^{-\kappa\left(D+R(1-\sin\theta)\right)}\right)\right\}\right] \quad (2.2.25)$$

For the opposite signed charge:

$F_{E2,tip\text{-}flat}(D)$

$$= \frac{64\pi\varepsilon_r\varepsilon_0(kT)^2}{3e^2}\left[R\kappa\gamma_1\gamma_2 e^{-\kappa D}\frac{3+3\gamma_1\gamma_2 e^{-\kappa D}+\left(\gamma_1\gamma_2 e^{-\kappa D}\right)^2}{\left(1+\gamma_1\gamma_2 e^{-\kappa D}\right)^3} + \frac{3+2\gamma_1\gamma_2 e^{-\kappa D}}{2\left(1+\gamma_1\gamma_2 e^{-\kappa D}\right)^2}\right.$$

$$\left. -\ln\left(1+\gamma_1\gamma_2 e^{-\kappa D}\right) + \frac{3}{2}\tan^2\theta\right]$$

$$-\left(1-\tan^2\theta\right)\left\{\frac{3+2\gamma_1\gamma_2 e^{-\kappa\left(D+R(1-\sin\theta)\right)}}{2\left(1+\gamma_1\gamma_2 e^{-\kappa\left(D+R(1-\sin\theta)\right)}\right)^2}-\ln\left(1+\gamma_1\gamma_2 e^{-\kappa\left(D+R(1-\sin\theta)\right)}\right)\right\}\Bigg] \tag{2.2.26}$$

2-3. Effects of AFM Tip Shape on Surface Forces

Here we simulate the tip-shape dependence of the van der Waals force and the electrical double layer force, taking typical values of the Hamaker constant, the Debye length and $\gamma_1\gamma_2$ for the above formulas. We take the Hamaker constant of $A = 2.1\times10^{-20}$ J, the temperature of 25 °C and a 1:1 electrolyte as an aqueous solution. The value of the Hamaker constant corresponds to that of Si_3N_4 and SiO_2 in water, which are usually used as materials for an AFM tip and a standard sample. The ionic concentrations are taken as 10^{-2}, 10^{-3} and 10^{-4} M, and then the Debye lengths $1/\kappa$ correspond to 3, 10, 30 nm, respectively. Assuming that the surfaces can be charged both positively and negatively, the values of 0.8, 0.2, 0.05, -0.05, -0.2 and -0.8 are taken for $\gamma_1\gamma_2$.

In order to compare the tip model mentioned above to the spherical tip model and the Derjaguin approximation, the equations for the spherical tip model and the Derjaguin approximation of the van der Waals force and the electrical double layer force are shown as follows:

for the van der Waals force,

$$F_{vdW,sph\text{-}flat}(D) = -\frac{A}{6}\left\{-\frac{1}{D}+\frac{R}{D^2}+\frac{1}{D+2R}+\frac{R}{(D+2R)^2}\right\} \tag{2.3.1}$$

$$\approx -\frac{AR}{6D^2} \tag{2.3.2}$$

for the electrical double layer force with the same-signed charged surfaces,

$F_{E1,sph\text{-}flat}(D)$

$$= \frac{64\pi \varepsilon_r \varepsilon_0 (kT)^2}{3e^2}\left[R\kappa\gamma_1\gamma_2 e^{-\kappa D}\frac{3+\left(\gamma_1\gamma_2 e^{-\kappa D}\right)^2}{\left(1-\gamma_1\gamma_2 e^{-\kappa D}\right)^3} - \frac{2\gamma_1\gamma_2 e^{-\kappa D}}{\left(1-\gamma_1\gamma_2 e^{-\kappa D}\right)^2}\right.$$

$$\left. + R\kappa\gamma_1\gamma_2 e^{-\kappa(D+2R)}\frac{3+\left(\gamma_1\gamma_2 e^{-\kappa(D+2R)}\right)^2}{\left(1-\gamma_1\gamma_2 e^{-\kappa(D+2R)}\right)^3} + \frac{2\gamma_1\gamma_2 e^{-\kappa(D+2R)}}{\left(1-\gamma_1\gamma_2 e^{-\kappa(D+2R)}\right)^2} - \ln\frac{1-\gamma_1\gamma_2 e^{-\kappa(D+2R)}}{1-\gamma_1\gamma_2 e^{-\kappa D}}\right.$$

(2.3.3)

$$\approx \frac{64\pi \varepsilon_r \varepsilon_0 (kT)^2 R\kappa\gamma_1\gamma_2 e^{-\kappa D}}{3e^2}\frac{\left\{3+\left(\gamma_1\gamma_2 e^{-\kappa D}\right)^2\right\}}{\left(1-\gamma_1\gamma_2 e^{-\kappa D}\right)^3} \qquad (2.3.4)$$

for the electrical double layer force with the opposite-signed charged surfaces,

$F_{E2,sph\text{-}flat}(D)$

$$= \frac{64\pi \varepsilon_r \varepsilon_0 (kT)^2}{3e^2}\left[R\kappa\gamma_1\gamma_2 e^{-\kappa D}\frac{3+3\gamma_1\gamma_2 e^{-\kappa D}+\left(\gamma_1\gamma_2 e^{-\kappa D}\right)^2}{\left(1+\gamma_1\gamma_2 e^{-\kappa D}\right)^3} + \frac{3+2\gamma_1\gamma_2 e^{-\kappa D}}{2\left(1+\gamma_1\gamma_2 e^{-\kappa D}\right)^2}\right.$$

$$\left. + R\kappa\gamma_1\gamma_2 e^{-\kappa(D+2R)}\frac{3+3\gamma_1\gamma_2 e^{-\kappa(D+2R)}+\left(\gamma_1\gamma_2 e^{-\kappa(D+2R)}\right)^2}{\left(1+\gamma_1\gamma_2 e^{-\kappa(D+2R)}\right)^3} - \frac{3+2\gamma_1\gamma_2 e^{-\kappa(D+2R)}}{2\left(1+\gamma_1\gamma_2 e^{-\kappa(D+2R)}\right)^2}\right.$$

$$\left. + \ln\frac{1+\gamma_1\gamma_2 e^{-\kappa(D+2R)}}{1+\gamma_1\gamma_2 e^{-\kappa D}}\right] \qquad (2.3.5)$$

$$\approx \frac{64\pi\varepsilon_r\varepsilon_0 (kT)^2 R\kappa\gamma_1\gamma_2 e^{-\kappa D}}{3e^2} \frac{\left\{3+3\gamma_1\gamma_2 e^{-\kappa D}+\left(\gamma_1\gamma_2 e^{-\kappa D}\right)^2\right\}}{\left(1+\gamma_1\gamma_2 e^{-\kappa D}\right)^3} \qquad (2.3.6)$$

Figure 2-4 (a) shows the van der Waals force-distance curves for a tip with an apex of 10 nm in radius and a sphere of 10 nm in radius, including the curve using the Derjaguin approximation for a sphere. The positive and the negative forces correspond to the repulsive and attractive force, respectively. The curve for the tip with a small 2θ is close to that for a sphere. As 2θ of the tip increases, the attractive force increases and the curve becomes different from that for a sphere. The Derjaguin approximation holds for $R \gg D$, and thus, for $R = 10$ nm and $0 < D < 50$ nm, the approximation can not be applicable and gives quite different values from those calculated without the approximation.

Figure 2-4 (b) shows the calculated van der Waals force for the tips with $R = 10$, 100, 1000 nm and $2\theta = 30$, 90° and for the spherical model. When 2θ is small ($2\theta < 30°$) for any R, the curves of the tip model are close to the one for the spherical model. When R is less than 10 nm, the curves for various 2θ are splitting each other, and show the 2θ dependence definitely. The 2θ dependence diminishes for large R's and the curves almost agree with that for the spherical tip model. The curve calculated with the Derjaguin approximation, which is not shown in Fig. 2-4 (b), also agrees with that in the range of R as large as the curves for the tip model and the spherical tip model agree each other.

Figure 2-5 (a) and (b) show the electrical double layer force-distance curves with $\gamma_1\gamma_2 = 0.2$ and -0.2, respectively, which are calculated for the tip

model, the spherical model and the Derjaguin approximation with parameters of R = 10, 100, 1000 nm, and 2θ = 30, 90° and $1/\kappa$ = 10 nm. The positive sign of $\gamma_1\gamma_2$ means that both surfaces are charged at the same sign, and the exerting force is repulsive. The negative sign of $\gamma_1\gamma_2$ means that both surfaces are charged at the opposite sign, and the force is attractive. For R < 10 nm, the curves are split with various 2θ values. For R > 100 nm, there is less 2θ dependence. The curve for the Derjaguin approximation does not agree with those for the tip model and the spherical model, which are close each other. On the other hand, for R > 1000 nm, the curves for these models and the approximation agree quite well each other.

Based on the above results, the resultant force of the van der Waals force and the electrical double layer force is evaluated, which is so-called the DLVO force. Figure 2-6 (a)-(c) show the force-distance curves under the condition of $1/\kappa$=10 nm and $\gamma_1\gamma_2$ = 0.05, 0.2 and 0.8. The DLVO force is normalized with the geometric parameter R. The force increases with large $\gamma_1\gamma_2$, which corresponds to a large product of the surface potential $\Psi_{0,1}$ and $\Psi_{0,2}$ as in eq.(2.2.12). For R=10 nm and any surface potential ($\gamma_1\gamma_2$), the 2θ dependence exists so that the curves are split increasing with 2θ. The force normalized with R for the spherical model is the smallest. On the other hand, for R > 100 nm, all of the normalized curves is overlapping each other, denoted by white marked lines as shown in Fig. 2-6 (a)-(c). With the Derjaguin approximation generally used, all of the normalized curves are brought in the same curve, and it exhibits the proportionality of the force to the geometric parameter R. But, for small R, the force is not proportional to R as the split normalized curves are shown here, and the validity of the approximation is broken.

For $\gamma_1\gamma_2$ = 0.8 in Fig.2-6 (c), assuming the same potential for the tip and

the sample surfaces, the value of Ψ_0 is about 150 mV. When the distance D between the tip and the sample becomes smaller than twice the Debye length and the double layers of both surfaces are about to be overlapped, the high surface potential gives a strong repulsive force caused by the electric static potential. The characteristics are consistent with those of the curves measured with the AFM [10]. However, if the following approximation [7] generally used for the potential is applied,

$$\Psi_z = \frac{4kT}{e}\operatorname{arctanh}\left(\gamma e^{-\kappa z}\right) \approx \frac{4kT}{e}\gamma e^{-\kappa z} \qquad (2.3.7)$$

the calculated curves don't agree with the measured curves. If the above approximation is employed, the calculated double layer forces for a tip-flat sample and a sphere-flat sample configuration are evaluated as follows:
for a tip-flat sample,

$$F_{\text{tip-flat}}(D) = \frac{64\pi\varepsilon_r\varepsilon_0(kT)^2}{e^2}\gamma_1\gamma_2 e^{-\kappa D}\left\{\kappa R + \left(1+\tan^2\theta\right)e^{-\kappa R(1-\sin\theta)} - 1\right\} \qquad (2.3.8)$$

for a sphere-flat sample,

$$F_{\text{sphere-flat}}(D) = \frac{64\pi\varepsilon_r\varepsilon_0(kT)^2}{e^2}\gamma_1\gamma_2 e^{-\kappa D}\left\{\kappa R + \left(\kappa R+1\right)e^{-2\kappa R} - 1\right\} \qquad (2.3.9)$$

$$\approx \frac{64\pi\varepsilon_r\varepsilon_0(kT)^2\kappa R\gamma_1\gamma_2 e^{-\kappa D}}{e^2} \qquad (2.3.10)$$

These equations are consistent with those calculated in this study for $\gamma_1\gamma_2 < 0.2$. But the deviation of these approximated equations become large with $\gamma_1\gamma_2$

larger than the value.

Here we make mention of other assumptions used in this study to be considered particularly in the proximity. We neglect the effects of the so-called Stern layer, where some basis are stickily adsorbed, and the charge regulation in a small gap separation, where the dissociation constants of ions may change caused by increasing the pressure. In this study, we assumed that the ions near each surface with potential Ψ_0 distribute accordingly to the Boltzmann distribution, and then the total ion distribution in the gap between two surfaces is given by the sum of the ion distributions from each surface, which is isolated from the other surface. In the AFM setup, the tip is very small and sharp, and thus the charge regulation effects are possibly negligible due to a small pressure effect [11].

Figure 2-7 shows the DLVO force normalized with R for surfaces charged at the opposite sign. The vertical axis is inverted and coordinated logarithmically. The electric attractive force increases as the absolute value of $\gamma_1\gamma_2$ increases. For R = 10 nm, as well as for the same-signed charge, the force curves depend on 2θ, and the curves are split more by increasing 2θ. The other characteristics depending on the tip geometry are also similar to those for the opposite sign charge, excepting that the van der Waals force exerts additionally and the resultant force becomes large at small separation D. Approaching the tip closer to the sample, the double layers of the tip and the sample start overlapping. The force for $\gamma_1\gamma_2 > 0$ is stronger than that for $\gamma_1\gamma_2 < 0$ in the vicinity to the sample, as shown in Fig.2-8. For $\gamma_1\gamma_2 < 0$ with the opposite signed charge, the electric charges in the overlapped layer, trend to cancel and then show no abrupt increase in the force. However, for $\gamma_1\gamma_2 > 0$ with the same signed charge, the neutralization doesn't occur, and an increase

in the ion charge concentration is caused in-between.

Figure 2-9 (a)-(c) show the $1/\kappa$-dependence of the double layer force with the same tip geometries and $\gamma_1\gamma_2 = 0.2$ in the 1:1 electrolyte solutions of 10^{-2} M and the Debye length of $1/\kappa = 3$ nm, 10^{-3} M and $1/\kappa = 10$ nm, and 10^{-4} M and $1/\kappa = 30$ nm, respectively. As $1/\kappa$ increases, corresponding to the decrease in the ion concentration, the 2θ dependence becomes large, and the splitting between the curves for the tip model and the spherical model increases. The curves for the tip model and the spherical model with $1/\kappa < 3$ nm are overlaps, which are not shown here, but the tendency is found in the data. This is attributed to a increase in κ in the factor of the first term in eqs. (2.2.25) and (2.2.26). The first term becomes dominant for large κ, corresponding to the regime of the Derjaguin approximation, and the other terms can be negligible. Consequently, in concentrated solutions, there is less dependence on the tip geometry, and the spherical approximation is applicable. Coupling the R-dependence pointed out in Figs.2-4 and 2-5, for $R\kappa > 10$, the force curves for any tip geometry are in agreement with that for the spherical model with an error less than 10%, and the Derjaguin approximation can be applied.

2-4. Conclusion

The force-distance curves were calculated assuming that the force comprises the van der Waals force and the electrical double layer force in an electrolyte in the AFM, considering account the tip geometry with a realistic shape. The calculation was undertaken on the assumption of the Boltzmann distribution of the ion near the surface and the total ion distribution given by the sum of that near the surfaces of the tip and the sample, which were electrically isolated each other. The approximation restricting the range of the

surface potential, which is generally used, was not adopted in this study. Therefore the derived formula holds for any surface potential. The force-distance curves were drawn for typical parameters of the electrolyte and the materials of the tip and the sample. Consequently, for $R\kappa > 10$, the spherical model is a good approximation independently of the tip shape, and the Derjaguin approximation can be applied. Conversely, for $R\kappa \ll 10$, since the parameter 2θ affects the force curves distinctly, the interaction force should be modeled by taking the tip geometry into account.

References

1. G.Binnig, C.F.Quate and Ch.Gerber, Phys. Rev. Lett., **56** (1986) 930.
2. W.A.Ducker, T.J.Senden and R.M.Pashley, Langmuir, **8** (1992) 1831.
3. J.L.Hutter and J.Bechhoefer, J. Appl. Phys., **73** (1993) 4123.
4. X.Y.Lin, F.Creuzet and G.Arribart, J. Phys. Chem., **97** (1993) 7272.
5. B.V.Derjaguin and L.Landau, Acta Physicochim., USSR **14** (1941) 633.
6. E.J.W.Verwey and J.T.G.Overbeek, *Theory of the Stability of Lyophobic Colloids*, Elsevier, Amsterdam, 1948.
7. J.N.Israelachvili, *Intermolecular and Surface Forces*, 2nd ed., Academic Press, San Diego, 1991.
8. H.C.Hamaker, Physica, **4** (1937) 1058.
9. P.Delahay, *Double Layer and Electrode Kinetics*, Interscience, New York, 1965.
10. T.Arai and M.Fujihira, J. Electroanal. Chem., **374** (1994) 269.
11. T.Arai and M.Fujihira, to be published.

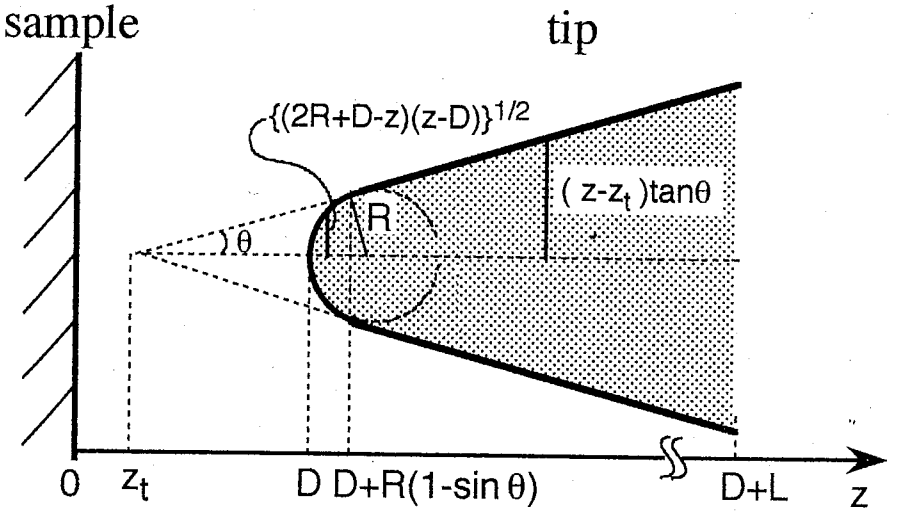

Figure 2-1. Schematic model of a realistic AFM tip used for calculation. The tip apex is a sphere with a radius R, and the shank is a tapered cone with a cone angle 2θ circumscribing to the sphere.

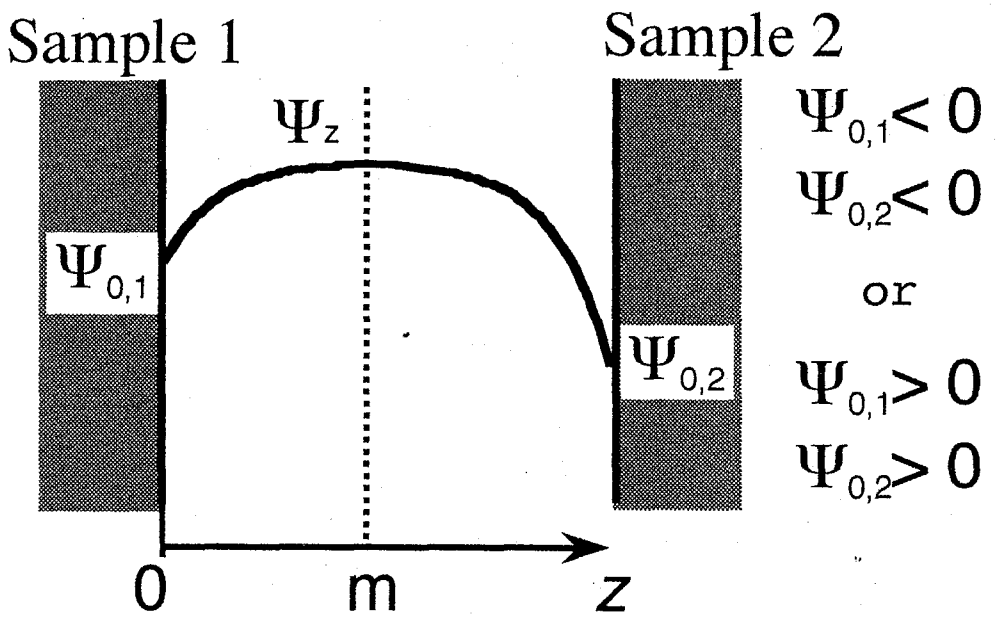

Figure 2-2. Schematic model of electrostatic potential Ψ_z, when two faced surfaces are charged with the same sign in aqueous solution. The surface potentials on each surface are $\Psi_{0,1}$ and $\Psi_{0,2}$.

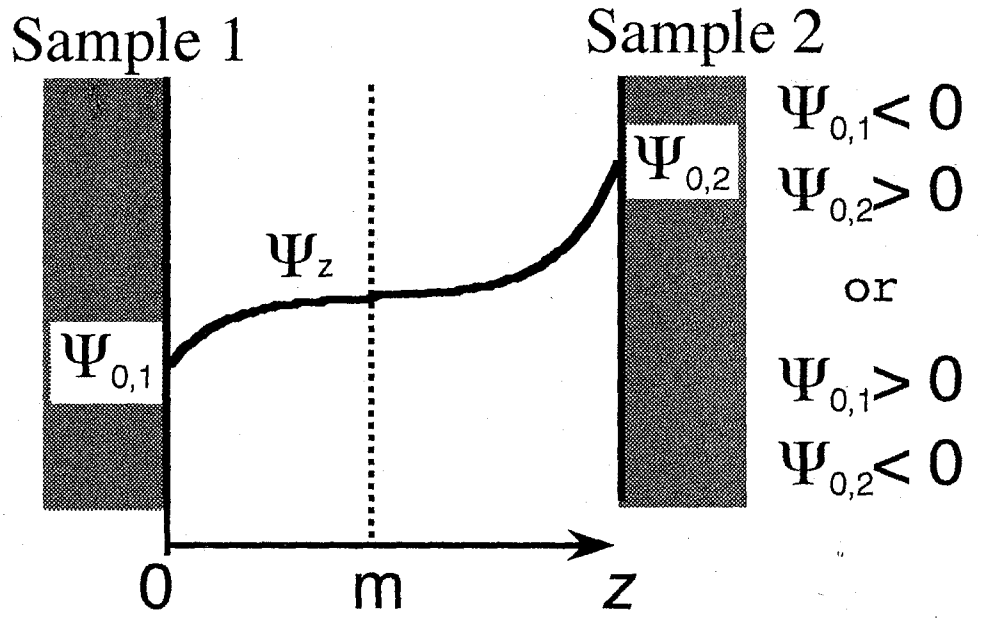

Figure 2-3. Schematic model of electrostatic potential Ψ_z, when two faced surfaces are charged with opposite sign in aqueous solution. The surface potentials on each surface are $\Psi_{0,1}$ and $\Psi_{0,2}$.

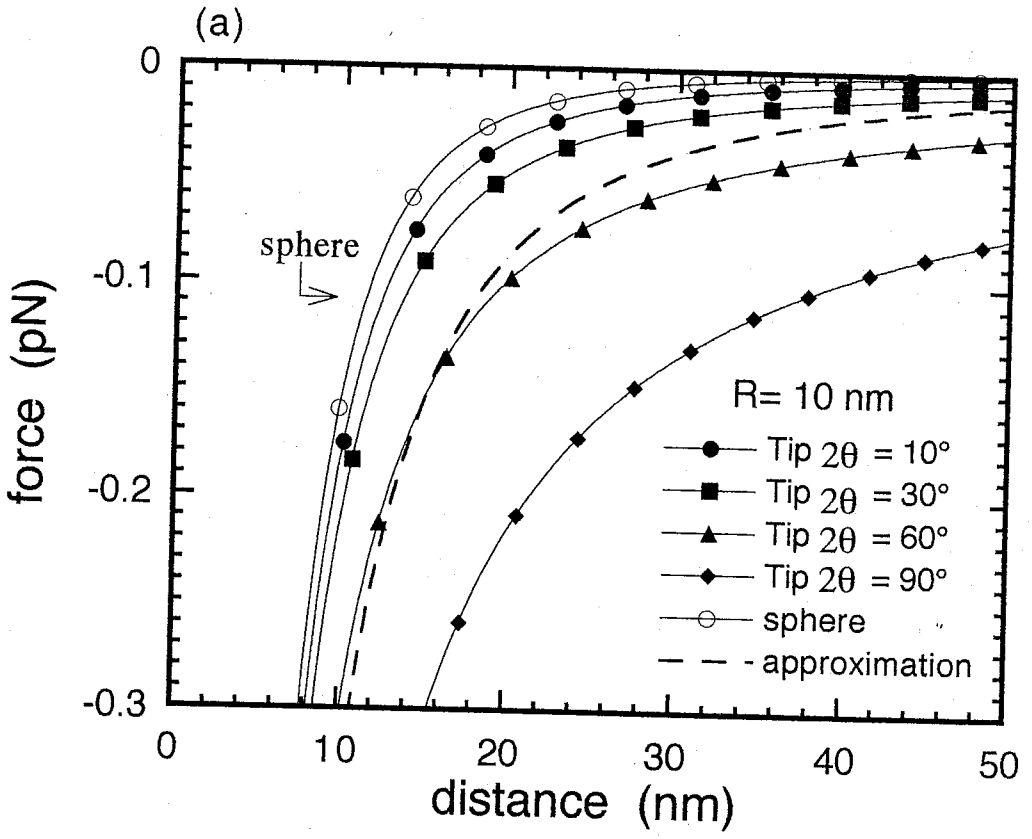

Figure 2-4.(a) Van der Waals force - distance curves for tips of R = 10 nm with 2θ = 10, 30, 60, 90 and 120°, a sphere of R = 10 nm and the Derjaguin approximation.

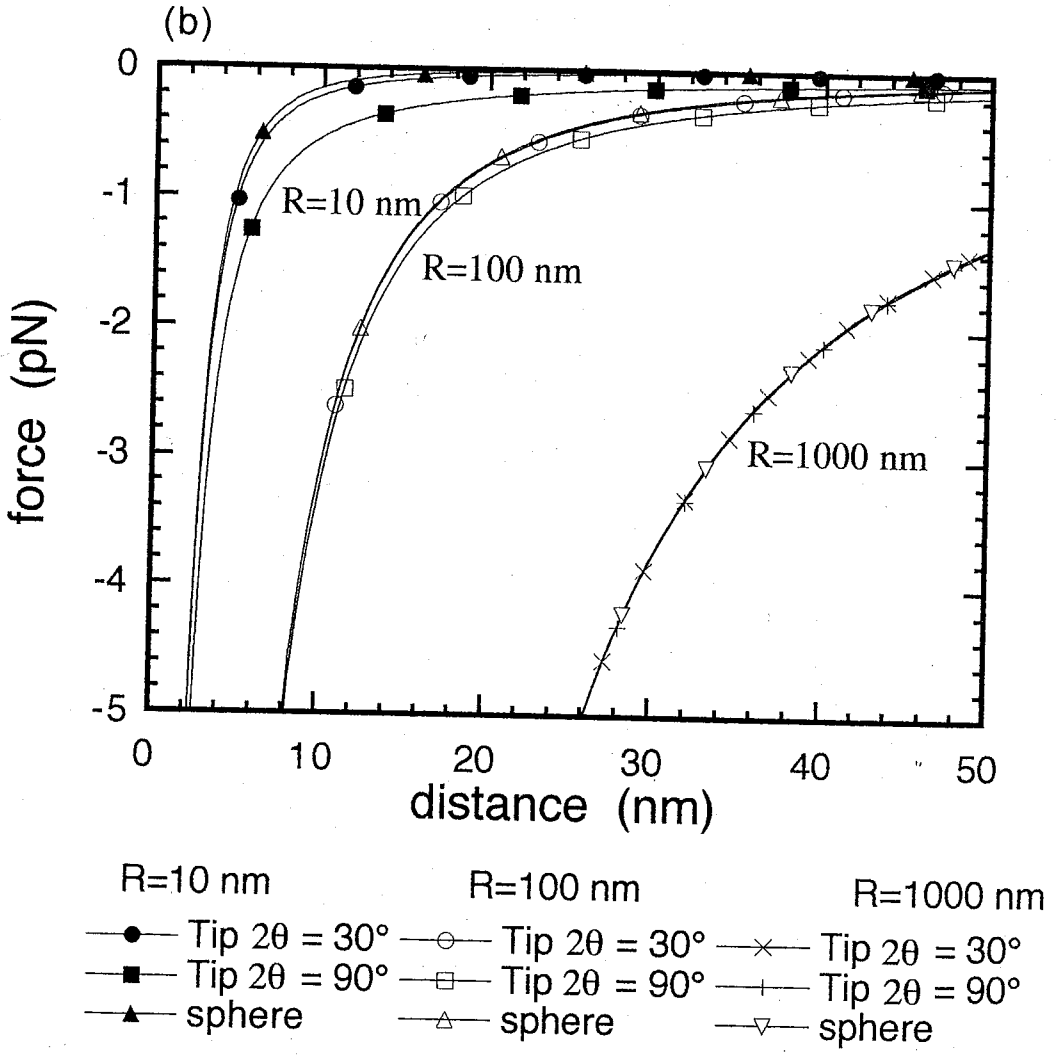

Figure 2-4.(b) Van der Waals force - distance curves for tips of R = 10, 100 and 1000 nm with 2θ = 30 and 90°, and spheres of R = 10, 100 and 1000 nm.

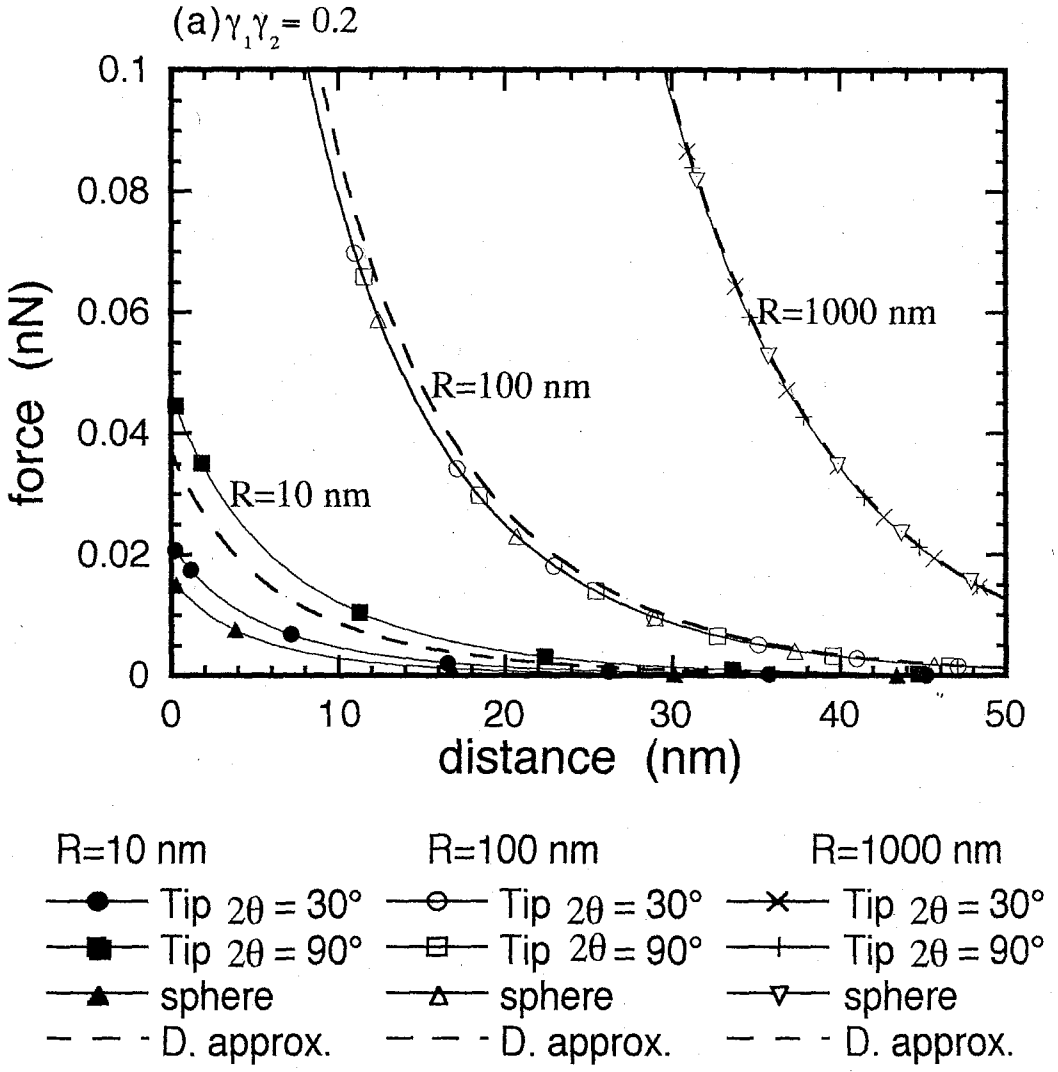

Figure 2-5.(a) Electrical double layer force - distance curves. For surfaces of the tip and the sample charged with the same sign. The tip radius R is 10, 100 and 1000 nm with 2θ of 30 and 90°. The sphere of R = 10, 100 and 1000 nm and the Derjaguin approximation are included.

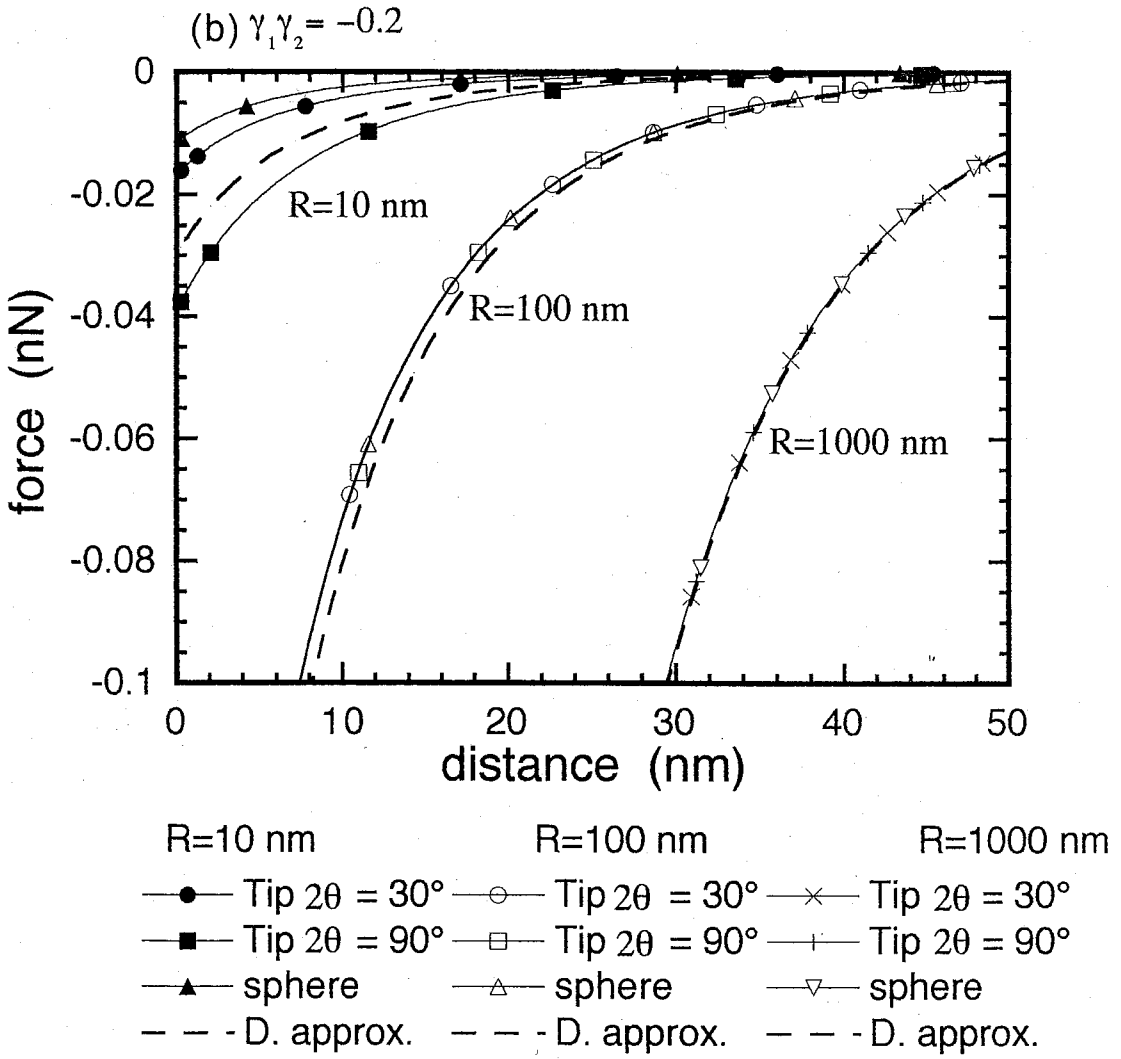

Figure 2-5.(b) Electrical double layer force - distance curves. For surfaces of the tip and the sample charged with the opposite sign.

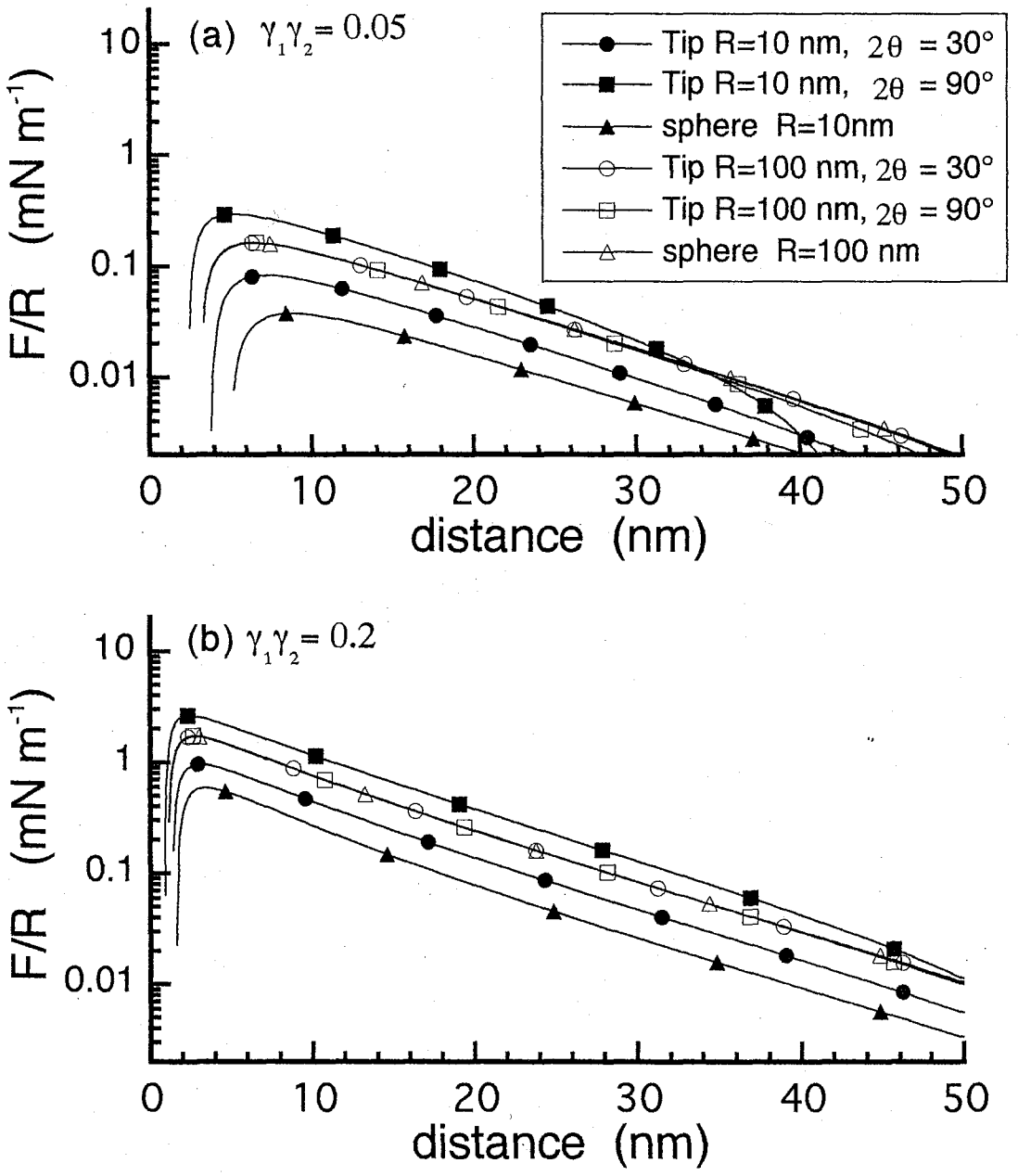

Figure 2-6. DLVO force - distance curves for $\gamma_1\gamma_2$ = (a) 0.05 and (b) 0.2. The force is normalized with R. Black marked lines for tips of R=10 nm with 2θ of 30 and 90°, and a sphere of R=10 nm. White marked lines for R=100 nm.

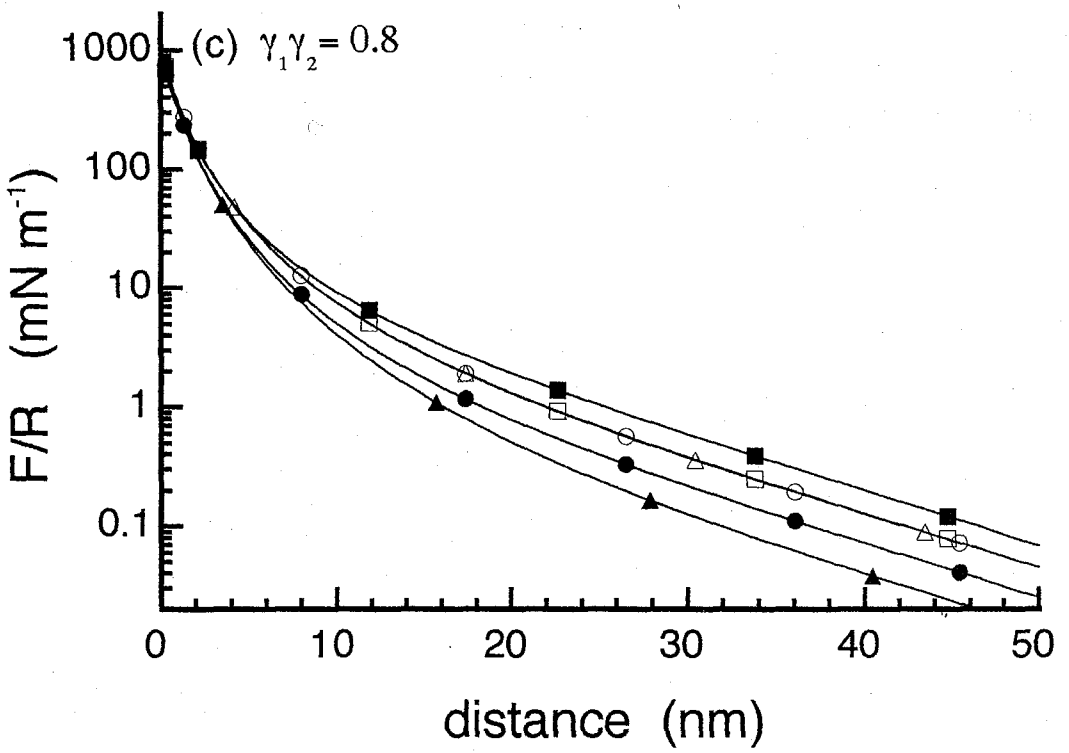

Figure 2-6.(c) DLVO force - distance curves for $\gamma_1\gamma_2 = 0.8$.

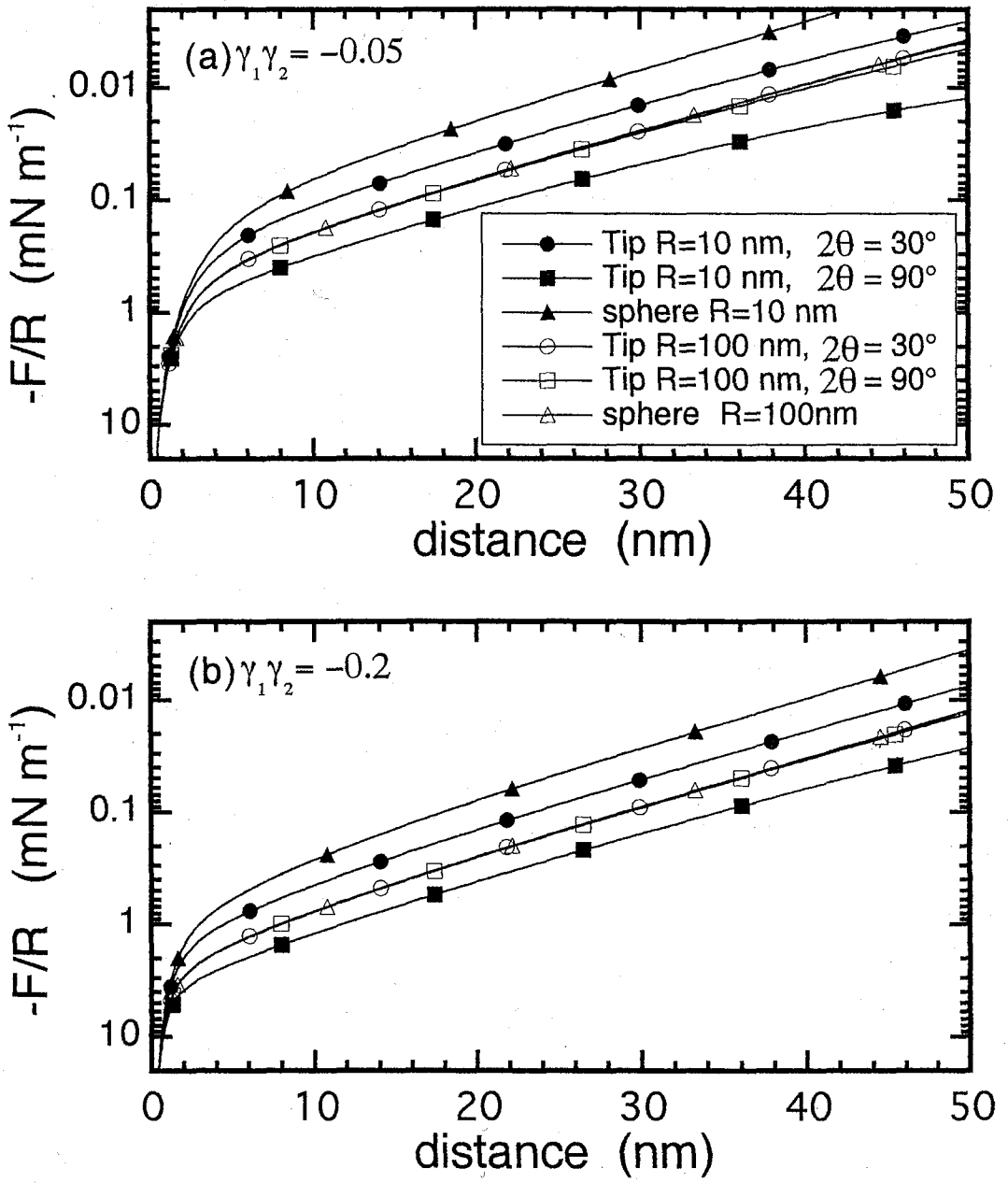

Figure 2-7. DLVO force - distance curves for $\gamma_1\gamma_2$ = (a) -0.05 and (b) -0.2. The force is normalized with R. Black marked lines for tips of R = 10 nm with 2θ of 30 and 90°, and a sphere of R = 10 nm. White marked lines for R = 100 nm.

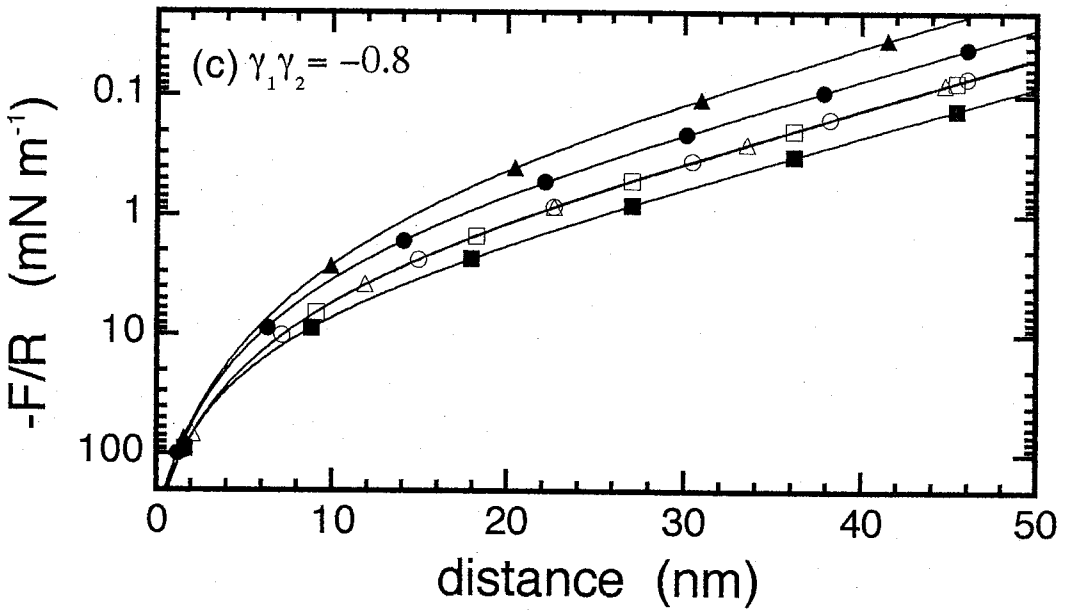

Figure 2-7.(c) DLVO force - distance curves for $\gamma_1\gamma_2 = -0.8$.

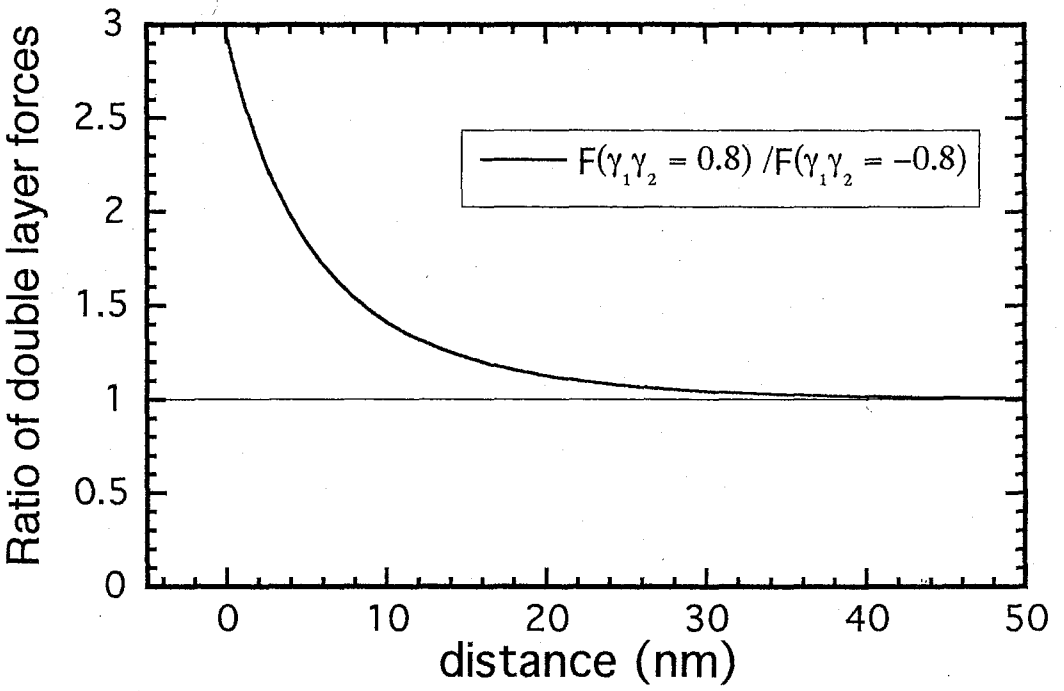

Figure 2-8. Ratio of double layer force for $\gamma_1\gamma_2 = 0.8$ to that for $\gamma_1\gamma_2 = -0.8$ changing the distance with a spherical tip of R = 100 nm. The curve corresponds to that in Figs.2-6(c) and 2-7(c) excluding the van der Waals force.

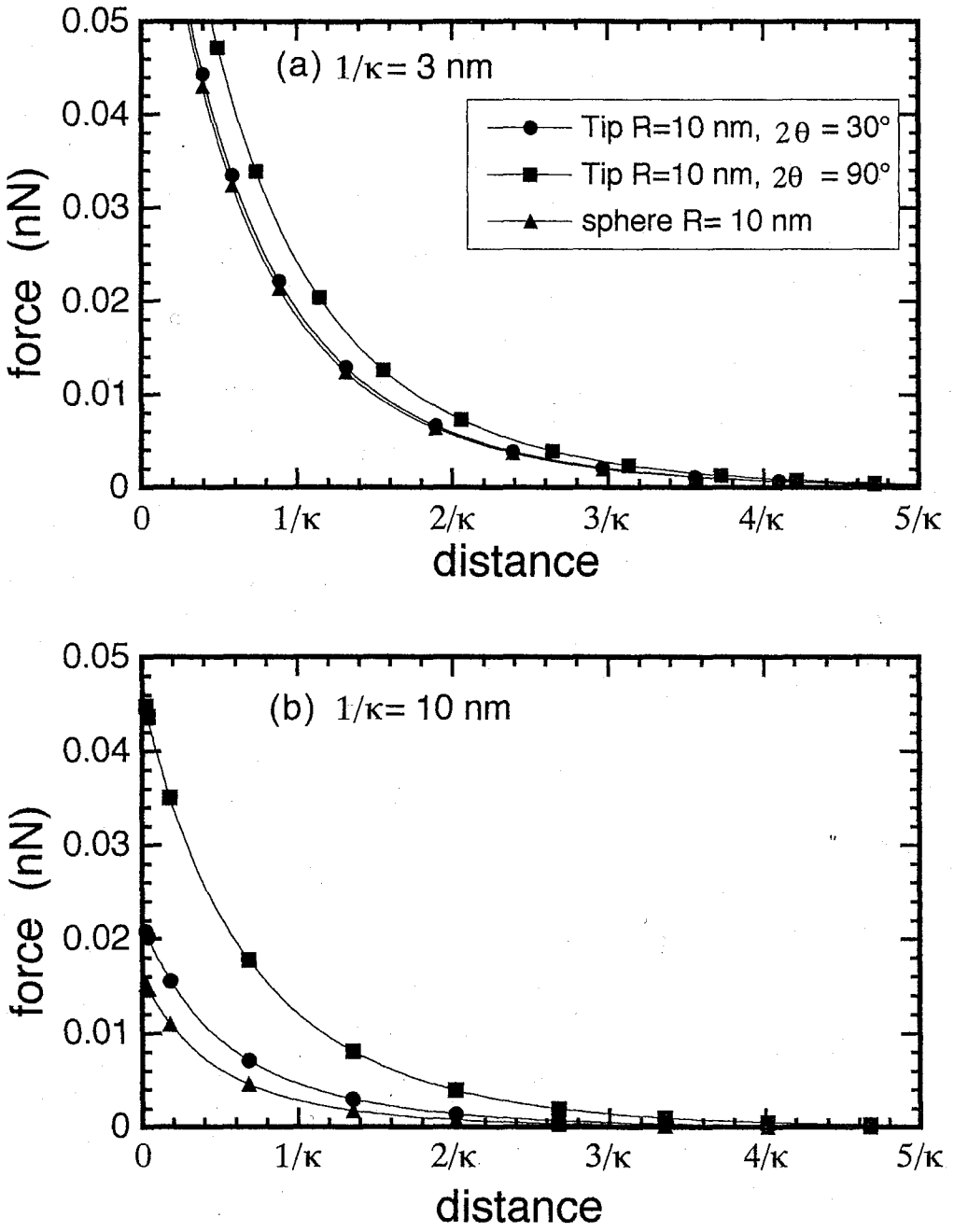

Figure 2-9. Double layer force - distance curves for $1/\kappa$ = (a) 3 and (b) 10 nm with $\gamma_1\gamma_2 = 0.2$. The horizontal unit of the distance is normalized with the Debye length $1/\kappa$. The tip radius R is 10 nm and the cone angle 2θ is 30 and 90°. The curves for a sphere with R = 10 nm is included.

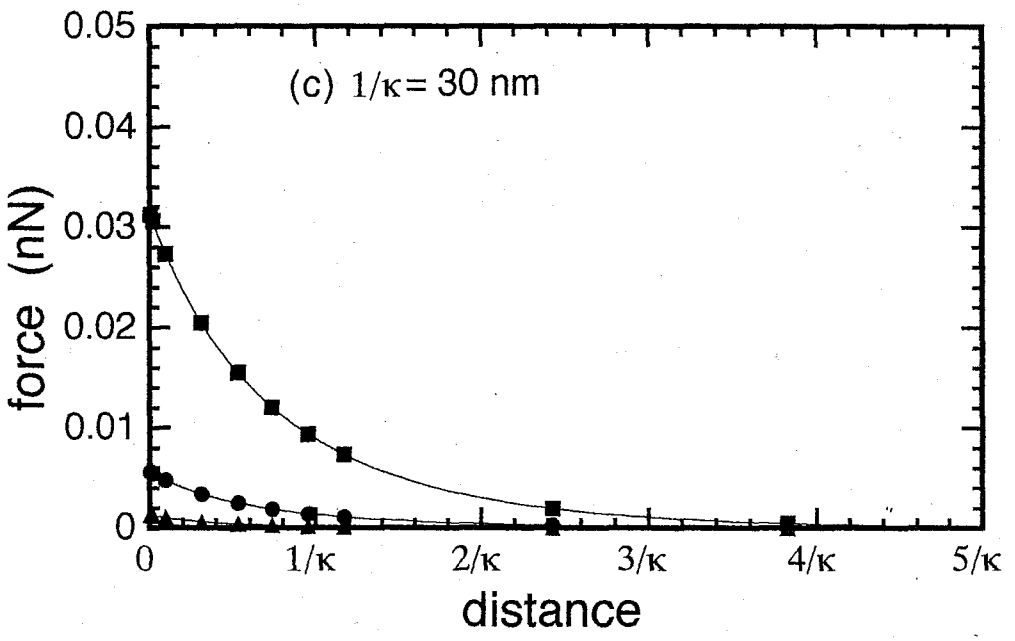

Figure 2-9.(c) Double layer force - distance curves for $1/\kappa = 30$ nm with $\gamma_1\gamma_2 = 0.2$.

Chapter 3

Surface Forces between Oxides and Silicon Nitride Tips

3-1. Introduction

It has been well established that an oxide suspended in an aqueous solution can acquire surface charges by absorbing H^+ or OH^- ions [1,2]. The total quantity of surface charge is well-known to change with pH of the solution; the pH at which a solid has no net surface charge is defined as the isoelectric point (IEP) [3]. The surface charge and IEP of colloidal particles can be evaluated by the electrophoresis experiments [4]. The surface charge estimated by electrophoresis is an average of net charge on a particle. The electrophoresis method can not define charge distribution on the surface with local inhomogeneity.

Then to study the interaction force between surfaces in an aqueous solution, it is required to map the inhomogeneous charges with a high lateral resolution. The analysis can reveal the structure of the double layer [5-7]. The IEP on a small surface area is evaluated on the basis of a pH dependence of the interaction force with an atomic lateral resolution of AFM.

In this chapter, the force-distance curves are measured with the AFM in aqueous electrolyte solutions, and compared to the theoretical curves calculated in chapter 2 according to the DLVO theory [8,9] on the assumption that the tip has a spherical apex and the circumscribing tapered shank. In the calculation of the electrical double layer force, the constant surface potentials at the tip

and the sample and the Boltzmann distribution of the ion concentration are assumed. The effects of the surface potential are also evaluated without the low potential approximation, mentioned in chapter 2.

The force-distance curves on several oxides, such as SiO_2, SnO_2, and Al_2O_3 in aqueous electrolytes, were measured by AFM with a sharpened tip of Si_3N_4. The IEP of each oxide was estimated from the pH dependence of the interaction force.

3-2. Experimental

3-2-1. Force measurement

All measurements of the surface force and topographic imaging were performed using a commercial AFM (a SEIKO Instruments, SPA 300 AFM unit with a controller SPI-3700). The force was measured by a laser beam deflection caused by bending of a cantilever with the force constant of 0.089 N m^{-1} (Olympus Co.,ltd). The cantilever has a specially-sharpened tip on a small pyramidal hill, made of silicon nitride (Si_3N_4). The sharpness of the tip was confirmed by an FE-SEM (JEOL LTD), shown in Fig.3-1. The radius of the tip apex and the cone angle 2θ of the shank was about 20 nm and 30°, respectively. The sample and the cantilever were immersed in an electrolyte in a Teflon cell, which is placed on top of a piezo tube scanner of the AFM. The tube scanner can position the sample 3-dimensionally within several μm on an atomic scale by changing the applied voltages to XYZ electrodes of the piezo. The piezo can expand and shrink with the voltage. The force-distance curves were recorded by changing the sample position z with respect to the tip. The sample position was calculated from the voltage applied to the piezo Z-electrode. Fig.3-2(a) shows the surface force-sample position curve. The

position does not correspond directly to a separation between the tip apex and the sample surface, because the cantilever bends a little depending on the force. Thus the distance was calibrated and plotted to show the true separation in the figure, subtracting the lever deflection from the sample position, as shown in Fig.3-2(b). The origin was chosen as a position, from which a linear repulsive change started in the contact regime. In addition, there was a hysteresis in the piezo displacement distinctively in the retracting curve, thus only the approaching direction curve to the tip was adopted to evaluate the interaction from the force-distance curves. The approaching speed was about 20 nm s^{-1}.

3-2-2. Materials and sample preparation

Electrolytes with pH values of 3 to 11.4 were used for the measurement of force-distance curves: $HClO_4$ for pH 3 to 4, phosphate buffer solutions for pH 5 to 8.5 and NaOH or KOH for pH 10 to 11.4. The ion concentrations in phosphate buffer solutions (KH_2PO_4 + NaOH) were adjusted so that the Debye length κ^{-1} became 10 or 30 nm. The electrolytes with the Debye length of 10 and 30 nm correspond to the solutions containing a 1:1 electrolyte of 10^{-3} and 10^{-4} M, respectively. The chemicals used were commercially available G.R. grade reagents and were used as received.

The samples for measuring surface forces were a silicon wafer covered with a natural oxide layer, a quartz (SiO_2) plate, a sapphire (Al_2O_3) plate, and a SnO_2 film deposited on a glass plate. The samples were prepared as follows. The silicon wafer was cleaned with an alkali detergent, rinsed with mill-Q water, and then heated at 80 °C in an RCA alkali solution (H_2O_2 : NH_4OH : H_2O = 1:1:5) [10] for 30 min and rinsed with mill-Q water to be hydrophilic. The silicon surface was covered with an oxide layer, about 1 nm thick [10].

The quartz plate was immersed in an RCA alkaline solution at 80 °C for 30 min and rinsed with Milli-Q water. The sapphire plate was cleaned in an ultrasonic bath with ethanol and rinsed with Milli-Q water. The glass plate coated with SnO_2 was cleaned with an alkali detergent, Milli-Q water, and ethanol, and then rinsed with Milli-Q water.

3-3. Results and discussion

3-3-1. Comparison of the measured force with the theory

The calculation of the van der Waals force in section 2-2-1 was required the values of the Hamaker constant [11] for our samples. In the non-retarded limit, the Hamaker constant between two bodies with a third intervening medium can be calculated using the Lifshitz theory [12]. Although the Lifshitz theory gives an exact formula for the Hamaker constant, the expression requires a representation of the dielectric responses of the media involved up to ultraviolet frequencies [13,14]. In this thesis, it is sufficient to consider an approximate from for the Hamaker constant due to Israelachvili [15],

$$A = \frac{3}{4}kT\left(\frac{\varepsilon_1-\varepsilon_3}{\varepsilon_1+\varepsilon_3}\right)\left(\frac{\varepsilon_2-\varepsilon_3}{\varepsilon_2+\varepsilon_3}\right)$$

$$+\frac{3h\nu_e}{8\sqrt{2}}\frac{(n_1^2-n_3^2)(n_2^2-n_3^2)}{(n_1^2+n_3^2)^{1/2}(n_2^2+n_3^2)^{1/2}[(n_1^2+n_3^2)^{1/2}+(n_2^2+n_3^2)^{1/2}]} \qquad (3.3.1)$$

where the ε_i's are the static dielectric constants and the n_i's are the optical refractive indices. The subscription indices 1 to 3 correspond to (1) the tip, (2) the samples, and (3) the immersion medium, aqueous solution. In eq. (3.3.1), ν_e is the electronic absorption frequency, which is assumed to be equal

for all materials. Table 3-1 summarizes the Hamaker constants for the silicon nitride-water-samples system calculated with eq. (3.3.1). The Hamaker constant for the silicon was calculated without consideration of natural oxide on the Si, because the oxide layer was very thin.

Figure 3-3 shows comparison between the experimental and the theoretical force-distance curves between a silicon wafer and a tip of R = 20 nm and $2\theta = 30^\circ$ in an electrolyte of pH 11.4 with KOH. The calculated curves here include the van der Waals force in addition to the double layer force. The solid line shows the calculation using eq. (2.2.4) and (2.2.25) without the approximation of a low electrostatic potential, and the dashed line using eq. (2.2.4) and (2.3.8) with the approximation, eq. (2.3.7).

The experimentally obtained curve, denoted by circles, clearly shows the strong repulsive force in the vicinity of the surface ($z < 10$ nm) in Fig. 3-3. The solid line agrees quite well to the experimental data, but the dashed line does not. The fitting value of $\gamma_1\gamma_2$ can be obtained from the solid line calculation: γ_1 and γ_2 are determined by the surface potentials of the tip and the sample, respectively, as in eq. (2.2.12), but here each of the value are undetermined. The $\gamma_1\gamma_2$ was 9.6 in fig.3-3. If γ_1 and γ_2 is the same value, $\Psi_{0,1}$ and $\Psi_{0,2}$ are estimated to be more than 200 mV from $\gamma_1\gamma_2 = 0.96$. As being clear from the discussion below, pH of the solution (pH 11.4) is extremely higher than the isoelectric points of the two surfaces. This means the approximation of a low electrostatic potential can not be applicable for such a high surface potential. It did not hold for the other electrolytes with the different pH values. For a low surface potential, the approximation curve also coincided with the experimental curve.

3-3-2. pH dependence

On the above fitting procedure, the fitting values of $\gamma_1\gamma_2$ can be obtained for every systems with difference pH. The surfaces of oxides immersed in an aqueous solution are covered with -OH groups, which are protonated into $-OH_2^+$ at low pH and dissociated into $-O^-$ at high pH [3] as follows:

$$-OH + H^+ \Leftrightarrow -OH_2^+ \qquad (pK_{aI}) \qquad (3.3.2)$$

$$-OH \Leftrightarrow -O^- + H^+ \qquad (pK_{aII}) \qquad (3.3.3)$$

Under these conditions, the oxide surface charges positively and negatively at lower and higher pH than the IEP, respectively. When two surfaces are brought so close as to allow the electrical double layers to overlap, the force becomes attractive or repulsive depending on the combination of the charge polarities over the two surfaces, according to section 2-2-2. The double layer force is attractive when $\Psi_{0,1}$ and $\Psi_{0,2}$ have the opposite sign to each other ($\gamma_1\gamma_2 < 0$) and repulsive when $\Psi_{0,1}$ and $\Psi_{0,2}$ have the same sign ($\gamma_1\gamma_2 > 0$). Figure 3-4 shows the expected behavior of the double layer force parameter, $\gamma_1\gamma_2$, as a function of the electrolyte pH. When the pH value crosses the IEPs, the sign of the surface potential at the surface changes and the interaction turns from repulsive to attractive or vice versa.

The pH dependence of $\gamma_1\gamma_2$ for the silicon nitride-water-silicon system, which is the same system of section 3-3-1, is shown in Fig.3-5. The negative values of $\gamma_1\gamma_2$ observed at pH less than 5 indicate that the surfaces are charged oppositely in sign, while the positive values of $\gamma_1\gamma_2$ at pH larger than 5 correspond that both the surfaces are charged negatively. The curve crosses

with a line of $\gamma_1\gamma_2 = 0$ at ca. pH 5. Thus, the pH 5 can correspond to the isoelectric point, $\Psi_0=0$, of Si_3N_4 or silicon oxide. According to a literature value of the isoelectric point of silica around pH 2 [1], the isoelectric point pH 5 found in this study can be assigned to that of Si_3N_4 other than silicon oxide. This indicates that the present fitting method can be used to determine the isoelectric points of the localized areas and thus the lateral distribution of the acidic and basic sites can be obtained.

In order to estimate the IEPs of samples, the sign of the force (repulsive or attractive) at each pH value is important. For instance, the force-distance curves between the silicon nitride tip and silica in several solutions were obtained as shown in Fig.3-6. The contribution of the van der Waals force was very slight at the distance lager than 2 nm. Then, the sign of the measured force should be the same with that of the double layer force at the distance lager than 10 nm. The force at a constant distance, i.e lager than 10 nm, changes as shown in Fig.3-7, which is similar to Fig.3-4.

Figure 3-8 shows the pH dependence of the measured force between a silicon nitride tip and the oxide samples at a distance of $1/2\ \kappa^{-1}$. The Debye lengths (κ^{-1}) of the 1:1 electrolyte solutions of 10^{-3} and 10^{-4} M are 10 and 30 nm, respectively. Here the Debye length (κ^{-1}) of the phosphate buffer solution shown here was adjusted to be 30 nm. On all the oxides, the sign of the force changed around pH 5-6. Table 3-2 summarizes the IEP values reported by other workers using other techniques [1,16,17]. According to the comparison, the change in the sign around pH 5-6 can be attributed to the IEP of Si_3N_4. Since the IEP of SiO_2 is reported to be around pH 2, the crossing point was not found in this experiment. The reported IEP of SnO_2 is close to that of Si_3N_4. This agrees with the experimental finding, in Fig. 3-8, that a distinct

attractive region was not found. For Al_2O_3 in Fig. 3-8, the double layer force changes from attractive to repulsive at about pH 10. The value is close to those reported previously [1,16,17].

3-4. Conclusion

The experimentally obtain data were compared with the calculation of the force-distance curves consisting of the van der Waals force and the electrical double layer force in an electrolyte in the AFM with a realistic shape tip without the approximation of a low electrostatic potential. The comparison showed had a good agreement. The pH dependence curves of $\gamma_1\gamma_2$ and the force at a constant distance showed that the force-distance curves can be used to estimate the IEPs for oxide surfaces. The measured interaction force was between a sharpened tip and a small area on a sample surface. The map of charge distribution on the inhomogeneous surface can be obtained by repeating this force measurement. The IEP for local area can also be estimated.

References

1. G. A. Parks, Chem. Rev., **65** (1965) 177.
2. R.H. Yoon, T. Salman, and G. Donnay, J. Colloid Interface Sci., **70** (1979) 483.
3. R.J.Hunter, *Foundations of Colloid Science*, Oxford University Press, New York, 1987.
4. R.J. Hunter, Zeta Potential in Colloid Science, Academic Press, London (1981).
5. W.A.Ducker, T.J.Senden and R.M.Pashley, Langmuir, **8** (1992) 1831.
6. J.L.Hutter and J.Bechhoefer, J. Appl. Phys., **73** (1993) 4123.
7. X.Y.Lin, F.Creuzet and G.Arribart, J. Phys. Chem., **97** (1993) 7272.
8. B.V.Derjaguin and L.Landau, Physicochim., URSS **14** (1941) 633.
9. E.J.W.Verwey and J.T.G.Overbeek, *Theory of the Stability of Lyophobic Colloids*, Elsevier, Amsterdam, 1948.
10. W.Kern and D.A.Poutinen, RCA Rev., **31** (1970) 187.
11. H.C.Hamaker, Physica, **4** (1937) 1058.
12. E.M.Lifshitz, Soviet Physics JETP (Engl. Trandl.) **2** (1956) 73.
13. B. W. Ninham and V. A. Parsegian, Biophys. J., **10** (1970) 646.
14. D. B. Hough and L. R. White, Adv. Colloid Interface Sci., **14** (1980) 3.
15. J.N.Israelachvili, *Intermolecular and Surface Forces*, 2nd ed., Academic Press, San Diego, 1991.
16. D. L. Harame, L. J. Bousse, J. D. Shott and J. D. Meindl, IEEE Trans. Electron Devices, ED-**34** (1987) 1700.
17. L. Bergstrom and E. Bostedt, Colloids Surf., **49** (1990) 183.

Table 3-1. Calculated Hamaker constants between oxides and silicon nitride in an aqueous solution using eq. (3.3.1).

	Hamaker constant A ($\times 10^{-20}$ J)
Si - H_2O - Si_3N_4	21.7
SiO_2 - H_2O - Si_3N_4	2.08
Al_2O_3 - H_2O - Si_3N_4	4.99
SnO_2 - H_2O - Si_3N_4	7.15

Table 3-2. Summary of the isoelectric points for oxides reported by other workers [1,16,17].

	Si_3N_4	SiO_2	SnO_2	α-Al_2O_3
IEP	5-7	1.8 - 2.8	4.5 - 7.3	9 - 10

(a)

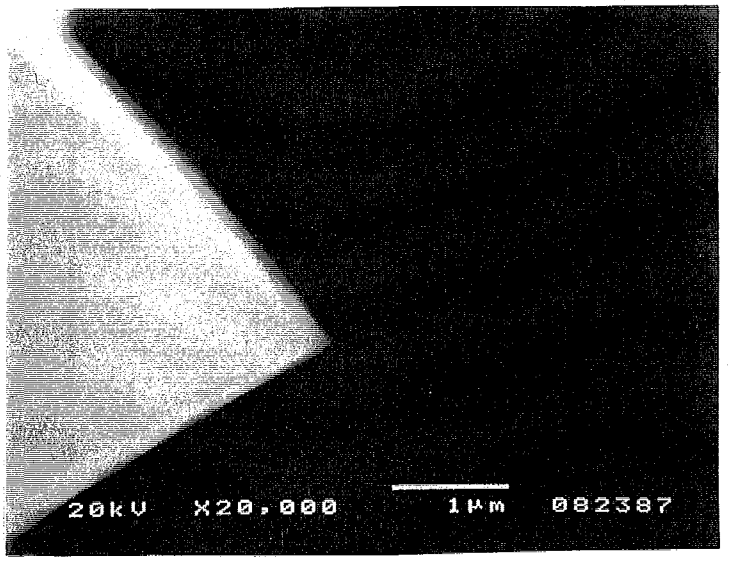

(b)

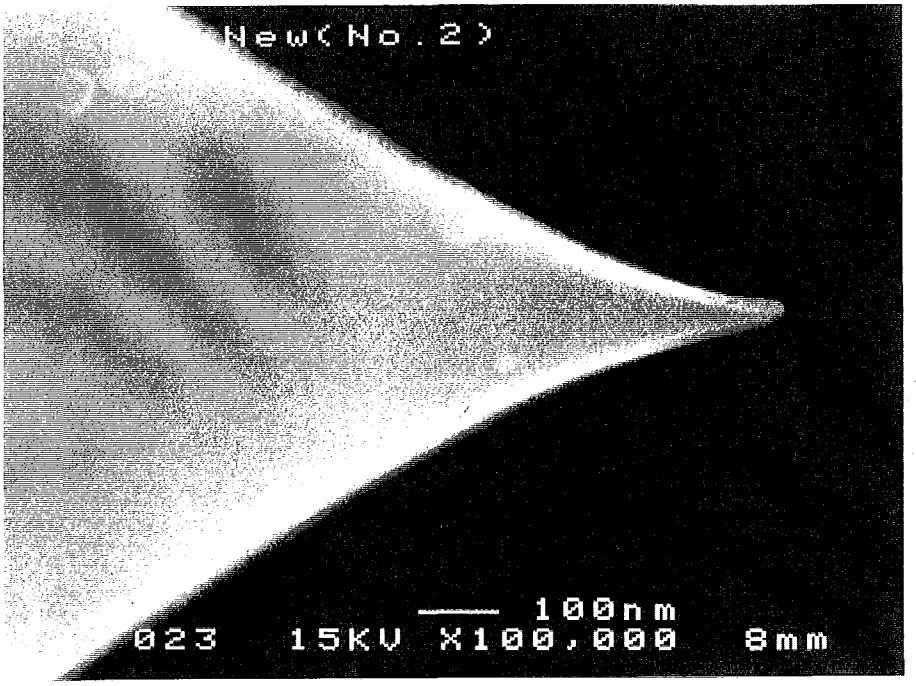

Figure 3-1. (a) SEM image of a cantilever with a specially-sharpened tip on a small pyramidal hill, (b) FE-SEM image of the apex of the sharpened tip.

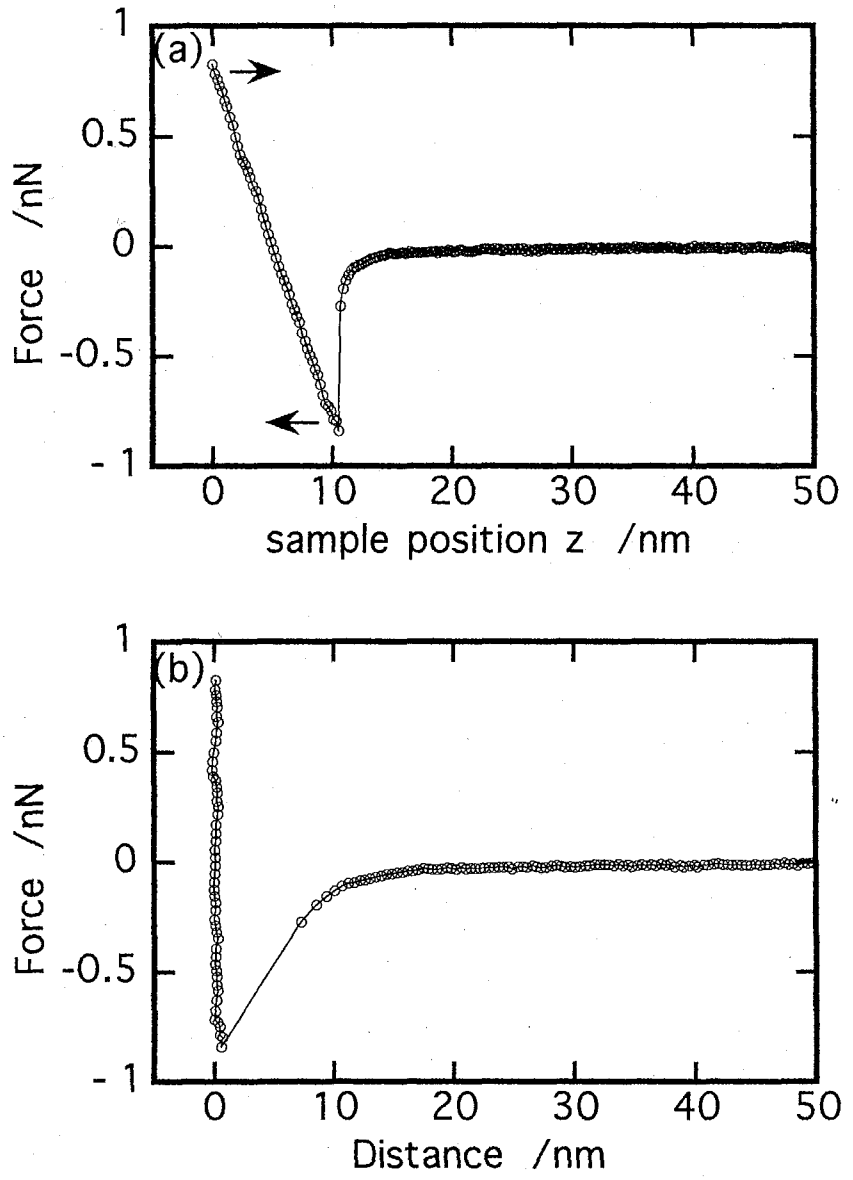

Figure 3-2. (a) Relation between the surface force and the sample position. The sample position was calculated from the voltage applied to the piezo Z-electrode. (b) The force-distance curve. The distance was calibrated from the true separation between the tip apex and the sample surface by taking account of the cantilever bends.

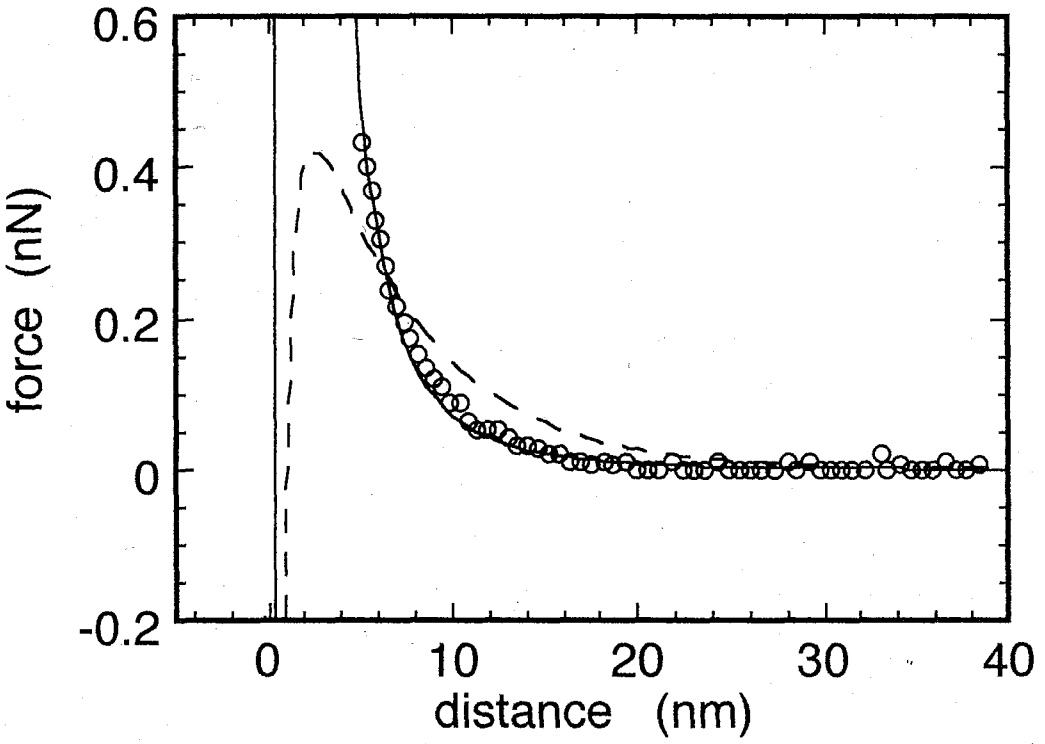

Figure 3-3. Comparison of the experimentally obtained data with the calculated force-distance curves. The circles show the experimental data, the dashed and the solid line show the calculated curves with and without the approximation of a low electrostatic potential, respectively. R=20 nm, $2\theta = 30^{\circ}$, pH = 11.4.

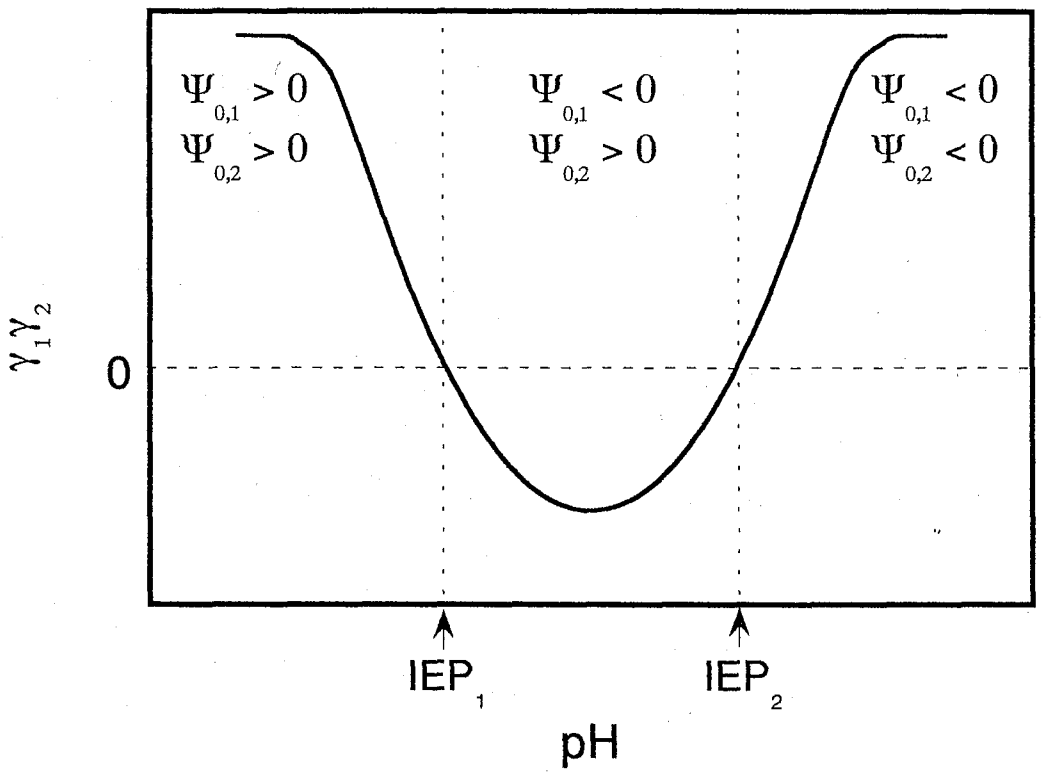

Figure 3-4. Estimated characteristics of $\gamma_1\gamma_2$ as a function of the pH in the electrolyte, which was determined by the curve fitting between two surfaces with different IEPs.

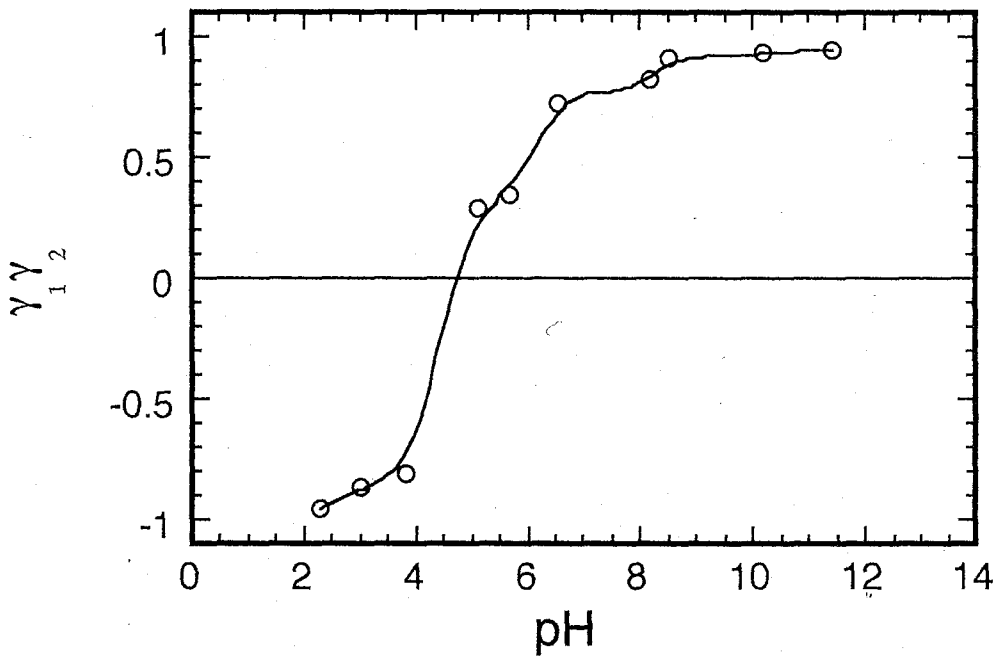

Figure 3-5. pH dependence of $\gamma_1\gamma_2$, which was determined by the curve fitting between the measured and calculated curves for silicon nitride - aqueous solution - silicon wafer.

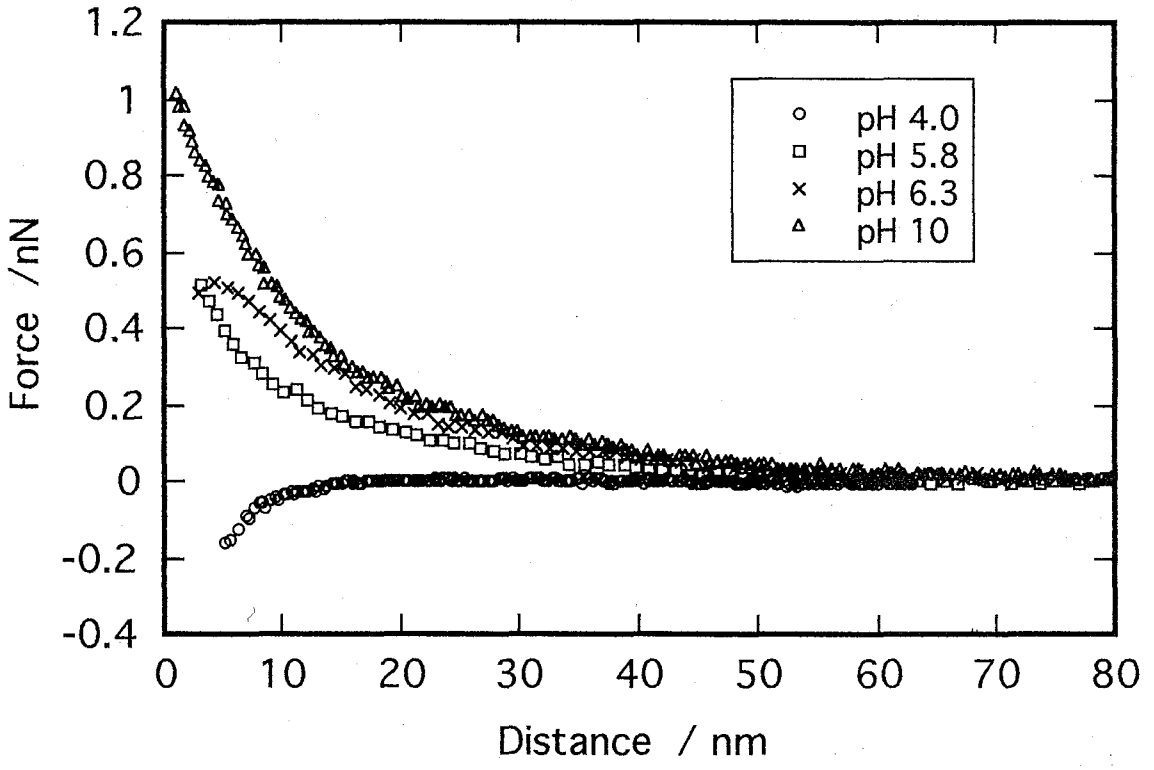

Figure 3-6. The force-distance curves between the silicon nitride tip and silica in several solutions. The Debye lengths (κ^{-1}) in all the solutions were 30 nm. κ^{-1} of the 1:1 electrolyte solutions in 10^{-4} M are 30 nm.

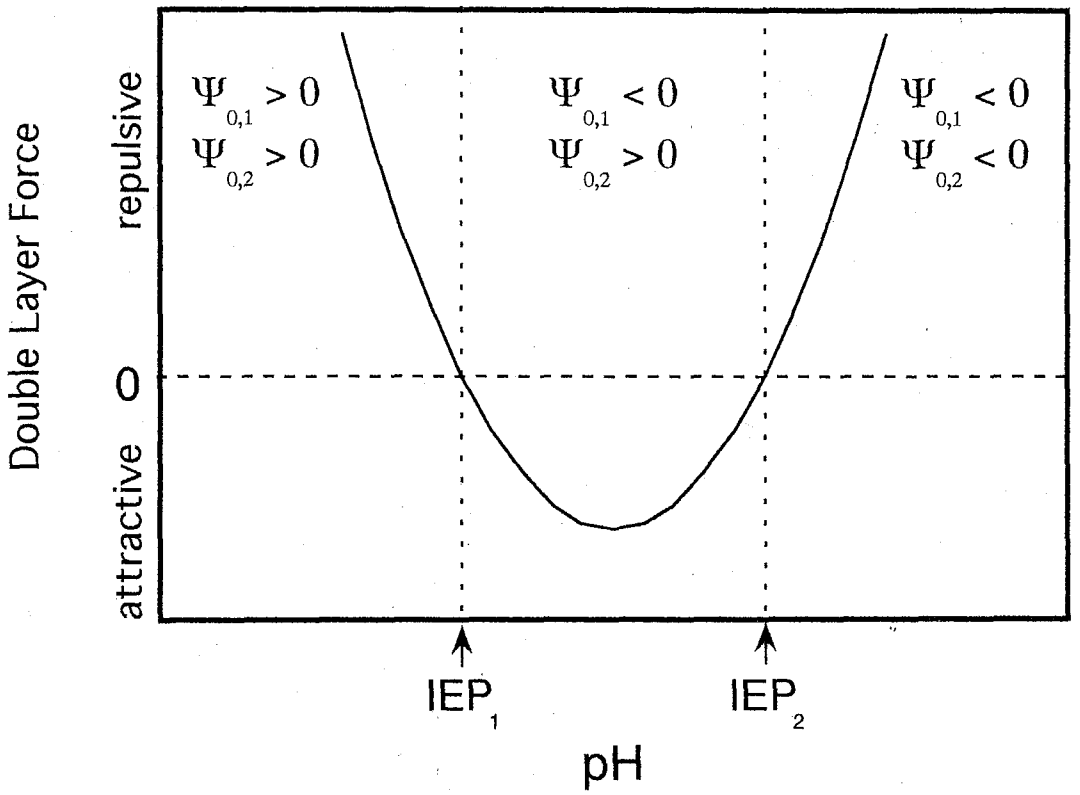

Figure 3-7. Estimated characteristics of the double layer force between two surfaces with different IEPs at a constant distance as a function of the pH in the electrolyte.

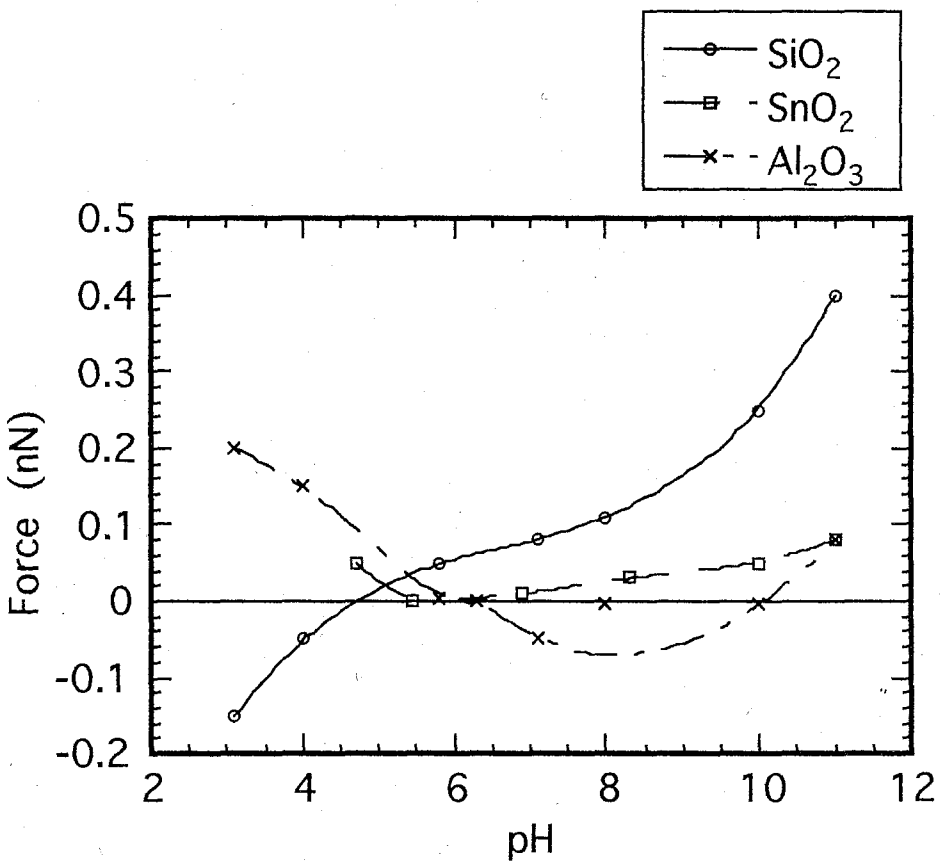

Figure 3-8. pH Dependence of surface forces at a distance of a half of the Debye length between a Si_3N_4 tip and a surface of SiO_2, SnO_2 or Al_2O_3.

Chapter 4

Langmuir-Blodgett Films on Oxides

4-1. Introduction

In chapter 3, the electrical double layers over the oxide surfaces were analyzed from the force measurements with the AFM, assuming that they were homogeneous. There the analyzed oxide surfaces met the demanded condition of surface homogeneity. In this chapter, the surfaces partially covered with dielectric thin films are studied to clarify the effects of the coverage on the double layers; the AFM is extremely powerful to observe the spatial variation on the sample surfaces [1-3]. To compare bare oxide surfaces with oxide surfaces covered with dielectric films using the AFM, the partially covered surfaces, which consists of the bare oxide regions and the dielectric covered regions within the AFM scanning range, are formed by a novel method [4]. The film thickness is adjusted to be less than the Debye length of the double layer, 10-30 nm in chapter 3, to facilitate the comparison with the AFM in respect of the vertical dynamic range.

In principle, the AFM depicts sample topography by scanning a tip over a sample surface, while maintaining a constant separation between the tip and the sample [1]. To maintain it, the feedback system of the AFM refers the measured force, which depends on the separation. The AFM imaging force, however, has not been well-characterized analytically. The condition of a constant force does not necessarily mean the constant separation, depending on natures of the forces on the different surface regions. For example, if charges

inhomogeneously distribute over a flat sample surface in a liquid, the AFM image with a small load force mainly reflects the charge distribution on the surface [5]. Thus, to depict the true topography, it is indispensable to make a correction of the topography for a surface with an inhomogeneous charge distribution. The clue to understanding the nature of the detected force is in the distance dependence of the force, which can be measured by the AFM. Then the force-distance curves have been measured and analyzed to characterize the force in aqueous electrolytes by the AFM [6].

To clarify the effects of the organic molecular films on the oxides on the charge distribution, a novel method [4] is adopted to form a quartz surface covered partially with organic molecular films. The technique is related to the phase-separated Langmuir-Blodgett (LB) films [7-10]. The effect of the organic molecular films on the charge distribution is discussed in this chapter.

Here the LB films are referred briefly: in 1935, Langmuir first reported the systematic study of monolayers of amphophilic molecules at the water-air interface [11], followed by Blodgett and Langmuir's reports about the built-up multilayer films [12,13]. Then the built-up monolayer assemblies formed by their method is call the LB films. The method using a trough to assemble the LB films is schematically illustrated in Fig. 4-1. At first, a spread monolayer on a subphase is compressed by a barrier. When the monolayer changes into a solid phase, the monolayer formed on the subphase is transferred on a substrate. The monolayer physically lies on the substrate. On the other hand, a monolayers can be also realized by chemical bonding with the substrate through the substrate base (e.g. -OH) and the end base of the molecule (e.g. -S-Cl_3) [14]. The novel method adopted here to form a partially covered films utilizes both features. At present, the troughs and the related apparatus are

commercial available, and various LB films were formed, characterized and applied in many fields.

4-2. Experimental

4-2-1. Chemicals

Electrolytes with pH values of 3 to 11 were used for the measurement of force-distance curves: $HClO_4$ for pH 3 to 4, phosphate buffer solutions for pH 5 to 8.5 and NaOH for pH 10 to 11 were used. The ion concentrations in phosphate buffer solutions (KH_2PO_4 + NaOH) were adjusted so that the Debye length κ^{-1} became 10 or 30 nm. The electrolytes with the Debye length of 10 and 30 nm correspond to the solutions containing a 1:1 electrolyte of 10^{-3} and 10^{-4} M, respectively. The chemicals used were commercially available G.R. grade reagents and were used as received.

4-2-2. Preparation of a partial modified surface with an organic molecule by the LB method

Fujihira et al. reported previously that the formation of a polyion complexed LB film of a mixture of carboxylic acids with a hydrocarbon (HC) and a fluorocarbon (FC) long tail, results in HC islands on top of a FC sea [7-10]. When a mixed LB film of a long alkyl (HC) trichlorosilane compound and a FC-carboxylic acid was deposited on a quartz surface, the formation of a "side by side" structure [10], i.e. HC islands surrounded by a FC sea, was found [4]. In the deposited single monolayer, the HC-silane coupling reagent was found to be polymerized and bound chemically on the quartz substrate, while the FC-carboxylic acid was adsorbed via electrostatic interaction. The sea part consisting of the FC-carboxylic acid was easily removed by

ultrasonication in ethanol [4]. An outline of the silanization on a quartz surface is illustrated in Fig. 4-2.

In the present work, quartz surfaces were chemically modified in the same procedure. A 1 mM chloroform solution of a 2:1 molar mixture of octadecyltrichlorosilane, $CH_3(CH_2)_{17}SiCl_3$ (n-OTS) and partially fluorinated carboxylic acid, $C_9F_{19}C_2H_4O$-C_2H_4-COOH (PFECA) was spread on an aqueous subphase containing 0.2 mM $CaCl_2$, and 0.05 mM $NaHCO_3$. The LB film deposition was carried out with an LB trough (Kyowa Interface Science). The compression speed was 14 cm^2 min^{-1} and the lifting speed of the substrate was 5 mm min^{-1}. The monolayer film was transferred to the quartz plate. The temperature for the LB film preparation and deposition was 15 °C. The monolayer film on the aqueous subphase was deposited at a transfer ratio of unity when the immersed quartz substrate was withdrawn at 20 mN m^{-1}. The quartz plate covered with the mixed monolayer of polymerized n-OTS (p-HC-siloxane) and PFECA was put into an 80 °C oven for 1 day to promote chemical binding of p-HC-siloxane to the quartz surface. Finally, it was cleaned in an ultrasonic bath with ethanol in order to remove PFECA.

Force measurements were performed in the similar way with chapter 3.

4-3. Results and Discussion

The LB films formed in this study are expected to be composed of the islands of p-HC-siloxane on the quartz substrate, since the FC is removed and only p-HC-siloxane remains due to the Si-O- chemical bonding to the substrate (Fig. 4-2). Figures 4-3(a) and (b) show an AFM and a friction force microscopy (FFM) [15,16] image of the chemically modified surface recorded in air, respectively. About 2 nm height of the islands from the substrate level

in Fig. 4-3(a), which is much larger than the height difference between the HC islands and the FC sea observed before ultrasonication, confirms the removal of the FC sea [4]. The FFM image shows that the friction over the island is much lower than that over the exposed quartz surface. The friction loop [7], which the indicates friction - X curve measured during forward and backward scan along a line in Fig. 4-3(b), is shown in Fig. 4-4. It clearly shows that the difference in friction between the film covered and uncovered surfaces. The difference is much greater than that between the HC islands and the FC sea [4,17]. This result also indicates that this sample has the HC islands on the quartz substrate without the FC sea.

Figure 4-5 shows the force-curves on the covered and the uncovered region in a $HClO_4$ solution of pH 3. In accordance with the result at pH 3 in Fig. 3-8 in chapter 3, where the Si_3N_4 tip was charged positively and the SiO_2 surface negatively, the attractive force was found on the uncovered region. The attractive force on the HC covered region was, however, lower than that on the uncovered region. As shown in Fig. 4-6, the force-distance curves at pH 6.8 exhibit that the force was slightly repulsive and the magnitude was almost equivalent over the covered and the uncovered region. A small repulsive force might be induced by a slight negative charge on the Si_3N_4 tip, because the IEP of Si_3N_4 is slightly lower than pH 6.8. Figure 4-7 shows the force-distance curve at pH 10. At this pH, it is expected that the dissociation of the -OH group on Si_3N_4 advances and thus both surfaces of the quartz substrate and the tip charge negatively, which results in the strong repulsive force, as shown in Fig. 4-7. The repulsive force over the covered region is weaker than that over the uncovered region.

As described above, both at the low and the high pH, the force of the

electrical double layer over the HC covered region was weaker than that over the uncovered region, independently of the repulsive or attractive force. The reason why the force was weakened has not been clarified yet. One of the possible explanation is, however, that the silane reagent reacts with some -OH sites on SiO_2 and the surface density of the -OH group decreases by the silanization reaction. Since the film was formed by the LB method, the film was almost pin-hole free. It is, however, impossible to reduce the number of the -OH group on the quartz surface completely due to the steric structure of the molecule. The remaining -OH sites show the lower double layer force. Another explanation is that the dissociation of -OH groups into $-O^-$ on the modified surface was suppressed in comparison with the uncovered surface due to lowering in dielectric constant in the vicinity of the surface -OH groups.

4-4. Conclusion

The quartz surface covered with the HC islands showed that the force-distance curve was different from that over the uncovered surface at low and high pHs. The pH dependence of the electrical double layer forces at the uncovered and the modified surfaces was interpreted in terms of the acid-base equilibrium of the surface -OH groups and the effect of chemical modification on the surface acid-base reaction.

References

1. G. Binnig, C. F. Quate and Ch. Gerber, Phys. Rev. Lett., **56** (1986) 930.
2. Y. Kim and C. M. Lieber, J. Am. Chem. Soc.,**113** (1991) 2333.
3. J. Frommer, Angew, Chem., Int. Ed. **31** (1992) 1298.
4. M. Fujihira, D. Aoki, Y. Okabe, H. Hokari, and J. Frommer, Langmuir, submitted.
5. T. J. Senden, C. J. Drummond, and P. Kekicheff, Langmuir, **10** (1994) 358.
6. T. Arai and M. Fujihira, J. Electroanal. Chem., **374** (1994) 269.
7. E. Meyer, R. Overney, R. Lüthi, D. Brodbeck, L. Howald, J. Frommer, H.-J. Güntherodt, O. Wolter, M. Fujihira, H. Takano and Y. Gotoh, Thin solid films, **220** (1992) 132.
8. M. Fujihira and H. Takano, Thin solid films, **243** (1994) 446.
9. R. M. Overney, T. Bonner, E. Meyer, M. Rüetschi, R. Lüthi, L. Howald, J. Frommer, H.-J. Güntherodt, M. Fujihira and H. Takano, J. Vac. Sci. Technol. B **12** (1994) 1973.
10. M. Fujihira and H. Kawate, Thin solid films, **242** (1994) 163.
11. I. Langmuir, J. Am. Chem. Soc., **39** (1917) 1848.
12. K. B. Blodgett, J. Am. Chem. Soc., **57** (1935) 1007.
13. K. B. Blodgett and I. Langmuir, Phys. rev., **51** (1937) 964.
14. L. Netzer and J. Sagiv, J. Am. Chem. Soc., **105** (1983) 674.
15. C. M. Mate, G. M. McClelland, R. Erlandsson and S. Chiang, Phys. Rev. Lett., **59** (1987) 1942.
16. G. Meyer and N. M. Amer, Appl. Phys. Lett., **57** (1990) 2089.
17. E. Meyer, R. Overney, D. Brodbeck, L. Howald, R. Lüthi, J. Frommer, and H.-J. Güntherodt,Phys. Rev. Lett., **69** (1992) 1777.

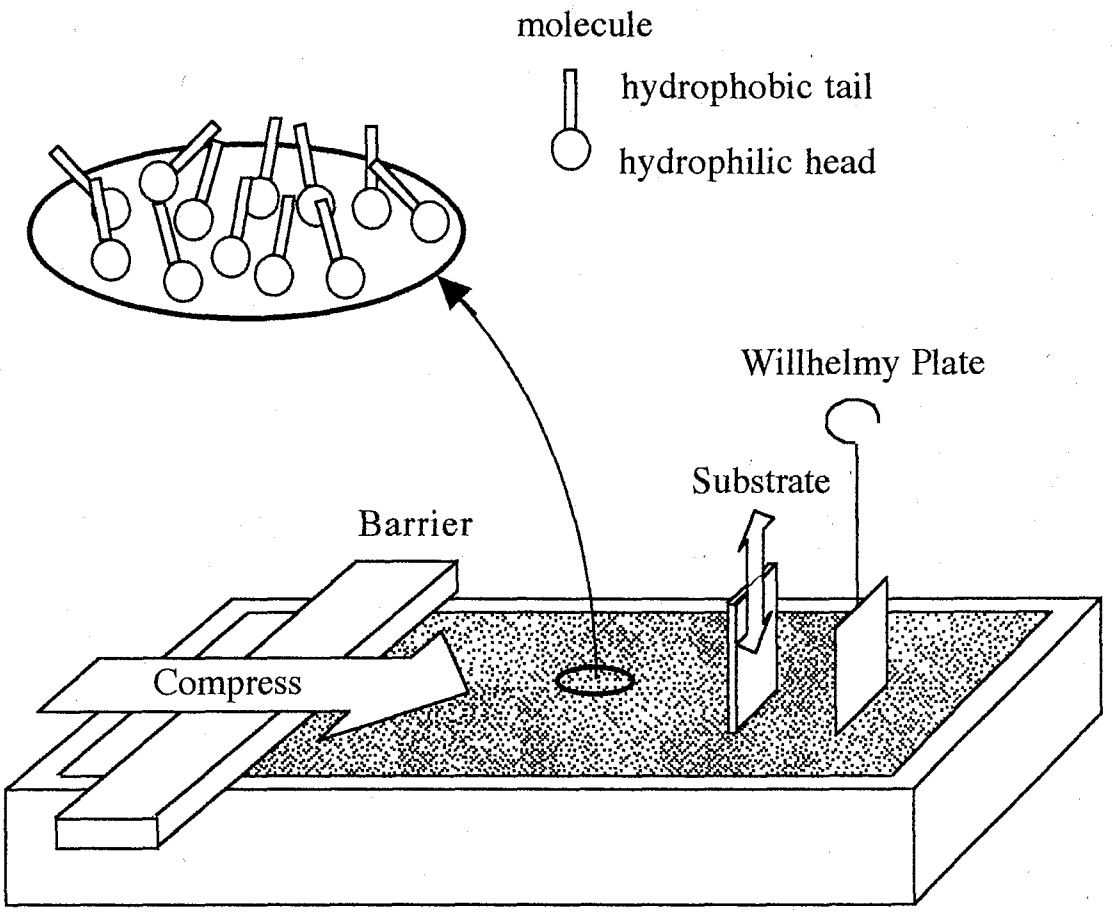

Figure 4-1. Schematic illustration of a conventional Langmuir trough.

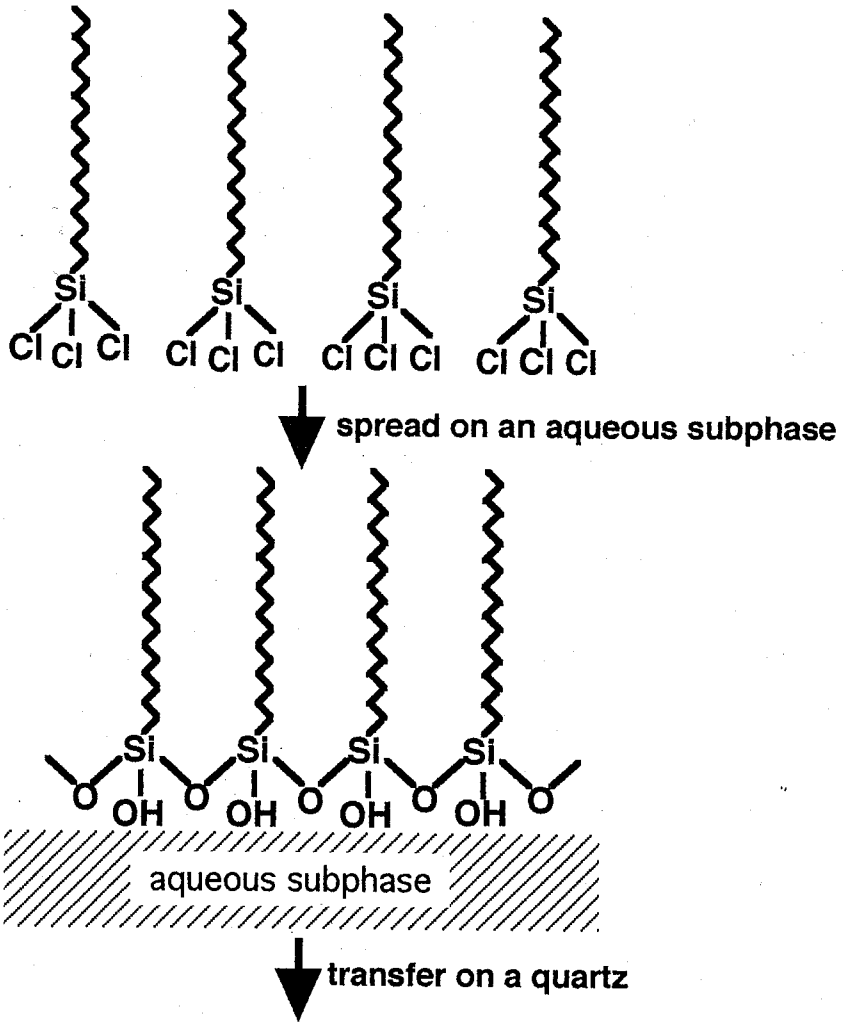

Figure 4-2. Schematic illustration of silanization reaction on a quartz surface.

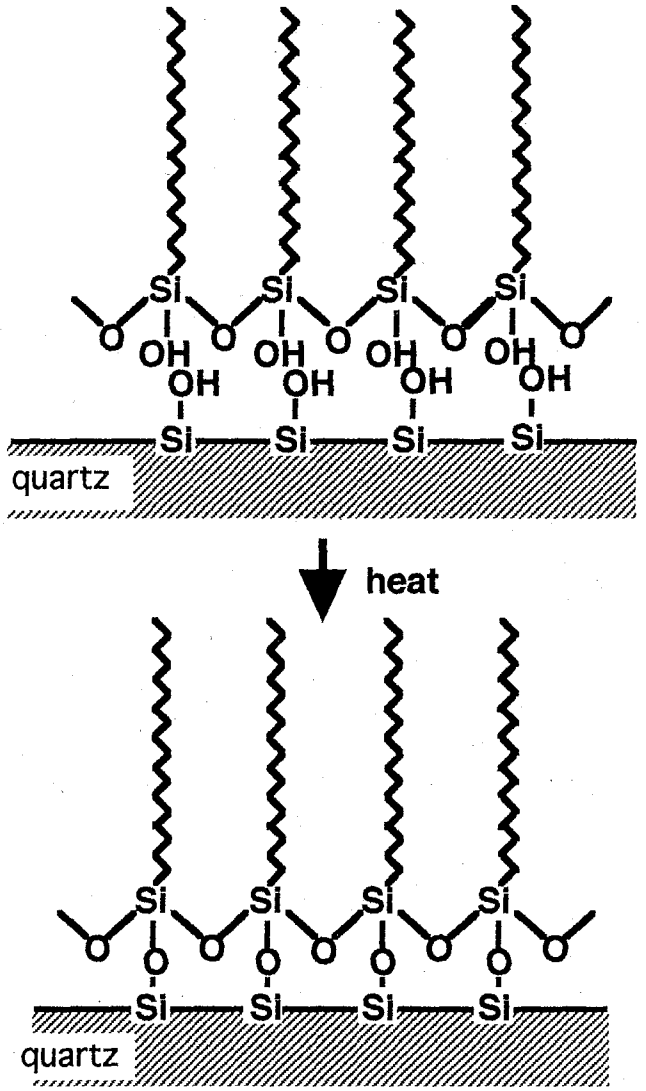

Figure 4-2. Continued.

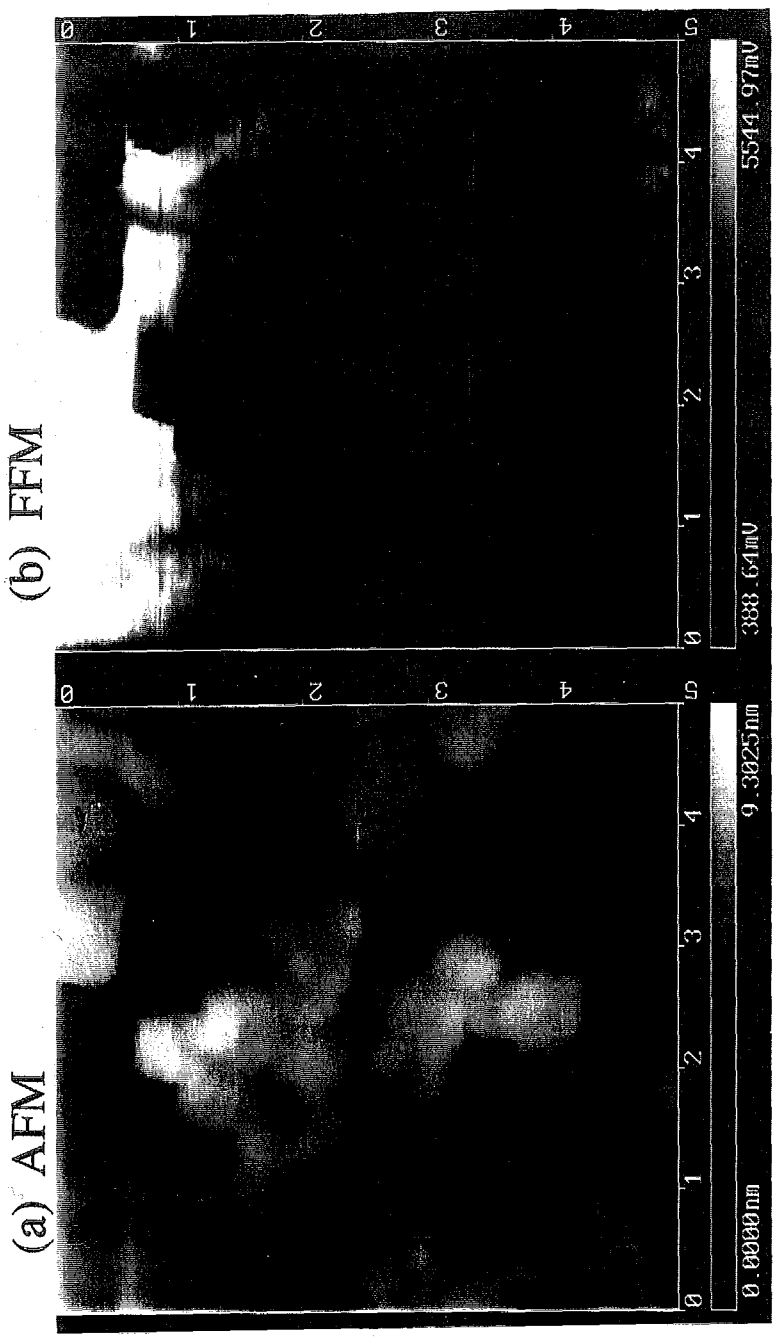

Figure 4-3. An AFM (a) and an FFM (b) image of a quartz substrate partially covered with p-HC siloxane islands in air. The scanning area is 5x5 μm^2.

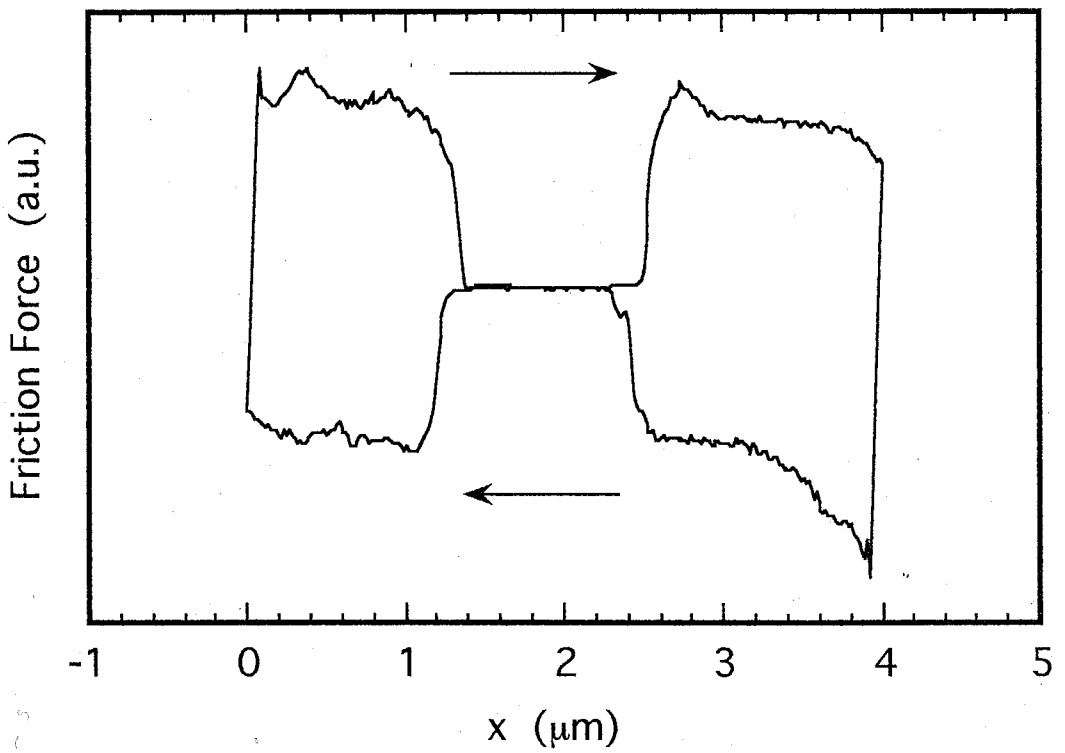

Figure 4-4. A friction loop corresponding to the friction -X curve measured during forward and backward scans along a line in Fig. 4-3(b).

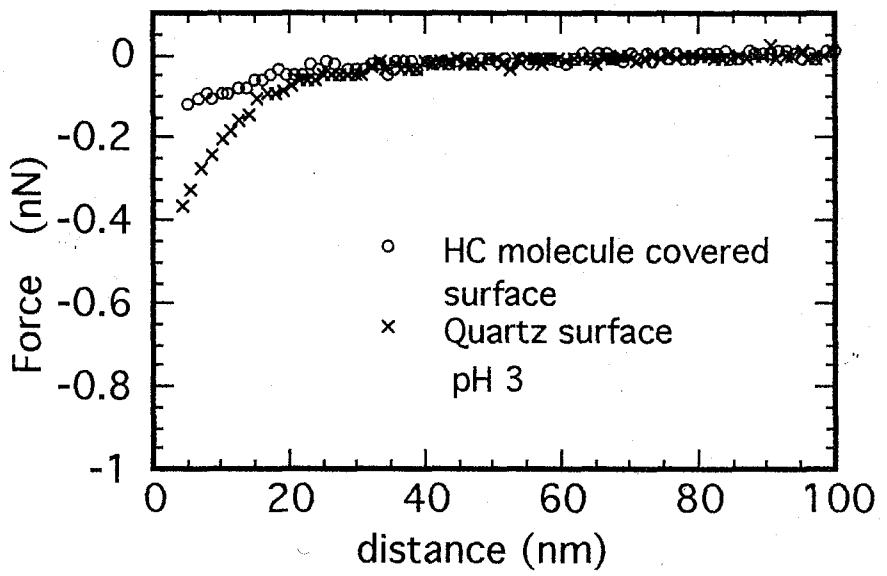

Figure 4-5. Force-distance curves over the p-HC siloxane island and an exposed quartz surface of the chemically modified quartz in $HClO_4$ with pH 3 (the Debye length 10nm).

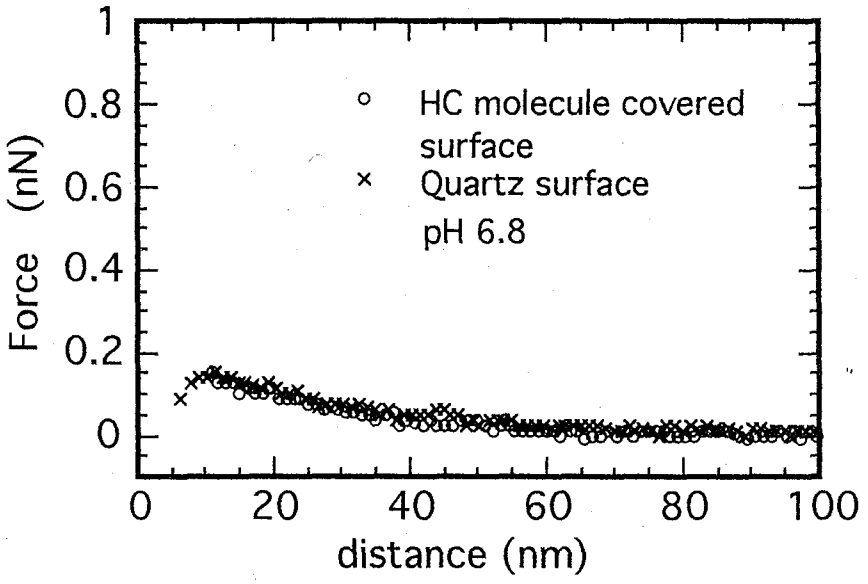

Figure 4-6. Force-distance curves over the p-HC siloxane island and an exposed quartz surface of the chemically modified quartz in a phosphate buffer solution of pH 6.8 (the Debye length 30nm).

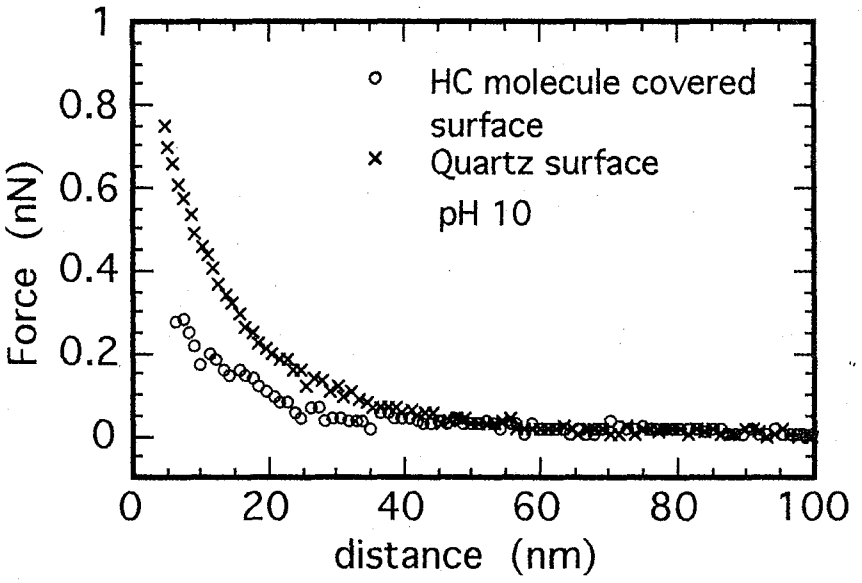

Figure 4-7. Force-distance curves over the p-HC siloxane island and an exposed quartz surface of the chemically modified quartz in NaOH with pH 10 (the Debye length 30nm).

Chapter 5

Electrical Double Layer on Potential Controlled Gold Films

5-1. Introduction

In chapter 3 and 4 [1,2], the interaction between oxide surfaces and a silicon nitride (Si_3N_4) tip in electrolyte solutions was studied by AFM. For the insulating samples and tip, their surface charges are regulated by the pH of the electrolyte [3]. The DLVO theory [4,5] is readily applicable to the case where surfaces approach each other under the condition of constant potential or constant charge [3,6]. For oxide surfaces, however, the protonation and dissociation of surface acid-base sites can be affected by the close proximity of a second surface. This is called charge regulation [7]. In this case interactions should be analyzed based the model which is intermediate between constant potential and the constant charge condition. Since early times in electrochemistry, the double layer on an isolated electrode has been studies [8-11], but there had been no concept that the interaction is induced by approaching of two electrodes, which potentials are controlled electrochemically. The surface potentials of metal electrodes can be kept constant during approach, when the potentials are controlled electrochemically by a potentiostat. Here a question arises: does the boundary condition of constant potential used in the DLVO theory hold on the approaching?

The models of the electrical double layer are also based upon a nonrealistic geometrically flat and chemically homogeneous surface, while real

electrode surfaces have roughness and inhomogeneity ranging from atomically flat to polycrystalline. The surfaces of liquid Hg and single crystals are examples of the former and the film surfaces vapor deposited with high deposition rates are examples of the latter.

The surface charge of a metal electrode is equal to zero at a potential which is called potential of zero charge (pzc) [10]. The pzc's, which are known to be related to the work functions, depend not only on the kind of metal but also on the particular crystal face of a single crystal of a metal [10,11]. Therefore, the pzc of a polycrystalline electrode surface changes from place to place and the observed large-scale pzc is the average value of these distributed pzc's from the micro scale. It is of interest to develop a new method which provides the distribution of pzc on the micro scale.

In this chapter, the interaction between a flat Au surface and a Au-covered or bare Si_3N_4 tip in an aqueous electrolyte is analyzed. When the sample and the tip are Au, the same potential is applied to both of the Au surfaces by a potentiostat. In order to minimize the effect of the charge regulation on the charge on the bare Si_3N_4 tip, a sufficiently high pH of 10.9 compared with the isoelectric point of Si_3N_4 (pH 5-6) [1] is used. The effects of the controlled potentials on the surface forces are discussed.

5-2. Experimental

An AFM (Nanoscope III, Digital Instruments (DI)) was employed to obtain force-distance curves in an electrolyte solution. An electrochemical cell supplied from DI was used. The force was measured by a laser beam deflection caused by bending of a cantilever with a spring constant of 0.12 N m^{-1}. The cantilever was made of Si_3N_4 with a pyramidal tip. Some tips were

covered by a sputtered Au film with a thickness of 30 nm. The bare tip radius and the cone angle 2θ of the shank were about 50 nm and 70°, respectively. The force-distance curves were measured by changing the sample position z with respect to the tip. The sample position was determined by the voltage applied to the piezo z-electrode corrected for the hysteresis, and the origin was chosen as a position from where a linear repulsive change started in the contact regime on a recorded deflection-sample position curve. Finally, the force curves were plotted with respect to the calibrated true separation between the sample surface and the tip apex, corrected for the cantilever bending.

The sample was formed by Au deposition on a mica sheet. The vacuum for the deposition was 2×10^{-8} Torr, the substrate temperature 400 °C, the deposition rate 0.1 nm s^{-1}, and the resulting Au thickness 200 nm. Figures 5-1 (a) and (b) show an AFM and an FFM image of a Au sample recorded in aqueous NaOH of pH 10.9, respectively. The film was not a perfect single crystal, but partially epitaxially grown with a (111) face.

The electrode potential was controlled by a potentiostat (NPGFZ-2501-A, Nikko-Keisoku). Pt wires were used as a reference and a counter electrode. The potential was expressed relative to the normal hydrogen electrode (NHE) in this study. The potential correction was performed by comparing a reduction peak potential of Au oxidation in a cyclic voltamograms (CVs) using the Pt reference electrode with the peak potential in a CV of the same Au surface in the same solution using a Ag/AgCl reference electrode. The electrolyte solution was aqueous NaOH of pH 10.9. In this solution, the thickness of the diffuse double layer, i.e. the Debye length (κ^{-1}), is 11 nm. The apparatus was set in a glove box filled with pure nitrogen gas to reduce the oxygen concentrations in the atmosphere and in the electrolyte solution.

Before all measurements, the electrolyte was bubbled with nitrogen for longer than 30 min for deaeration. Differential capacitance-potential (C-E) characteristics and CVs were measured in situ before and after the force-distance curve recording. The capacitance was measured by a two-phase lock-in amplifier with a sinusoidal modulation of 30 Hz, 5 mV in amplitude.

5-3. Results and Discussion

5-3-1. Electrochemical measurements

Figures 5-2 (a) and (b) show CVs in a 7.5×10^{-4} M NaOH aqueous solution (κ^{-1} = 11 nm) for a Au film and a Au-covered tip electrode, respectively. The separation between the sample and the tip was fixed to be about 50 μm where the electrical double layer interaction between these two electrodes can be completely neglected. The dotted lines in the figures, whose ordinate shifted by -10 mA cm^{-2}, are the CVs observed by the potential sweep between -300 and +300 mV. This potential region is called the double layer region, where no surface reactions such as oxide formation proceed. The more positive potential for oxide formation observed on the tip than on the film in the CVs with the wider potential sweep (solid lines) suggests that the sample's film surface is cleaner, perhaps due to its preparation under higher vacuum. The higher capacitive current observed in the double layer region on the tip than on the film indicates that the surface roughness on the sputtered Au tip surface is higher than the Au sample film prepared under UHV at a high temperature. The roughness difference between these two surfaces was also confirmed by the capacitance measurement described below. The following experiments were carried out only at the potentials in the double layer region.

The C-E characteristics of the film and the tip Au electrode in the double

layer region are shown in Figs. 5-3 (a) and (b), respectively. The ordinate refers to the differential capacitance per unit area, where the roughness factor of the sample surface is not taken into account. The higher differential capacitance measured on the sputtered Au tip than on the Au film confirms again the greater roughness of the former electrode. Although a slight hysteresis less than 50 mV between the voltage sweep directions was found, only the C-E curve observed under the positive sweeps is shown. A minimum near -100 mV was found for both curves, which probably corresponds to the pzc for these sample surfaces. The minimum potentials of -100 mV are much more negative than the reported pzc values ranging from +570 mV to +160 mV for different crystal faces of Au single crystals and polycrystalline Au as listed in Table 5-1. All literature values of the pzc's were measured in a solution of $HClO_4$ [12] or NaF [13], in which no specific adsorption of anions was expected to occur. The results shown in Fig.5-3 suggest that strong specific adsorption of OH^- anions occurred on both Au surfaces, which agrees with results reported by others [14,15].

5-3-2. Interaction force measurements between a Au film and a Si_3N_4 tip

The interaction force was measured between a Au film, whose potential was controlled by a potentiostat, and a Si_3N_4 tip, immersed in a 7.5×10^{-4} M NaOH solution of pH 10.9, as shown in Fig.5-4 schematically. The surface of the Si_3N_4 tip charges negatively in an electrolyte solution of pH 10.9 because the isoelectric point of the Si_3N_4 tip was determined to be about 5 as reported previously [1,2]. The force would be attractive if the Au sample surface were positively charged, and repulsive if it were negatively charged. The forces

were measured, however, always to be repulsive, independent of the potential being on the negative or positive sides of the pzc, as shown in Fig.5-5.

To clarify the electrical double layer contribution, the measured force at a constant separation of 13 nm was plotted as a function of the electrode potential as shown in Fig.5-6. At this separation of 13 nm, the van der Waals attractive force contribution to the measured force was found to be negligible, which was consistent with the theoretical calculation. The diffuse double layers on both surfaces were overlapped significantly at this separation to give the measurable electrical double layer force, because the Debye length was 11 nm at the electrolyte concentration used. The electrical double layer force was expected to be weak near the pzc of the film Au electrode and in fact the minimum in the force was observed near -100 mV. The potential was very close to that for the minimum of the C-E characteristics shown in Fig.5-3(a). A repulsive force, on the other hand, was observed at potentials on both sides of the pzc and increased as the potentials diverged from the pzc. The increase in repulsive force on the negative side of the pzc is understandable in view of the repulsive electrical double layer interaction between the charged surfaces with the same sign [4,5]. However, on the positive side of the pzc, an attractive electrical double layer force was expected according to theories of interactions between dissimilar surfaces [16,17]. An increase in the negative diffuse double layer potential even at the positive side of the pzc has been reported at Hg electrodes where anions were adsorbed specifically [18]. Our results strongly support the specific adsorption of OH^- anions on the Au electrode surface; the adsorbed OH^- anions overcompensate the positive charge at the Au surface at potentials more positive than the pzc. Figure 5-7 shows a schematic image of the electrical double layer on the Au surface in aqueous

NaOH. In this way, the double layer force measurements can provide us the direct evidence of specific anion adsorption.

5-3-3. Interaction force measurements between a Au film and a Au-covered tip

The potential value of each surface can not be estimated from the measurement of the surface forces between two different materials, because the measured forces depend only on the product of the two potential values [16,17]. It should be noted here that the surface potential used in colloid science corresponds to the potential at the outer Helmholtz plane, Ψ_2, used in electrochemistry. The force measurements between the same materials under the same controlled equivalent potential were performed to obtain the diffuse double layer potential near the surface, as shown in Fig.5-8 schematically.

In general, the pzc of even the same material changes at different crystal faces [10,13] as shown in Table 5-1. The Au-covered tip and the Au film electrode, however, showed similar C-E characteristics as shown in Fig.5-3, indicating that both surfaces have almost the same pzc. This coincidental agreement in the pzc between the polycrystalline Au-covered tip and the epitaxitially grown Au film electrode can be the influence of reconstruction of the Au single crystal face on the sample [13,19] or of the specific adsorption of OH^- [15]. In the present study, potentials were cycled before the C-E measurements in the potential region including Au oxidation. A detailed study on this point is now under investigation. In the following experiment, the potentials for both of the Au electrodes were kept the same by the potentiostat and thus both tip and sample were expected to have the same diffuse double layer potentials. The electrolyte used was the same 7.5×10^{-4} M NaOH solution

of pH 10.9 as in the above measurements.

Figure 5-9 shows the interaction force measured at the same separation of 13 nm as in Fig.5-6 as a function of the controlled potentials. The force decreased more steeply near the pzc than in Fig.5-6 and increased as the potential diverged from the pzc on both sides of the pzc. Since the tip and the sample were at the same potential, the forces were always expected to be repulsive regardless of the polarity of the potential. From the above result obtained with the bare Si_3N_4 tip and the Au sample film described in section 5-3-2, it can be safely concluded that the potential in the diffuse double layer is always negative regardless of the electrode potential. The more enhanced increase in the repulsive force between the Au-covered tip and the Au sample film near the pzc can be attributed to the simultaneous increase in the charge of the Au-covered tip in contrast with the constant negative charge of the bare tip under a constant pH.

The open circle dots in Fig.5-10 are the measured force curve at electrode potentials of +20 mV. The curve calculated from the DLVO theory under the constant potential condition is also plotted in Fig.5-10. In this calculation, for the electrical double layer force, the strict DLVO theory [3,5,9] was used rather than the previous approximate method [1] by taking into account tip geometry [1]. The Hamaker constant was estimated to be 40×10^{-20} J by Derjaguin [20] and the tip geometry was calculated by the radius described in the specification by the supplier (DI) and the estimated thickness of the sputtered Au film. From this fitting, the potential at the outer Helmholtz plane, Ψ_2, is estimated to be about -230 mV. Even taking into account the more negative pzc value of -140 mV shown in Fig.5-9 than -100 mV in Fig.5-3, the potential at the Au surface from the pzc was calculated to

be +160 mV. The potential at the outer Helmholtz plane, Ψ_2, should be smaller than this potential of +160 mV. This discrepancy may arise from i) too small an estimated value for the tip radius [1], ii) too large a value for the spring constant of the used cantilever [21], and/or iii) too large a value used as the Hamaker constant than realistic [22].

Throughout the present experiment, an inhomogeneous distribution of force in the x-y plane was not clearly observed. The result indicates that domain sizes of single crystal faces, especially after the reconstruction, were smaller than the lateral resolution of the electrical double layer force measurements. The lateral resolution was expected to be larger than the tip-sample distance used, i.e. 13 nm.

5-4. Conclusion

The interaction between two approaching electrodes, the potentials of which were electrochemically controlled, has been measured and characterized for the first time. Force-distance measurements with an AFM in an electrolyte solution can afford an analysis of the electrical double layer. The potential of the outer Helmholtz plane of the electrical double layer can be also estimated from the analysis. By controlling the electrode potentials of the sample surface and/or the metal coated tip, the pzc's of metals can be readily determined. Using this technique, pzc's were determined for a Au-covered tip and a Au sample film in a NaOH solution of pH 10.9. These results together with sign of the electrical double layer force confirmed the specific adsorption of OH^- to Au reported in the literature. The contribution from the AFM will expand the range of analytical techniques for the study of the electrical double layer structure, especially as a function of the distance from the electrode

surface [1,2,23], and for mapping the potential [24] at the outer Helmholtz plane, Ψ_2, with high lateral resolution in a x-y plane.

References

1. T. Arai and M. Fujihira, J. Electroanal. Chem., **374** (1994) 269.
2. T. Arai, D. Aoki, Y. Okabe, and M. Fujihira, Thin solid films (in press).
3. R. J. Hunter, *Foundations of Colloid Science*, Oxford University Press, New York, (1987).
4. B. V. Derjaguin and L. Landau, Physicochim., URSS **14** (1941) 633.
5. E. J. W. Verwey and J. T. G. Overbeek, *Theory of the Stability of Lyophobic Colloids*, Elsevier, Amsterdam, (1948).
6. J. N. Israelachvili, *Intermolecular and Surface Forces*, 2nd ed., Academic Press, San Diego, (1991).
7. T. W. Healy, D. Chan, and L. R. White, Pure Appl. Chem., 52 (1980) 1207.
8. D. C. Grahame, Chem. Rev., **41** (1947) 441.
9. J. T. G. Overbeek, *Colloid Science*, H.R.Kruyt Eds., Elsevier, Amsterdam, (1952).
10. P. Delahay, *Double Layer and Electrode Kinetics* , Interscience, New York, (1965).
11. R. Parsons, Chem. Rev., **90** (1990) 813.
12. Z. Borkowska and U. Stimming, J. Electroanal. Chem., **312** (1991) 237.
13. A. Hamelin, T. Vitanov, E. Sevastyanov, and A. Popov, J. Electroanal. Chem., **145** (1983) 225.
14. D. D. Bode, Jr., T. N. Andersen, and H. Eyring, J. Phys. Chem., **71** (1967) 792 .
15. S. Strbac, A. Hamelin, and R. R. Adzic, J. Electroanal. Chem., 362 (1993) 47.

16. R. Hogg, T. W. Healy, L. R. White, Trans. Faraday Soc., **62** (1966) 1638.

17 D. McCormack, S. L. Carnie, D. Y. C. Chan, J. Colloid Interface Sci., **169** (1995) 177.

18. D. C. Grahame and B. A. Soderberg, J. Chem. Phys., **22** (1954) 449.

19. H. Honbo, S. Sugawara, and K. Itaya, Anal. Chem., **62** (1990) 2424.

20. B. V. Derjaguin, Y. I. Rabinovich, and N. V. Churaev, Nature, **272** (1978) 313 .

21. J. P. Cleveland, S. Manne, D. Bocek, and P. K. Hansma, Rev. Sci. Instrum., **64** (1993) 403.

22. V. A. Parsegian and G. H. Weiss, J. Colloid Interface Sci., **81** (1981) 285.

23. C. J. Drummond and T. J. Senden, Colloids. Surf. A: Physicochem. Eng. Aspects, **87** (1994) 217.

24. T. J. Senden, C. J. Drummond, and P. Kekicheff, Langmuir, **10** (1994) 358 .

Table 5-1. Point of zero charge for the two type of Au electrodes in the present work and different crystal faces of Au single crystals and polycrystalline Au reported in Refs. 12 and 13.

Au	$7.5x10^{-4}$M NaOH (mV *vs.* NHE)	1 mM $HClO_4$ (mV *vs.* NHE)	10 mM NaF (mV *vs.* NHE)
Au film electrode	-100		
Au covered tip electrode	-100		
(111)			+570 [13]
(100)			+380 [13]
(110)			+190 [13]
polycrystalline		+190 [12]	+160 - +190 [13]

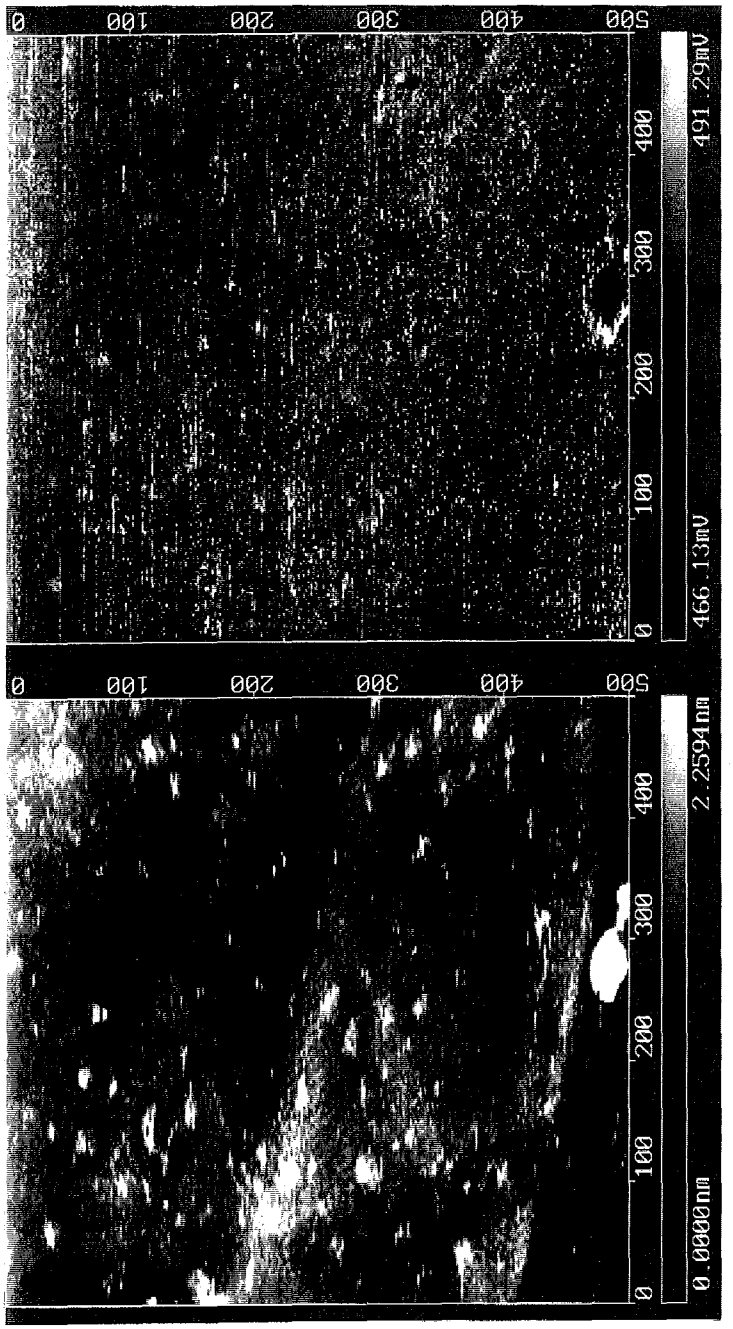

Figure 5-1. An AFM (a) and a FFM (b) image of a Au sample recorded in aqueous NaOH of pH 10.9. The scanning area is 5x5 μm^2.

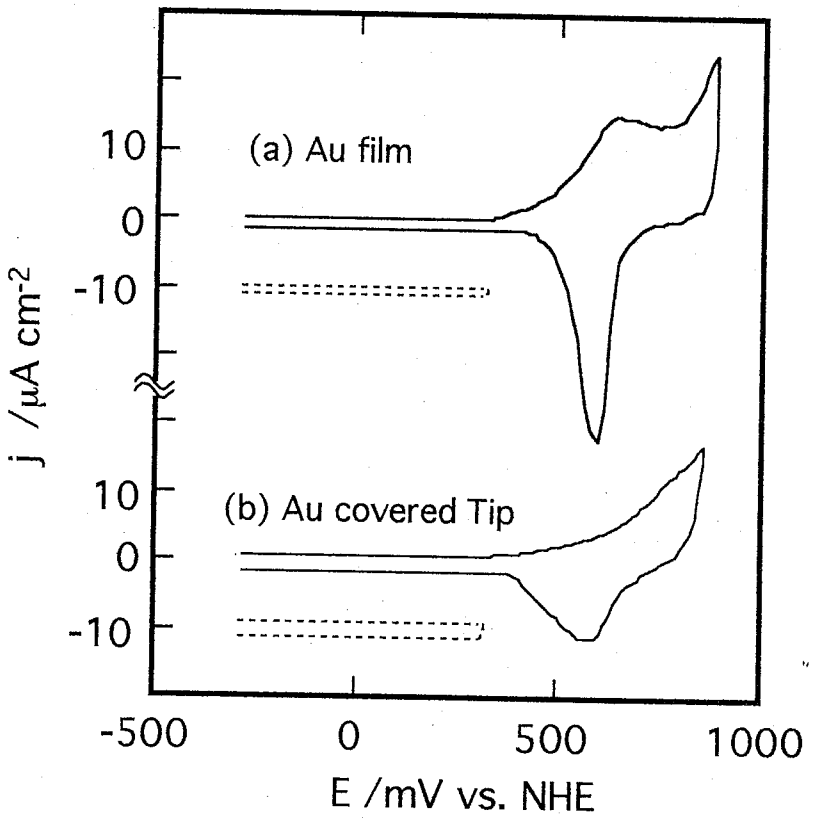

Figure 5-2. Cyclic voltamograms (CVs) for (a) a Au film on a mica sheet and (b) a Au-covered tip in 7.5×10^{-4} M NaOH. The sweep rate is 20 mV s^{-1}. The dotted lines are the CVs under a potential sweep only in the double layer potential region from -300 to +300 mV. The currents were normalized with geometric electrode areas.

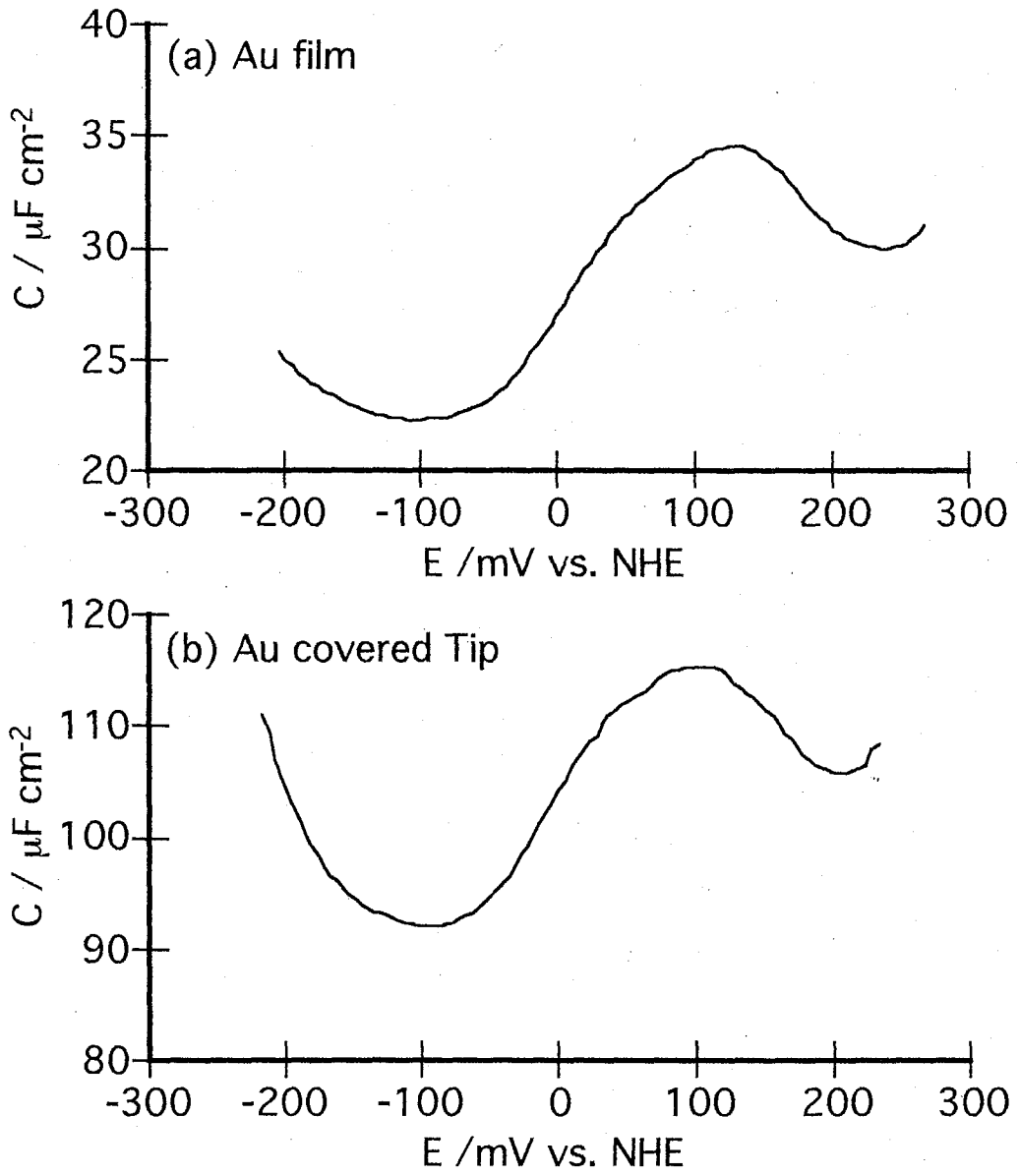

Figure 5-3. Differential capacity of (a) a Au film on a mica sheet and (b) a Au-covered tip in 7.5×10^{-4} M NaOH. The sine modulation was 30 Hz in frequency and 5 mV in amplitude, and the voltage sweep rate was 4 mV s^{-1}.

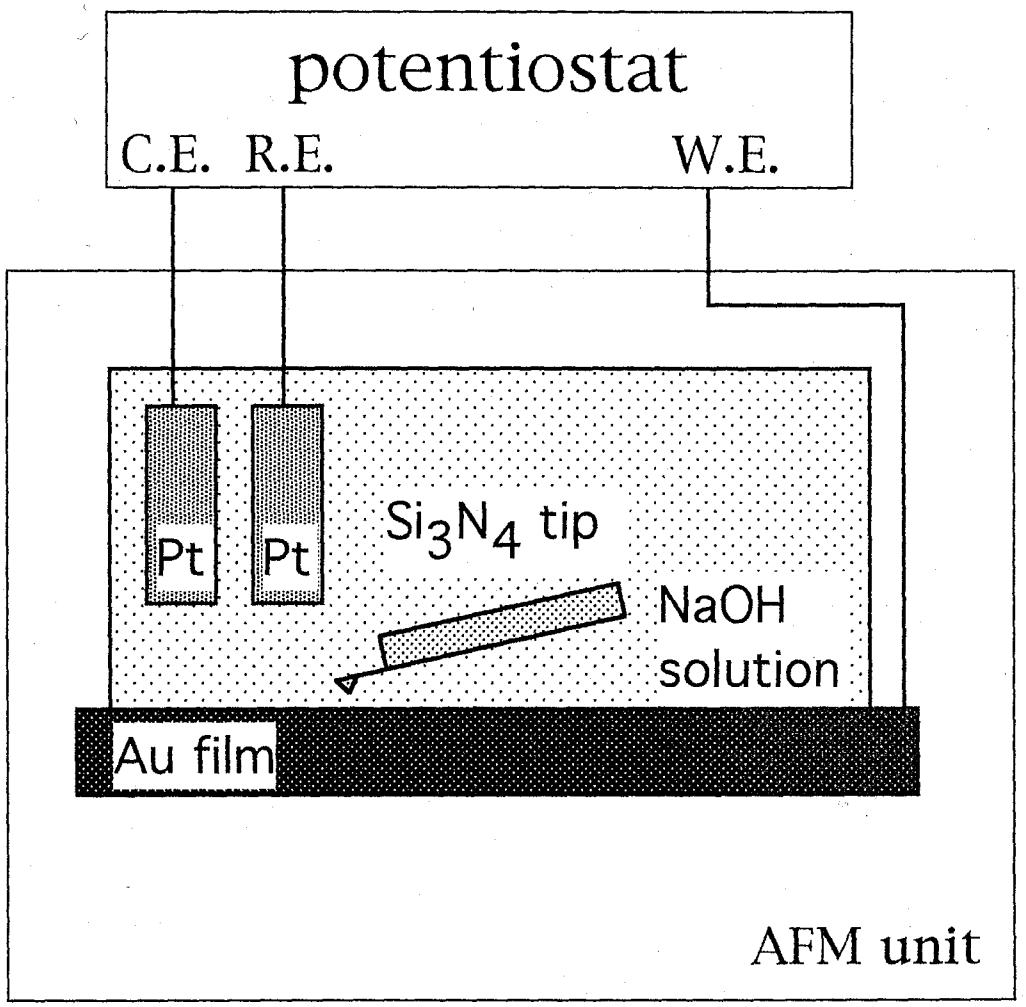

Figure 5-4. Schematic diagram of the experimental setup used in the force measurements between a Au film and a Si_3N_4 tip. A sample of Au film is set on a sample stage on top of a tube piezo scanner of the AFM, the potential of which is electrically connected to the working output of a potentiostat. Two Pt wires are inserted in the cell as a reference electrode and a counter electrode, respectively.

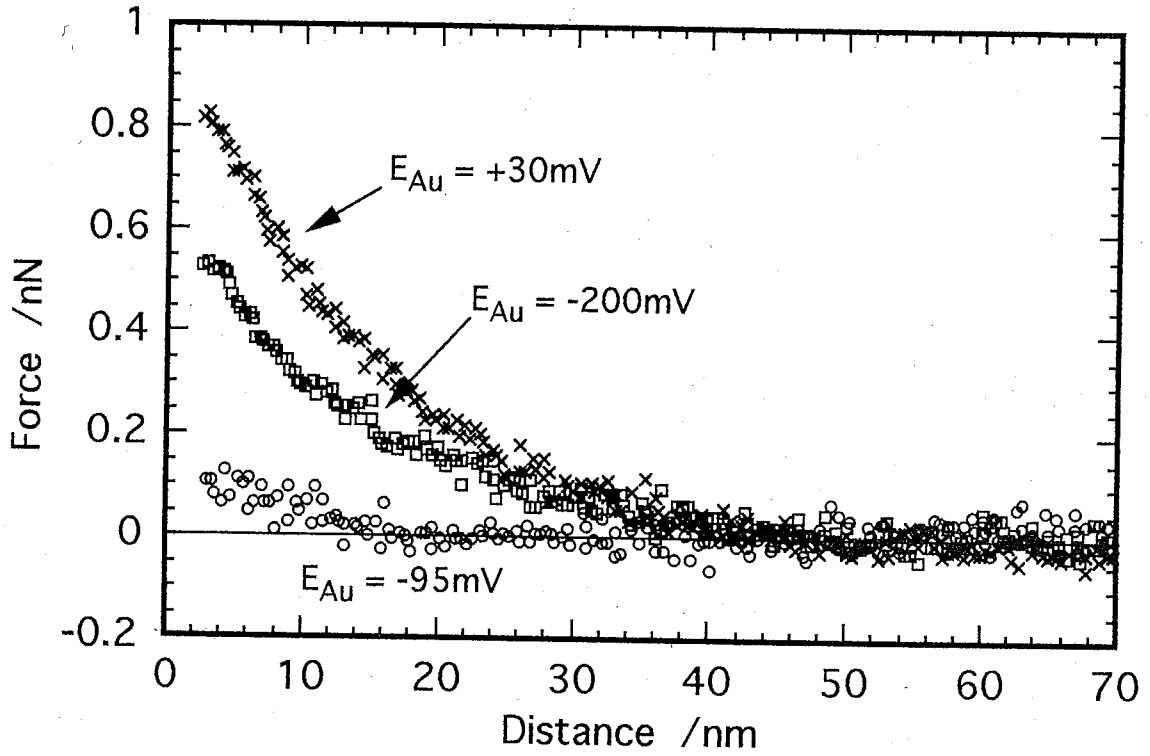

Figure 5-5. Force-distance curves between a Si_3N_4 tip and a Au film whose potentials were controlled at -200, -95, and +30 mV.

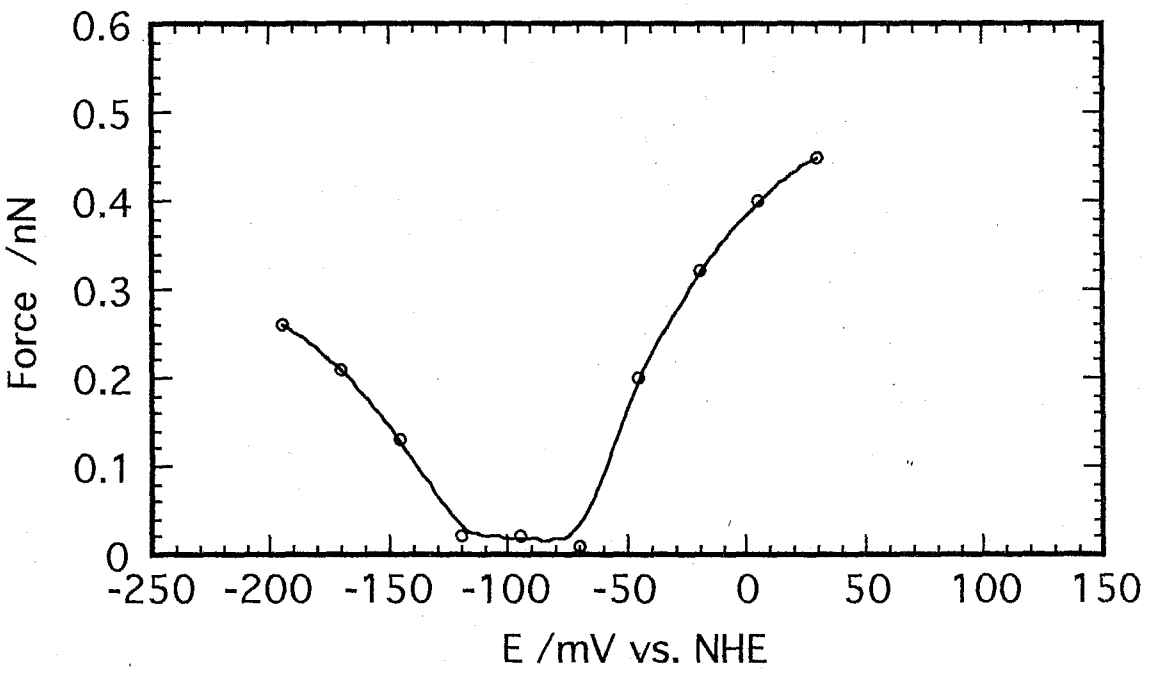

Figure 5-6. Potential dependence of surface forces at a separation of 13 nm between the Si_3N_4 tip and the surface of the Au sample film.

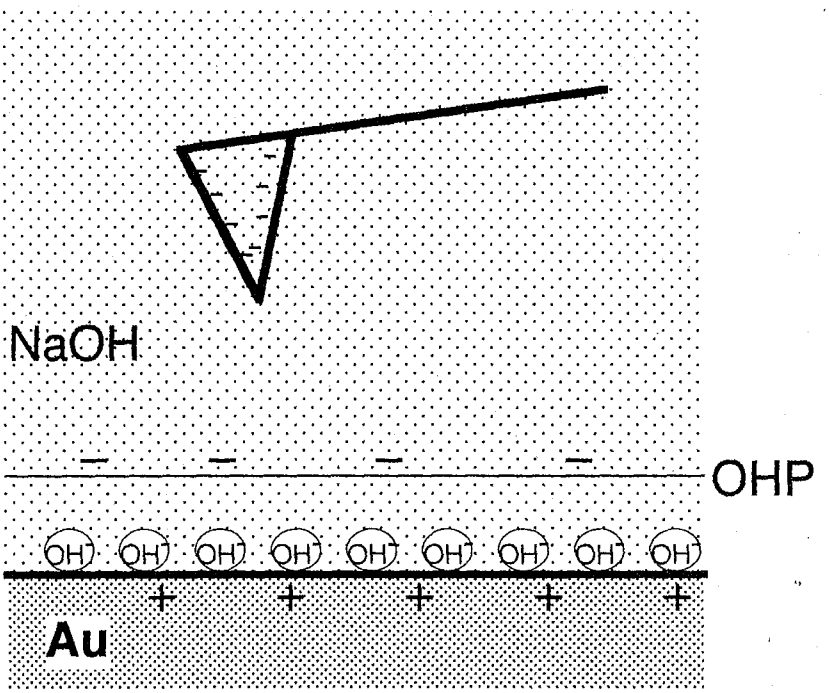

Figure 5-7. Schematic image of the electrical double layer on the Au surface in aqueous NaOH.

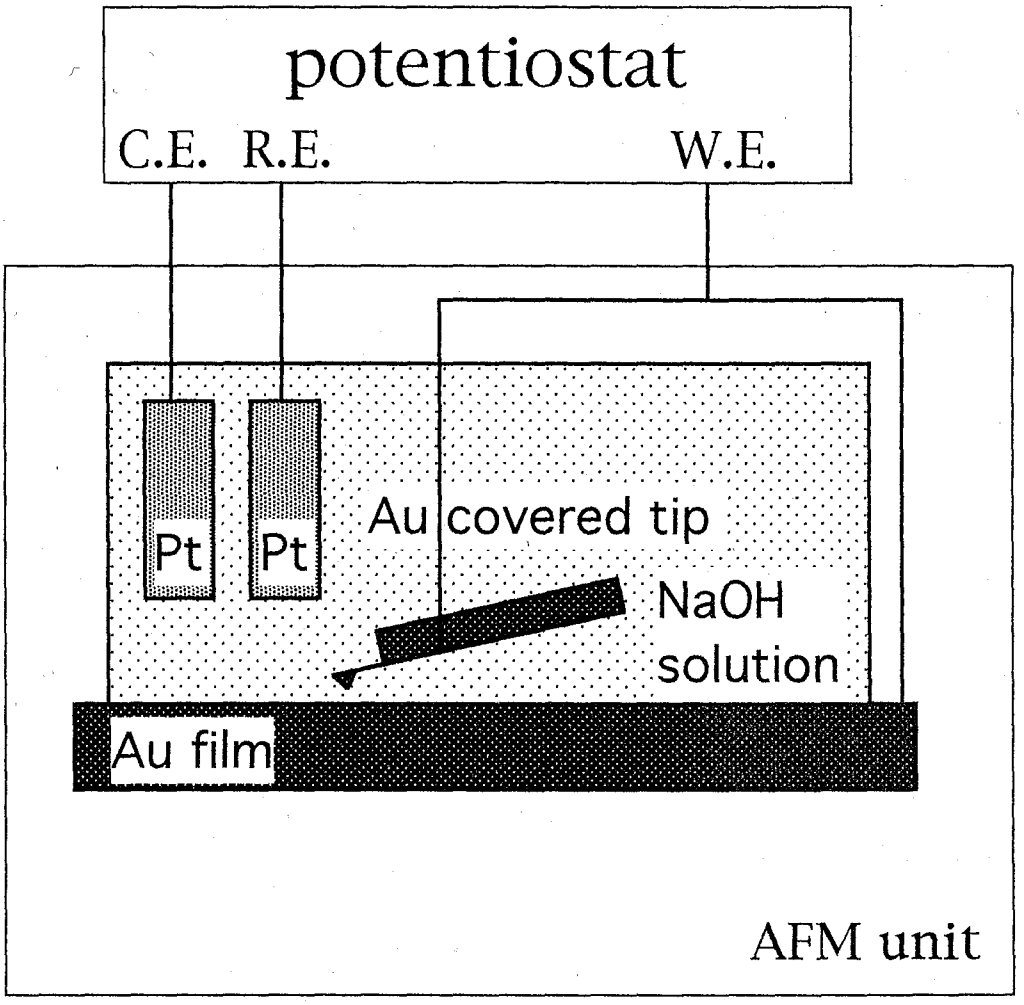

Figure 5-8. Schematic diagram of the experimental setup used in the force measurements between a Au film and a Au-covered tip. A Au film and a Au-covered tip are electrically connected and electrochemically controlled as a working electrode by a potentiostat. Thus the potentials of the two Au are the same.

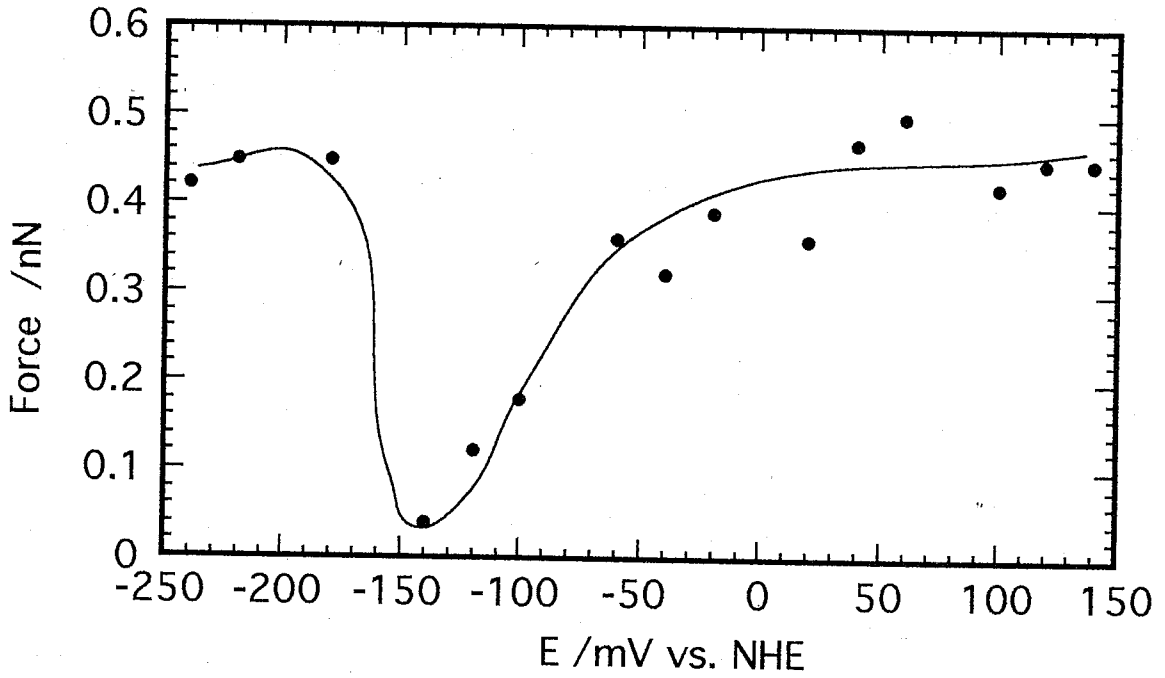

Figure 5-9. Potential dependence of surface forces at a separation of 13 nm between a Au-covered Si_3N_4 tip and the surface of Au film. The potentials for both Au surfaces were always the same.

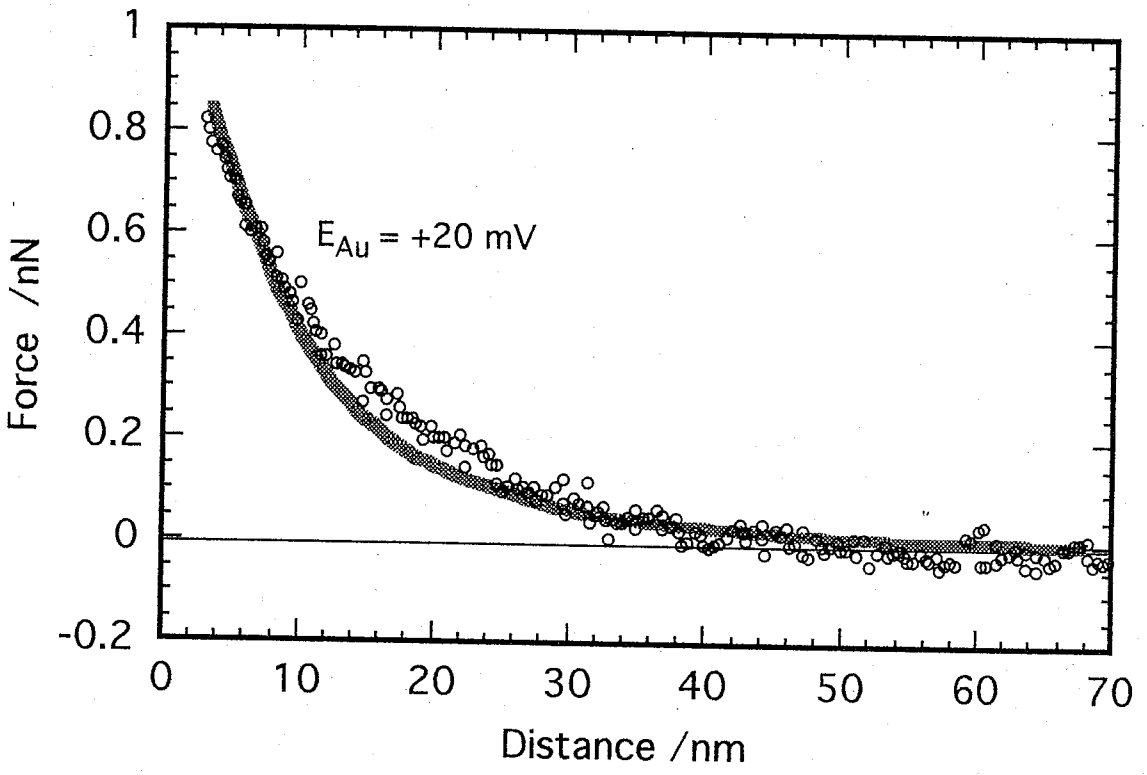

Figure 5-10. A force-distance curve between the Au-covered tip and the Au film whose potentials were controlled at +20 mV. The line indicates the DLVO fit, where 40×10^{-20} J [20] was adopted as the Hamaker constant for a Au/water/Au system.

Chapter 6

A New Method to Measure Surface Tension for Solid Electrodes

6-1. Introduction

Understanding the structures of electrical double layers formed at the interfaces between solids and liquids can be achieved through the detailed analysis for the surface excess and the surface charge density by measuring the double layer capacitance, the surface tension, and so on. The surface tension and the surface charge density are deeply interconnected according to the Lippmann equation [1]. The surface tension and the capacitance can be measured directly, and the potentials for the maximum of the surface tension and the minimum of the capacitance can be used to determine the point of zero charge (pzc). The pzc is electrochemically referred to the applied bias voltage giving no charge on the electrode surface. Grahame [2], Delahay [3], and Parsons [4] have independently reported the meaningful results for the electrical double layers of liquid mercury in aqueous solutions. However, their methods can not be applied to solid metal electrodes to obtain the surface tension. Although Beck suggested the method [5] to estimate surface tension by measuring the stretch of a metal ribbon with applied voltage, the ratio of the stretch to the ribbon length is small and then it is not easy to measure the surface tension precisely.

In this chapter, the author suggests a novel method to measure the change in surface tension on a solid electrode with applied bias voltage, using atomic

force microscopy (AFM) [6], which utilizes the laser beam deflection to measure the displacement of a microfabricated cantilever. As an example of measuring the surface tension of solid electrodes, Au films in contact with an $HClO_4$ aqueous solution is used. Since it was reported that ClO_4^- ions are hardly adsorbed specifically [7], many researches have carried out the capacitance measurements in the double layer of Au electrodes in aqueous $HClO_4$ solutions [7-9]. In chapter 5, the specific adsorption of OH^- was indicated from the results of the force measurements. In this chapter, therefore, the specific adsorption of OH^- on Au surface is also discussed on the basis of the potential dependence of surface tension, which is evaluated by this new method of surface tension.

6-2. Principle of Surface Tension Measurements

A schematic diagram of a novel method to measure the change in surface tension with applied voltage is shown in Fig.6-1. This setup utilizes an AFM apparatus with a microfabricated cantilever immersed in an electrolyte. On one side of the cantilever, a Au film (ca. 30 nm) was coated by spattering. The potential of the Au film was controlled by a potentiostat. The one-side Au coated cantilever is bent by the difference in surface tension between the bare side and the coated side. By AFM we can measure the deflection of the cantilever with high precision better than 0.1 Å. The cantilever is made of single crystal Si, and the oxidation layer formed on the bare surface exhibits electric insulating. Then the change in bending with applied voltage is attributed to the change in surface tension on the Au-coated surface.

Hereinafter the relation between the bending of the cantilever (δ) and the change in the surface tension (γ) will be described. Figure 6-2 shows a

schematic structure of a cantilever referred to a rectangular cantilever formed from a homogeneous material (Si). The left end of the cantilever is fixed to a thick Si body (a Si pad) and the other end stands free. The bottom side of the cantilever is coated with a very thin Au film. The mechanical properties of the cantilever, such as the Young's modulus, are assumed to be unchange by the coating. The bending force (F), which equals the surface tension time the width (w) of the cantilever, exerts at the bottom corner on the right end of the cantilever to the - x direction,

$$F = \gamma w \qquad (6.1)$$

Since the Au layer is thin compared with the thickness of the cantilever, the neutral plane of the bending is the middle plane of the cantilever, y=0. The bending moment at an arbitrary position on the x axis is given by

$$M = -\frac{d}{2} F$$

$$= -\frac{\gamma w d}{2} \qquad (6.2)$$

The bending δ and the bending moment is related as follows,

$$\frac{d^2\delta}{dx^2} = -\frac{M}{EI} \qquad (6.3)$$

$$I = \frac{wd^3}{12} \qquad (6.4)$$

where E is the Young's modulus, I the second moment of area. Thus integrating equation (6.3) two times, we obtain

$$\delta = -\frac{M}{EI}\left(\frac{1}{2}x^2 + C_1 x + C_2\right) \qquad (6.5)$$

At x=0, then $\frac{d\delta}{dx} = 0$ and $\delta = 0$, the above equation leads to

$$\delta = -\frac{Mx^2}{2EI} \qquad (6.6)$$

At the free side of the cantilever, $x=l$. Introducing (6.2) and (6.4) into (6.6)

$$\delta_{max} = -\frac{Ml^2}{2}$$

$$= \frac{3\gamma l^2}{Ed^2} \qquad (6.7)$$

Finally, the equation of the surface tension γ is obtained as follows:

$$\gamma = \frac{Ed^2}{3l^2}\delta_{max} \qquad (6.8)$$

For example, E=1.65x10^{11} Pa for Si, d = 1.7 μm, w = 48 μm and l = 439 μm for the cantilever used in this study, then the following formula is obtained,

$$\gamma\ [\text{mN m}^{-1}] = 0.825 \times \delta_{max}\ [\text{nm}] \qquad (6.9)$$

In our AFM measurements, only the change in the bending is evaluated. The change is expressed as follows:

$$\Delta\gamma = \gamma - \gamma_{max} \qquad (6.10)$$

where γ_{max} is the surface tension given at pzc.

6-3. Experimental

A commercial AFM (SPA300 with a controller of SPI-3700, SEIKO Instruments) was employed for the surface tension measurements. The laser beam deflection was measured by a 4-sectioned position sensor of a photodiode. The Si cantilever, which is made of single crystal silicon by microfabrication, is commercially available (Nanoprobe). The cantilever was cleaned with ethanol, acetone and ethanol again, and then heated at 80 °C in an RCA alkali solution (H_2O_2 : NH_4OH : H_2O = 1 : 1 : 5) [10] for 1 min and rinsed with milli-Q water. Since the RCA alkali solution is a strong oxidant, the above procedure not only removes organic contaminant, but also forms an oxide layer on the surface: the cantilever surface was covered with an oxide layer, about 1 nm thick [10]. Then the one side of the cantilever was Au-sputtered with a thickness of about 30 nm. The spring constant of the cantilever was 0.11 N m^{-1}, and the size was described in the above section. The Au film was electrically connected through a Au wire covered with resin of electric insulator. The potential of the Au film electrode was controlled by a potentiostat (NPGFZ-2501-A, Nikko-Keisoku). The Au-coated cantilever and two Pt wires were immersed in an electrolyte in an AFM electrochemical cell, where the Au film acted as a working electrode, Pt wires acted as a counter electrode and a reference electrode. The potential was referred to the normal hydrogen electrode (NHE). The potential correction was performed by comparing the rereduction peak potentials of the same Au film electrode in the same solution between cyclic voltamograms (CVs) using the Pt and a Ag/AgCl reference electrode. The electrolyte aqueous solution were 10^{-3} M $HClO_4$ and 10^{-3} M NaOH. The AFM apparatus was set in a glove box filled

with pure nitrogen gas to reduce the oxygen concentrations in the atmosphere and in the electrolyte solution. Before all measurements, the electrolyte was bubbled with nitrogen for longer than 30 min for deaeration. Additionally to the above surface tension measurement, the capacitance of the Au film was measured by a lockin amplifier.

6-4. Results and Discussion

Figures 6-3 (a) and (b) show cyclic voltamograms (CVs) in a 10^{-3} M $HClO_4$ (pH 3) and a 10^{-3} M NaOH (pH 11) aqueous solution for a Au film electrode, respectively. On sweeping the voltage positively, the Au surface was oxidized and the oxidation current was detected. On the other hand, negatively, the oxide surface was rereduced to a bare Au surface backwardly. The difference in the peak potentials in (a) and (b) comes from the different pHs of the solutions. On the negative side of the rereduction peak, the flat potential regions up to the H_2 generation are observed. This potential region is called the double layer region, where no surface reactions proceed such as oxide formation. The surface tension and capacitance measurements were carried out only in the double layer region.

Figure 6-4(a) shows the characteristics of surface tension versus the electrode potential in the double layer region in $HClO_4$ and NaOH solutions. The ordinate indicates the value $\Delta\gamma$, which is the decrease in the surface tension from the maximum value, expressed in eq.(6.10). The voltage sweep rate was 20 mV s^{-1}. Both of the curves exhibit parabolic. The parabolic shape of these are resembled to so called electrocapillary curves for liquid metals such as Hg [2]. The electrocapillary curves are also called the γ-E curve. The resemblance confirmed that the surface tension of the solid electrode was

measured successfully by the present method.

The maximum of the curve in $HClO_4$ was found to be about 200 mV. The potential at the maximum should correspond to the pzc: the maximum of the surface tension means that the repulsive interaction between the charges homogeneously distributed on the surface is the weakest, so that the charge should be zero at the maximum point, pzc. This result explicitly indicates that the method suggested in this study is a very powerful tool to determine the pzc value of solid electrodes, and moreover, by differentiating the curve the charge density can be evaluated.

To justify the method to measure the surface tension directly, an experiment with a cantilever without Au-coating and a pad with Au-coating was carried out. A Au wire was connected to the pad with Au-coating. If the reflectivity of Si were changed by the change in the potential, the photo-voltage of the diode would be affected by the change in intensity of the reflected beam, even if there were no difference in the surface tensions between the top and bottom part of the cantilever. Figure 6-4(b) shows the photodiode output observed with the bare cantilever in 10^{-3} M $HClO_4$ solution. No change with the potential was observed suggesting that difference in the surface tensions and the reflectivity of the bare Si were not affected by the potential control at the pad. In other words, Si was insulated by the oxide layer formed by the chemical oxidation. Therefore, it is obvious that the measured change with the Au-coated cantilever was caused by the change in the surface tension of the Au film electrode on the cantilever.

The capacitance-potential curve, which has been usually used for determination of pzc of solid electrodes, was measured in 10^{-3} M $HClO_4$ solution and is shown in Fig.6-5. The curve in Fig.6-5 shows a minimum at

the potential about 220 mV, which is close to the potential obtained from the maximum of the surface tension vs. potential curve. Because the polarity of the charge at the electrode surface changed at the pzc depending on the applied potential, the minimum of the capacitance curve and the maximum of the surface tension curve should agree with each other. The literature values of pzc [7,11,12] determined by the capacitance method.were +160 - +200 mV in the same electrolyte These are also close to the value obtained in this study.

The γ-E curve in Fig. 6-4(a) in a NaOH solution shows a maximum at about -100 mV. This pzc value agrees with those of the potentials in chapter 5, which were estimated from a minimum in the C-E characteristics or a minimum interaction force with the AFM tip as a function of the potential. Grahame measured mercury electrocapillary curves in various solutions and found that the maximum point was shifted negatively as the specific adsorption became stronger [2]. It is concluded from the results in chapter 5 and Fig.6-4(a) that the specific adsorption of OH^- anion shifted the pzc value of Au surface toward the negative potential by about -300 mV.

6-5. Conclusion

The author proposed a novel method to evaluate the surface tension of solid electrodes in an electrolyte, using an AFM apparatus with a cantilever with one-side Au coating. The pzc value was estimated from the maximum of the surface tension curve versus the applied potential, and the value was close to the pzc value obtained from the minimum of the capacitance-potential curve. This method is very useful to give the pzc and study the electrical double layer by measuring the surface tension of solid electrode in electrolyte.

The C-E characteristics with the specific adsorption shows no apparent

minimum except in very dilute solution less than about 10^{-3} M [3]. However, the γ-E curves can be expected to show a maximum independently of the electrolyte concentration and therefore will be useful to determine the pzc in a concentrated solution. This new method by measuring the γ-E curves shown in this study will contribute to the study of electrical double layers of solid electrodes particularly in the specific adsorption system.

References

1. G.Lippmann, Ann. chem. phys., **5** (1875) 494.
2. D.C.Graham, Chem. Revs.,**41** (1947) 441.
3. P.Delahay, Double Layer and Electrode Kinetics, Interscience, New York (1965).
4. R.Persons, Modern Aspects of Electrochemistry, Vol. 1, O'M. Bokris, editor, Butterworths, London (1954) pp.103-179.
5. T.R.Beck, J. Phys. Chem., **73** (1969) 466.
6. G.Binnig, C.F.Quate and Ch.Gerber, Phys. Rev. Lett., **56** (1986) 930.
7. J.Clavilier and C.N. van Huong, J. Electroanal. Chem., **80** (1977) 101.
8. G.M.Schmid and N.Hackerman, J. Electrochem. Soc., **109** (1962) 243.
9. F. Silva, M.J.Sottomayor, A.Hamelin, and L.Stoicoviciu, **295** (1990) 301.
10. W. Kern and D. A. Poutinen, RCA Rev., **31** (1970) 187.
11. Z. Borkowska and U. Stimming, J. Electroanal. Chem. **312** (1991) 237.
12. A. Hamelin, T. Vitanov, E. Sevastyanov, and A. Popov, J. Electroanal. Chem., **145** (1983) 225.

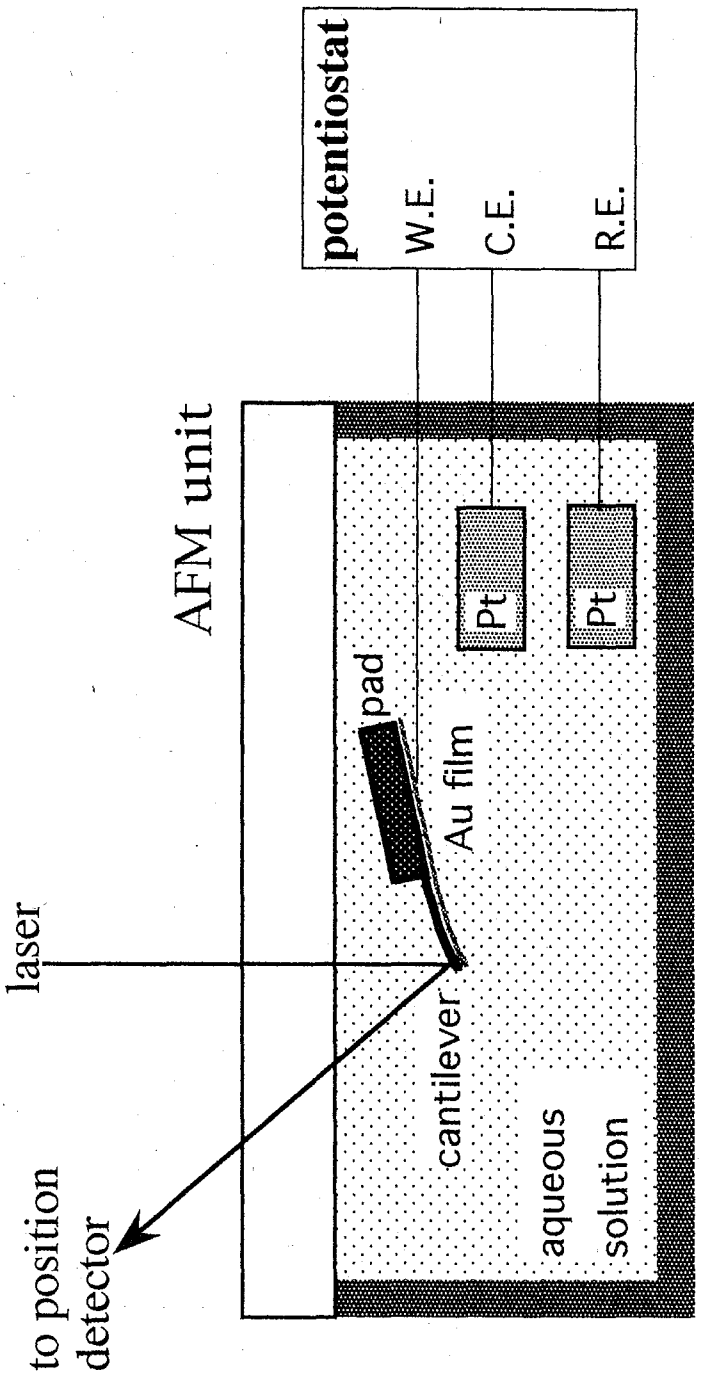

Figure 6-1 Schematic diagram of our experimental setup used in this study. The bending of the cantilever can be measured by the laser beam deflection. The microfabricated cantilever, the bottom plane covered with a thin Au layer, is immersed in an electrolyte and the electrical potential is controlled by a potentiostat.

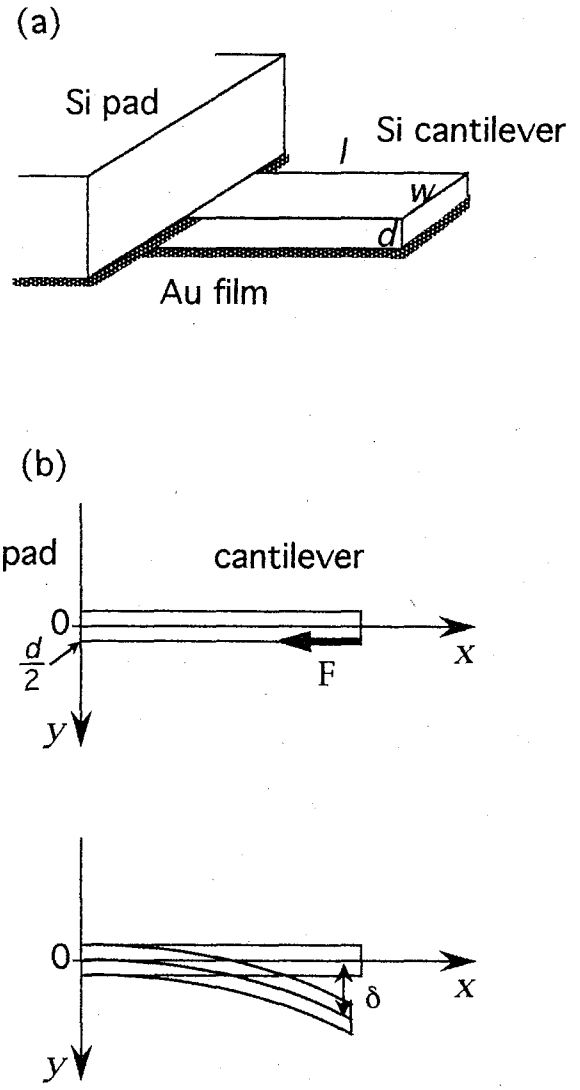

Figure 6-2 Simplified model of a bending cantilever. (a) perspective view. l the length of the cantilever, w the width, d the thickness. (b) side view. The coordinates are shown as x and y. The force F exerts at the bottom right corner. The neutral plane is taken as the middle plane of the cantilever referred to y=0.

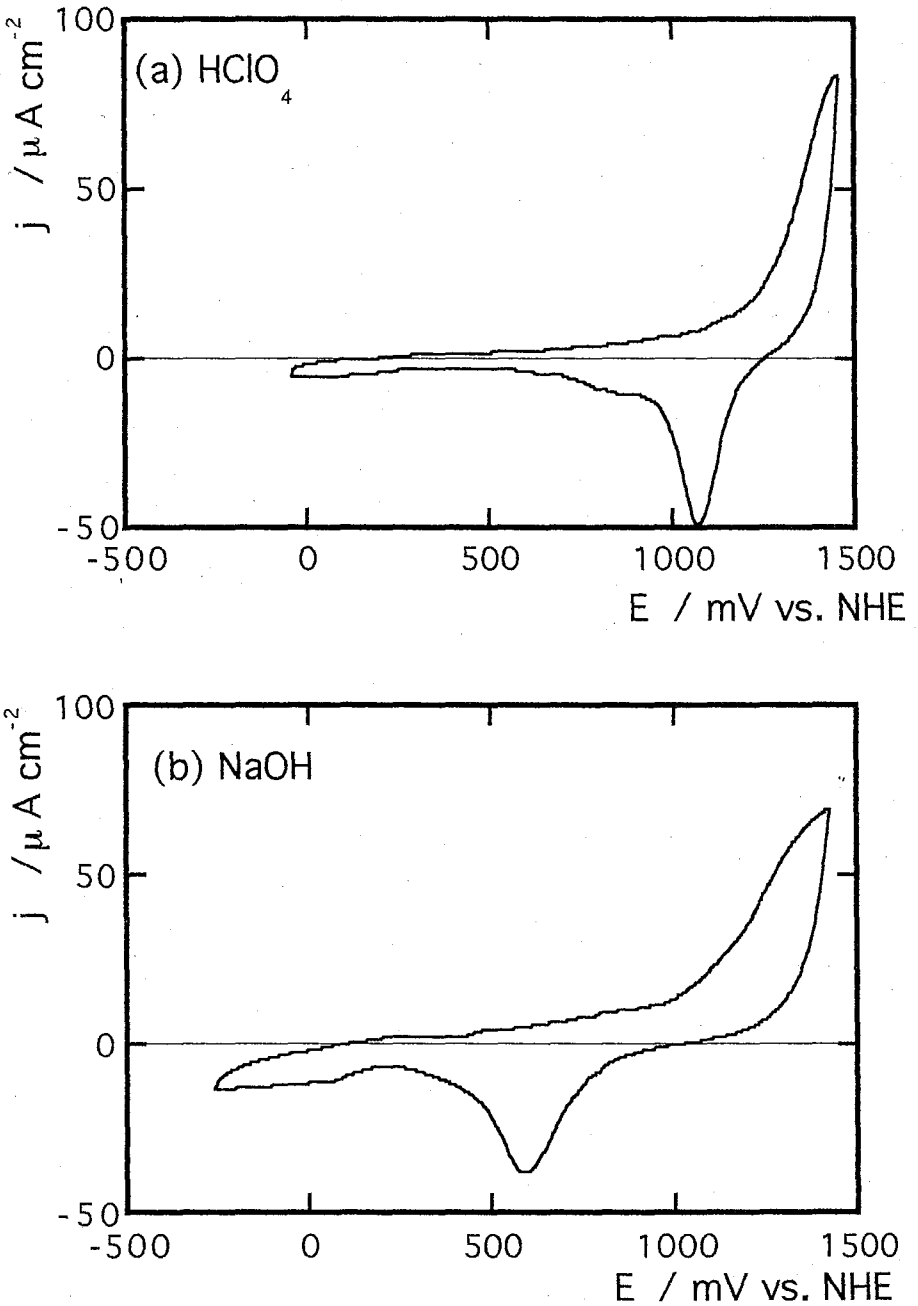

Figure 6-3 Cyclic voltamogram (CV) for a Au film electrode on a Si cantilever in (a) 10^{-3} M $HClO_4$ and (b) 10^{-3} M NaOH. The sweep rate 20 mV s^{-1}. The current was normalized with geometric electrode area, 0.024 cm^2.

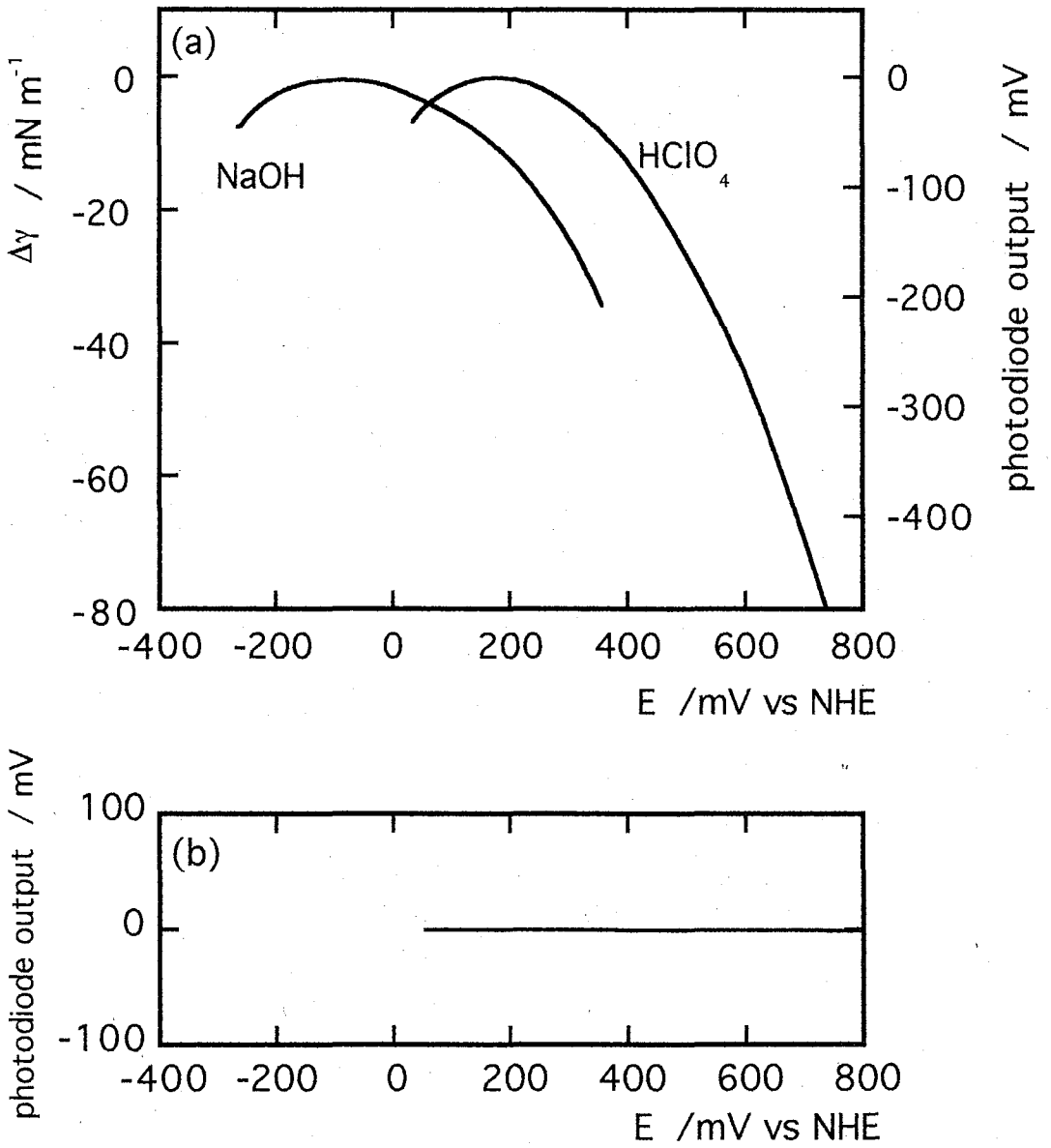

Figure 6-4 Characteristics of surface tension versus the electrode potential for (a) a Si cantilever with a Au-coated electrode in 10^{-3} M $HClO_4$ and 10^{-3} M NaOH, and (b) without a Au-coated electrode but with a Au-coated pad 10^{-3} M $HClO_4$.

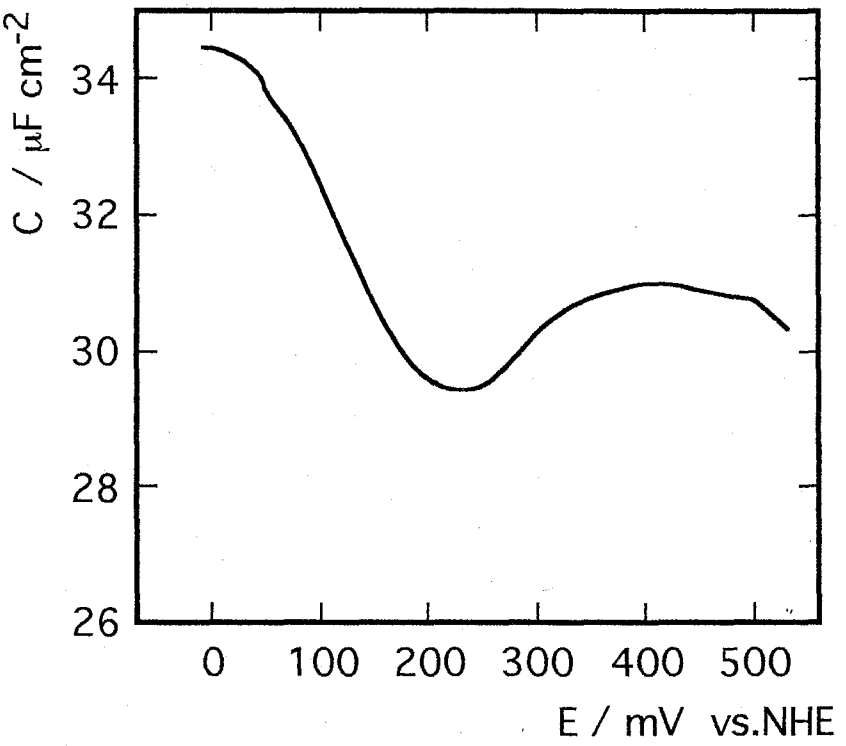

Figure 6-5 Differential capacitance of a Au film electrode on a Si cantilever in 10^{-3} M $HClO_4$. The sine modulation was 71 Hz in frequency and 5 mV in amplitude.

Chapter 7

Summary

In this thesis, the author has tried to evaluate the electrical double layer structure at the solid-liquid interface by the measurements of the interaction force with an AFM. For almost 100 years, the counter ions in the diffused double layer have been estimated to be distributed according to the Boltzmann distribution, although there was no direct measurement tool. Here, a new method with an atomically sharpened tip has been applied to study the double layer, which can measure the interaction force with a lateral resolution on a nanoscale, although the surface force apparatus (SFA) was used to evaluate the distribution by measuring the interaction force without lateral resolution. It is noteworthy that the author has evaluated the interaction force and introduced the concept of the interaction force between approaching electrodes in electrochemistry, where only a mechanically isolated electrode had been studied before. Furthermore, the author has suggested a new method to measure surface tension on the solid electrode easily, and then opened a new route for study of solid electrodes.

The summary for each chapter are mentioned below:

In chapter 1, the history of study of the electrical double layers were described. The features of SFA and SPM, in particular, AFM, which were recently developed as surface analytical tools, were pointed out, including the effective application for study of the double layer.

In chapter 2, force-distance curves with an AFM were calculated for tips with various shapes, immersed in electrolytes without the low potential approximation and the Derjaguin approximation. It was revealed that the interaction force measured with the AFM close to sample surface within several 10 nm strongly depends on the tip shape, then the importance of tip shape evaluation and correction was emphasized.

In chapter 3, for oxides, the agreement of the measured force-distance curves with the calculated curves was clearly shown: it proved that the calculation in chapter 2 was correct. Moreover, the author has suggested a new method to measure isoelectric points (IEP) from results of the interaction measurements.

In chapter 4, organic mono-molecular films were formed with partial coverages on quartz substrates by a new LB film method combined with silanization reaction. Compared the force on the covered surface with that on the uncovered surface, it was found that the surface interaction force becomes weak on the covered area.

In chapter 5, a new method to evaluate the potential at the outer Helmholtz plane (OHP) has been suggested: by measuring the interaction forces between the potential controlled electrode and the AFM tip charged with the polarity determined by the pH of the solution, and between both of the potential controlled electrodes. Using the method, the potential at OHP was estimated.

In chapter 6, using an AFM, the author has suggested a new method to measure surface tension of solid electrodes. This method can easily give the pzc value even in the system with strongly specified adsorption.

List of Publication

1. "Theoretical calculation of force between a sharpened tip and a flat surface in an electrolyte solution for atomic force microscopy.", to be submitted.
   (M. Fujihira) (Chapter 2)

2. "Effect of tip shape on force-distance curves of AFM in aqueous electrolytes."; J. Electroanal. Chem., 374, 269 (1994).
   (M. Fujihira) (Chapter 2 and 3)

3. "Analysis of surface forces on oxides in aqueous solutions using AFM."; Thin Solid Films, in press.
   (D. Aoki, Y. Okabe, and M. Fujihira) (Chapter 3 and 4)

4. "Effects of electric potentials on surface forces in electrolyte solutions."; J.Vac.Sci.Technol., in press.
   (M. Fujihira) (Chapter 5)

5. "Study of Electrical Double Layer Structure at Electrode-Solution Interfaces by Atomic Force Microscopy.", to be submitted.
   (M. Fujihira) (Chapter 2, 5 and 6)

Acknowledgments

I wish to express my appreciation to my research advisor, Professor Masamichi Fujihira, for his guidance, encouragement, and patience throughout the years of these studies.

I am grateful to Dr. Suga for his helpful suggestions and discussions.

I wish to thank Professor Atsushi Ikai for providing his DI AFM instrument for the present study.

I am also grateful to all staffs and colleagues in Fujihira laboratory for their kind help.